Synthesis and Characterization of some Nano Graphene Oxide Membranes for the Removal of some Water Pollutants

Thesis Submitted to

the College of Science / University of Misan as Partial Fulfillment

of the Requirements for the Master Degree of Science in Chemistry

By

Sammah Naeem Ghazi

B.Sc. Chemistry / Misan University (2018)

Supervisors

Asst. Prof. Safaa Sabri Najim
Asst. Prof. Dr. Ahmed Majeed Abbas

2023   **1445**

بسم الله الرحمن الرحيم

﴿قُلْ هَلْ يَسْتَوِي الَّذِينَ يَعْلَمُونَ وَالَّذِينَ لَا يَعْلَمُونَ إِنَّمَا يَتَذَكَّرُ أُولُو الْأَلْبَابِ﴾

سورة الزمر اية (9)

صدق الله العلي العظيم

Dedication

To The person who raised me and prayed for me in every prayer for success…

my grandmother (may Allah have mercy on her soul)

To The Sun and Moon Which Lighting my Life by Pave the Way to my Success…

My Father & My Mother

To Those who have Supported me and are Waiting for my Success…

My Sisters & My Close Friends

To The one who gave me his Time and Knowledge…

My Supervisor

Jammah

Acknowledgement

Supervisor Certification

We are the supervisors of **Sammah Naeem Ghazi**, certify that the thesis (**Synthesis and Characterization of some Nano Graphene Oxide Membranes for the Removal of some Water Pollutants**) was done and written under our supervision as a fulfillment of the requirement for the master degree of science in chemistry.

Signature…………   Signature ………….

Asst. Prof. Safaa Sabri Najim   **Asst. Prof. Dr. Ahmed Majeed Abbas**
Chemistry Department   *Chemistry Department*
College of Science   *College of Science*
Misan University   *Misan University*

Date: / 9 / 2023   Date: / 9 / 2023

Head of Chemistry Department Recommendation

According to the recommendation of the supervisors, this thesis is forwarded to the examination committee for approval.

Signature…………

Asst. Prof. Dr. Tahseen Saddam Findi

Head of Chemistry Department
College of Science
Misan University

Date: / 9 / 2023

"Examining Committee Certificate"

We the examining committee members, certify that we have read this thesis entitled **(Synthesis and Characterization of Some Nano Graphene Oxide Membranes for the Removal of some Water pollutants),** examined the MSc. student **(Sammah Naeem Ghazi)** in its contents and in our opinion it meets the standard of a thesis for the degree of master in Chemistry with **(Excellent)** grade.

Signature………….

Professor

Dr. Hassan Thamir Abd ul-Sahib

Collage of Science /Basrah University

Date: / / 2023

(Chairman)

Signature………….

Professor

Dr. Ali Kareem Abd ul-Hassan

Collage of Science /Misan University

Date: / / 2023

(Member)

Signature………….

Professor

Dr. Salim Namah Al-Bukhaty

Collage of Science /Misan University

Date: / / 2023

(Member)

Signature………….

Assistant Professor

Safaa Sabri Najim

Collage of Science /Misan University

Date: / / 2023

(Member and Supervisor)

Signature………….

Assistant Professor

Dr. Ahmed Majeed Abbas

Collage of Science /Misan University

Date: / / 2023

(Member and Supervisor)

I confirm the above approval decision of the Examination Committee

Signature………….

Professor

Dr. Tahseen Saddam Fendi

Date: / / 2023

(Dean of Science Collage)

Abstract

The water pollution problem is widespread throughout the world. Nowadays, growing industrial activities have resulted in the generation of huge amounts of hazardous; untreated industrial effluents and uncontrolled pollutants that are released into environmental water. Among them, dyes from textile industries generate a large amount industrial wastewater due to the huge water demand and frequently discharge into the environment throughout the production process and has a direct impact on human health , as a result, water pollution remediation is one of the imperative issues which the scientific community has given significant attention to with the primary goal of safeguarding and conserving natural water resources. This study includes three parts; Synthesis, Characterization and application of nano-graphene oxide (NGO) composites for the removal of some Water Pollutants.

Part one contains the synthesis of nano-graphene oxide (NGO) and three composites, nano-graphene oxide-chitosan (NGO-CS), nano-graphene oxide-Methionine (NGO-M) and nano-graphene oxide-Cysteine (NGO-C).

Part two includes the characterization of these composites by (FT-IR), (XRD) to find out the particles size (7.4, 10.8, 16.83 and 19.52 nm) for NGO, NGO-CS, NGO-M and NGO-C composites respectively through Debye-Scherrer equation, and used zeta potential analysis to study the surface charge of particle.

Part three contains the application of these composites for water treatment in order to remove the organic pollutants (bromophenol blue dye BPB) as well as inorganic pollutants, trace heavy metals. Through two methods; first method (adsorption) of the BPB dye on the three composite beads, determination the optimum conditions for each composite, the results are (pH =2,3 and1, composite dosage= 2,2 and 2 mg, contact time =75,60 and 60 min., Temperature= 45, 55 and 55°C. dye concentration=40, 25 and 25 mg.L^{-1}) for NGO-CS, NGO-M and NGO-

C composites respectively. As well as studying the adsorption isotherm, the isotherm curves show the general adsorption isotherms of the composites is S-type according to the Gilles classification, applying Freundlich and Langmuir models. In addition, studying the thermodynamics, estimated thermodynamic for the adsorption of BPB dye on NGO-CS, NGO-C and NGO-M composites, the process was endothermic, ΔH (+), ΔS (+) of the adsorption BPB dye on the three composites, confirmed spontaneously of the adsorption processes ΔG (-). The results show pseudo-second order kinetic model is more valid to describe the adsorption behavior of BPB dye on the three composites. Second method includes fabrication NGO, CS, NGO-CS, NGO-M and NGO-C membranes by vacuum filtration, and determination the average pore sizes by FESEM as follow (52.31-613.2), (63.14-972.4), (49.53-347.5), (84.8-326.0) and (55.32-147.01) nm respectively. The membranes used to separate an organic compound as a pollutant (BPB dye), the removal% are (85.65, 95.35, 98.52, 86.91 and 92.61%) respectively, the best membrane was NGO-CS. These membranes also used to separate trace heavy metal Ni^{2+}, Cd^{2+}, Co^{2+}, Cu^{2+} and Pb^{2+} ions from aqueous solutions, the experimental data shows the removal percentage of Ni^{2+} and Co^{2+} ions by the membranes were in the order NGO-CS > NGO-C >NGO-M > CS > NGO, the best membrane is NGO-CS, R% (48.47%) and (68.17%) ..While, Cd2+ ions follow the order CS > NGO-M > NGO > NGO-CS > NGO-C, the best membrane is CS, where R% (52.2 %).The Cu2+ ions follow the order NGO-M > NGO-C > NGO> NGO-CS> CS, the best membrane is NGO-M, ,where R% (66.47%) . On the other hand, Pb^{2+} ions follow the order NGO-CS > NGO >NGO-M > NGO-C > CS, the best membrane is NGO-CS where R% (67.04%).

Contents

Tables

Figures

XI

XII

XIII

List of Abbreviations

Abbreviations	Key
BPB	Bromophenol Blue Dye
BOD	Biological oxygen demand
CNTs	Carbon nanotubes
CS	Chitosan polymer
Ce	The concentration at equilibrium for adsorbate in (mg/L)
Ci	The initial concentration of adsorbate in (mg/L)
C_d	The desorbed dye concentration (mg L-1)
D	Particle size
DMF	Di Methyl Formamide
FESEM	Field Emission Scanning Electron Microscopy
FAAS	Flame Atomic Absorption Spectroscopy
FT-IR	Fourier transform infrared spectroscopy
$\Delta G°$	The standard Gibbs free energy (KJ∕mol)
$\Delta H°$	The standard enthalpy change (KJ∕mol)
K_L,a	Langmuir constants
K_2	Second-order rate constant (*g/mg.min*)
K_1	First-order rate constant (min^{-1})

K_f , n	Freundlich constants
K	Scherrer's constant equal 0.9
LOD	Limit of Detection
MF	Micro-Filtration
NF	Nano-Filtration
NGO	Nano- Graphene oxide
NGO-CS	Nano graphene oxide-Chitosan composite
NGO-M	Nano graphene oxide- Methionine composite

Abbreviations	Key
Qe	Adsorption capacity at equilibrium in (mg\g)
Qt	Adsorption capacity at in (mg\g)
$\%R$	Percentage removal rate
R_L	The dimensionless separation factor
RO	Reverse osmosis
rpm	Round per minute
$\Delta S°$	The standard entropy (J/mol. K)
SD±	Standard Deviation
T	The temperature (K)
THMs	Trihalomethanes
UF	Ultra-Filtration
UV-Vis	Ultraviolet-Visible Spectrophotometer
V_d	Volume of desorption solution (L)
VOCS	Volatile Organic Chemicals
XRD	X-Ray Diffraction Spectroscopy
0D, 1D,3D	Zero, one, three dimensions
λ_{max}	wavelength maximum
β	full width at half maximum (FWHM)

Chapter one

INTRODUCION

1.1 Importance of Water

Water is a gift from God, it is essential to life as we know it, water covers over 70 % of the surface of the globe, it is a biomolecule and as such, is essential for all biological processes. Water is required for the survival of all life forms on Earth. It makes up (55-78)% of the human body [1]. One of the most important critical challenges currently affecting the political and social spheres is the lack of water in many developing nations. Water transports and spreads a lot of diseases and dangerous things. Water regulates the temperature of the earth and all living things, transports everything, including nutrients and waste, and makes up the majority of the blood and other aqueous fluids in both human and animal bodies[2].

1.2 Water Pollution

Water pollution is a widespread issue across the world. Anthropogenic (man-made) or geological contamination is the cause of this problem [1]. An anthropogenic pollutants are caused by human activities such as industrial activities, agricultural actions, commercial activities, residential and waste disposal systems, pharmaceuticals and personal care products[3] Magnesium, calcium, chloride, nitrate, iron, fluoride, sulfates, and radionuclides are a few examples of natural elements and compounds that can contaminate groundwater if they are present in excessive proportions. In addition to the decaying of organic particles, there are other natural elements and compounds that may pollution of water too by passing water through sedimentary rocks and soils [3, 4]. Essentially, there are inorganic, and organic pollutants.

1

1.3 Types of Pollutants

1.3.1 Inorganic Pollutants

Inorganic contaminants of water are largely caused by both natural and man-made sources. Heavy metals, the nitrate and phosphate groups, as well as other elements like chloride and fluoride, are the main inorganic water pollutants.

1.3.1.1 Heavy Metals

A class of metals (and metal-like elements) with an atomic number larger than 20 and a density greater than 5 g/cm^3 are referred to as "heavy metals" [5]. At least 20 metals are categorized as hazardous, and 50% of them are released into the environment at a level that poses a risk to human health[6] .

1.3.1.2 Heavy Metals Sources

These substances are naturally present in the crust of the planet and may enter the environment due to human activity and rapid manufacture [7]. Through industrial processes, significant amounts of toxic heavy metals are released into the environment. Heavy metals like copper, chromium, cadmium, nickel, lead, zinc, and mercury are released into industrial wastewater and urban sewage as a result of a number of processes, including mining, battery production, and plating[8] .

1.3.1.3 Effects and Important of Heavy Metals

Some heavy metals are vitally important to the body, such as zinc, iron, and others, which are permitted and recommended medically, but within very regulated limits that take into account the type of food, as an excess of these elements leads to poisoning as well. On the other hand, other elements such as arsenic, cadmium,

and mercury are not of chemical or biological importance. Medicinal and even harmful even at very low traces [9]. Heavy metals cannot be broke down or destroyed, [10] because they tend to accumulate in living organisms , they can lead to a variety of fatal diseases, such a buildup in the human body may harm the bones, central nervous system, kidney structure and function, and hematological problems. Additionally, it might affect how the primary biochemical reaction proceeds, even in very small concentrations, the heavy metals are harmful to all living organisms [11]. Heavy metals contamination of water are risky to environmental issue that degrades water quality. The results include reduced water availability and aquatic production, rising purifying costs, and eutrophication of water bodies [12].

1.3.2 Organic Pollutants

In almost every ecosystem, there are organic chemicals that are either naturally occurring or man-made, these substances may be the primary causes of water contamination. The quantity of synthetic organic compounds is growing as a result of industrial advancements, which also increases the health dangers posed by their presence in water [13] . The most common organic contaminants include Trihalomethanes (THMs)[14],Volatile Organic Chemicals (VOCS)[1], Pesticide, Raw Materials of Plastic Manufacturing [15], Pharmaceuticals, Personal Care Products (PPCPs) [16] and dyes. This thesis discusses the dye as a significant contaminant.

1.3.2.1 Dyes

Dyes are colored compounds with unique structural characteristics, absorb light in the spectrum at specific wavelengths (400-700 nm), as shown in Table (1.1). Require a minimum one chromophore group that is chargeable for dye color, and also have a conjugated system and stability within the compound's forces due to

electron resonance. The majority of the time, chromophores are made up of one or more functional groups of delocalized electron systems with conjugated double or simple bonds (with a more or less extended pi electron). In the structure of a chromophore, heteroatoms containing non-bonding electrons, such as nitrogen, sulfur, and oxygen, are present. Chromophores generally have - N=N- (azo), C=S (Sulphur), =C=O (carbonyl), =C=C=, C=NH, -CH=N-, and NO or N-OH (nitroso) [17]. In addition to chromophores, dyes also contain other groups which are auxochromes. Their name belongs to their action that enhances the color, they are polar groups as carboxylic acid, sulfonic acid, amino, and hydroxyl groups, binds to the textile polar group, furthermore, they are used to influence dye solubility[18] .

Table (1.1): Wavelength light absorption & color in organic dyes[19]
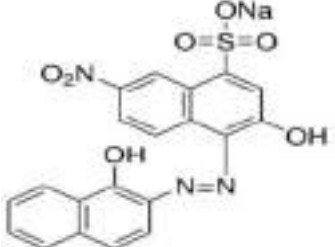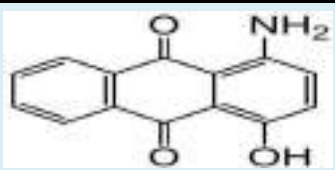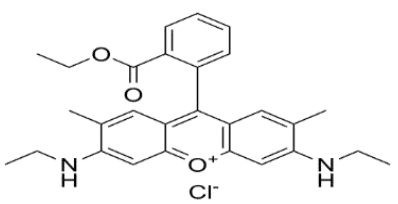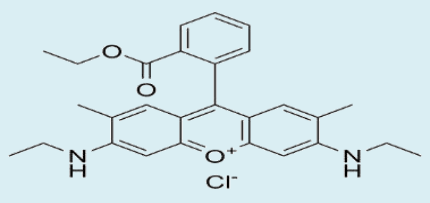
Wavelength Absorbed (nm)	Color Absorbed	Color Observed
400-435	Violet	Yellow-Green
435-480	Blue	Yellow
480-490	Green-Blue	Orange
490-500	Blue-Green	Red
500-560	Green	Purple
560-580	Yellow-Green	Violet
580-595	Yellow	Blue
595-605	Orange	Green-Blue
605-700	Red	Blue-Green

1.3.2.2 Classification of Dyes

The dyes are Classified based on:
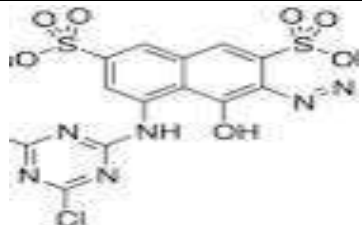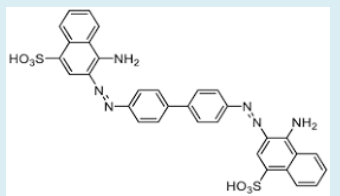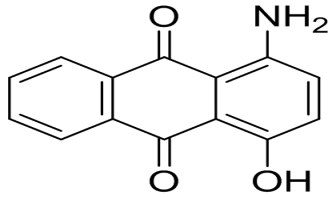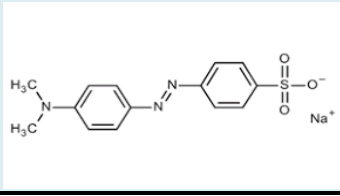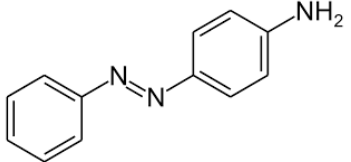
1- The chemical structure[20] as shown in Table (1-2).

Table (1-2): Classification of dyes based on the chemical structure[21]

Chemical group of dye	Example	structure
Azo dye	Eriochrome Black T	
Anthraquinone dye	Disperse Red 15	
Xanthene dye	Rhodamine (basic red 1)	
Phthalocyanine dye	Direct Blue 86	

2- Method of application to the substrate [21].

Table (1-3): Classification of dyes basaed on the methods of application [22]

Type of dye	Example	Structure
Reactive	Procion dye (2,4,6-tri chloro)1,3,5-triazine	
Direct	Congo red	
Disperse	Cellition fast pink B	
Acidic	Methyl orange	
Basic	Aniline yellow	

1.3.2.3 Influences of Dyes on Environment and Health

Over 8000 chemical compounds are consumed during the dyeing and printing process of textiles, and the majority of them have negative effects on health either directly or indirectly [23].The introduction of dyes into the water system causes a number of health and environmental problems: [24, 25]

• Dyes increases the water turbidity.

• Dyes have a major impact on the photosynthetic activity of the aquatic environment because they block the penetration of light into the water, thus inhibiting the growth of algae, which are not only important for oxygen production but are a pillar of the food chain[28, 29]

• Most of the dyes are carcinogenic (bladder, kidney, liver), mutagenic and toxic to living organisms.

• They can cause allergic reactions: skin, eye, mucous membrane irritation, dermatitis, respiratory problems.• They cause harm to aquatic environment, and may be toxic to aquatic organisms due to their aromatic, heavy metal and chlorine content[28, 29].

1.3.2.4 Separation and Elimination of Dyes from Water

Methods are used to treat the water from dyes can be classified into biological, chemical, and physical, additionally to various combinations of treatment techniques have been used to boost the efficacy of water treatments. Degradation and separation mechanism are utilized in water treatment from dyes, [30] as shown in Fig. (1-1).
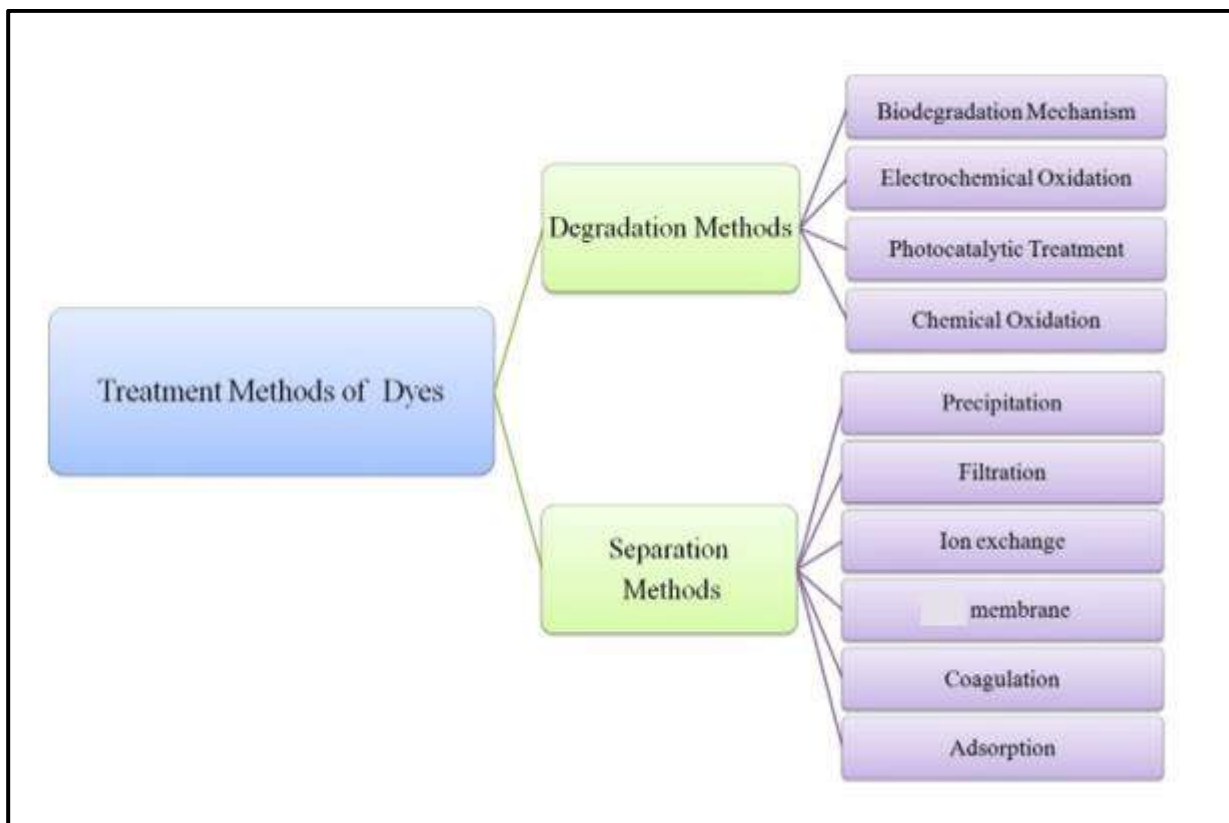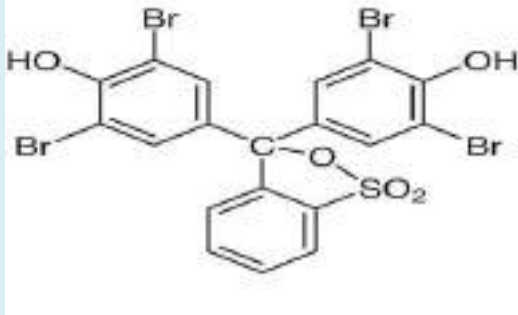
Fig. (1-1): Treatment methods of dyes[30]

1.3.2.5 Bromophenol Blue Dye

The bromophenol blue dye (3′, 3″, 5′, 5″-tetrabromophenol-sulfonphthalein), (BPB) has been used as a model molecule. It is derived from triphenylmethane and possesses potentially genotoxic derivatives,[31] as shown in Table (1-4). Triphenylmethane dyes are xenobiotic aromatic substances, alleged to be very harmful to mammalian cells and to be carcinogenic and mutagenic to humans, [47] in addition depending on how it is ingested, bromophenol blue dye might have negative consequences on one's health. It can irritate the skin, eyes, and respiratory system. Exposure to dyestuff dye might harm the cornea or conjunctiva of the eyes.

Table (1-4): Bromophenol blue dye properties [31]

Chemical Formula	$C_{19}H_{10}Br_4O_5S$
Structure	
Synonyms	Tetra-bromophenol blue, Bromophenol blue sultone form Tetra-bromophenol sulfonphthalein
Molecular Weight	670 g/mol
Class	Triary

1.4 Adsorption Phenomenon

The process of a substance (adsorbate) building up on the surface of a solid (adsorbent) is known as adsorption. The adsorbate can be either in a gas or liquid phase, as shown in Fig. (1-2). The adsorption phenomenon is the foremost commonly method used to evaluate the adsorbate capability to bind with adsorbents [32]. Due to their effectiveness in removing pollutants, adsorption techniques, recently become more popular. As a result, dye-loaded wastewater has been treated using adsorption techniques, which have been determined to be among the best and most reliable. The waste water is quickly separated into its aqueous and adsorbate phases.
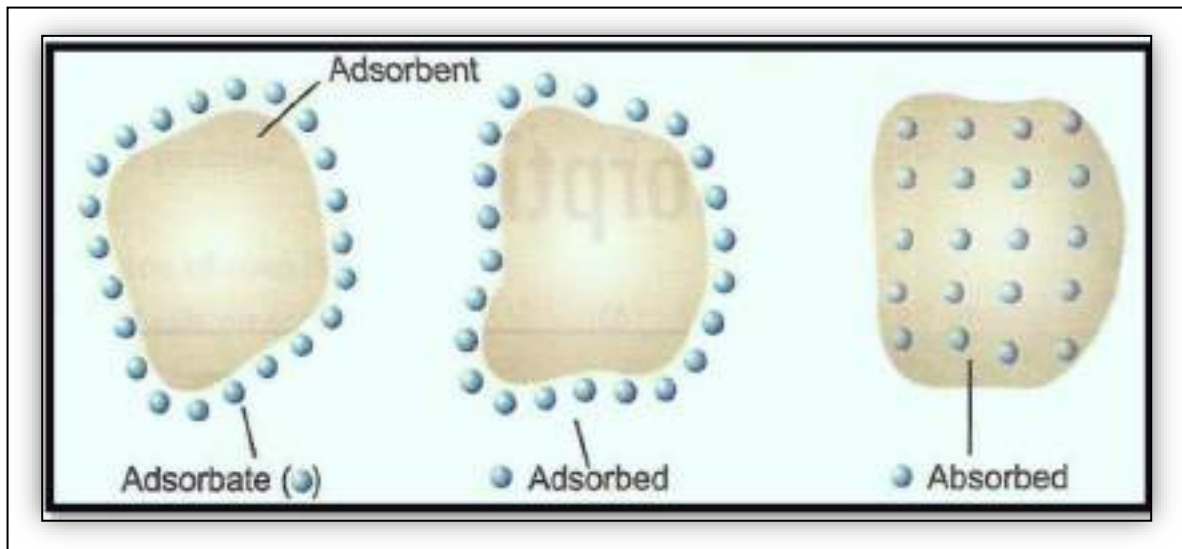
Fig. (1-2) adsorption versus absorption [32]

1.4.1 Forces affect the adsorption

The following forces are frequently taken into account when analyzing the adsorption process in solution[33] :

1- Ion-exchange: substitution of similarly charged solute ions for the double layer's counter ions.

2- Ion pairing: interactions between counter ions that are electrostatic.

3-Acid-base interaction: formation of a hydrogen-bond between solute and adsorbent.

4- Adsorption by polarization of π-electrons: interaction between positive charges and aromatic molecule groups at the adsorbent surface.

5- Adsorption by dispersive forces.

6-Hydrophobic bonding: Hydrophobic adsorbent groups and hydrophobic solute molecule groups interact in a desirable way.

1.4.2 Types of Adsorption[34]

1.4.2.1 Physical adsorption

Physisorption type of adsorption in which the adsorbate adheres to the surface only through weak intermolecular interactions, considered to be an effective method for quickly lowering the concentration of dissolved dyes in an effluent, can characterized by: [32, 33].

a) Low temperature, always under the critical temperature of the adsorbate.

b) Type of interaction: Intermolecular forces (van der Waals forces).

c) Low enthalpy: $\Delta H < 40$ KJ/mol.

d) Adsorption takes place in multilayer.

e) Low activation energy.

f) Reversible.

1.4.2.2 Chemical Adsorption

Chemisorption is a type of adsorption whereby a molecule adheres to a surface through the formation of a chemical bond, as opposed to physical adsorption. It is characterized by: [32,33]

a. High temperatures.

b. Type of interaction: strong; covalent bond between adsorbate and surface.

c. High enthalpy: $\Delta H \sim 400$ KJ/mol.

d. Adsorption takes place only in a monolayer.

e. High activation energy [34].

f. Irreversible.

1.4.3 Adsorption Equilibrium

The adsorption performance and characteristics of the adsorbents are researched for various adsorption isotherms, kinetic, and thermodynamic models [36].The adsorption capacity (the equilibrium adsorption amount) qe(mg/g) and The % removal efficiency determined by Equation (1.1) and (1.2), respectively.

$$Qe = \frac{(Ci - Ce)VL}{Wt} \quad .... \ (1.1)$$

$$\%R = \frac{Ci - Ce}{Ci} \times 100\% \quad .... \ (1.2)$$

Where: Qe adsorption capacity (mg/g), Ce (mg/L) is the concentration at equilibrium for adsorbate dye, Ci (mg/L) is the initial concentration of adsorbate, V (L) is the volume of sample, Wt (g) is the mass of adsorbent, $\%R$ removal efficiency [27].

1.4.4 Adsorption Isotherm Model

Although there are other isothermal models that are typically fitted for the relationship between Qe and Ce, Langmuir and Freundlich adsorption isotherms are the most widely used models for quantifying the dye adsorbed on the adsorbent [37].

1.4.4.1 Langmuir Isotherm

Langmuir developed an equation to describe adsorption in 1916. The possibility of adsorbing particles is determined, accordance to Langmuir, the presence of sites on the adsorbent surface, where the adsorbent surface contains empty sites, others occupied by adsorbed particles, and other free sites that are in

equilibrium with the particles adsorbed on the surface. Langmuir equation is written in linear form and is applicable to monolayer adsorption onto a perfectly homogenous surface with a finite number of identical sites and with minimal interaction between molecules that are adsorbed, as follows in Equation (1.3).

$$\frac{Ce}{Qe} = \frac{1}{K\text{L}} + \frac{a}{K\text{L}.Ce} \quad \dots\dots\dots\dots\dots \textbf{(1.3)}$$

Where: Q_e is the adsorption capacity at equilibrium in (mg\g), Ce the equilibrium concentration of adsorbate in (mg/L), a, K_L are Langmuir constants.

Can be calculate the dimensionless separation factor R_L, it determines the adsorption nature, either the adsorption process is favorable or not [38]. Equation (1.4) represents a way to calculate R_L factor, which described in Table (1-5)

$$\textbf{R}_\textbf{L} = \frac{1}{1+K\text{L Ci}} \quad \dots\dots\dots\dots \textbf{(1.4)}$$

Table (1-5) Adsorption isotherm supported the R_L value

Value of R_L	Adsorption
$R_L > 1$	Unfavorable
$R_L = 1$	linear
$0 < R_L < 1$	Favorable
$R_L < 1$	Irreversible

1.4.4.2 Freundlich Isotherm

The Freundlich isotherm, assumes a heterogeneous sorption surface, based on the idea that the adsorption depending on the energy of the adsorption sites. The Freundlich model can be represented as follows in Equation (1.5).

$$Qe = K_f\, C_e^{\,1/n} \text{ .... (1.5)}$$

Where: Qe the adsorption capacity at equilibrium in (mg/g), Ce the equilibrium concentration of the adsorbate in (mg/L), n and K_f Freundlich constants being indicators of the adsorption capacity and adsorption intensity, respectively.

The Freundlich constants can be obtained from the intercept and slope of the plot between the (log Qe) versus (log C_e) after taking logarithms of both side of Equation (1.6).

$$\text{Log } Qe = \text{Log } K_f + 1/n \text{ Log } C_e \text{ .... (1.6)}$$

The slope of the line will give the value of (1/n) and the intercept gives the value of (log K_f), if 1/n value is equal one it means the adsorbent is homogeneous with a regular pore size and surface chemistry, but if 1/n values are less than one which shows much of heterogeneity that are resulted from diversity within the shapes and sizes of the adsorbent pores as activated carbons.

Table (1-6): Type of adsorption isotherm supported the 1/n value [38]

1/n value	Type of isotherm
1/n = **0**	Irreversible
0 < 1/n < **1**	Favorable
1/n > **1**	Unfavorable

1.4.5 Thermodynamic of Adsorption

Thermodynamic parameters like standard enthalpy change ($\Delta H°$) and standard entropy change ($\Delta S°$) and the values for standard free energy ($\Delta G°$) are determined by the Equation (1.7).

$$\Delta G° = \Delta H° - T\Delta S° \ .... \ (1.7)$$

Where: ($\Delta H°$) is the standard enthalpy change (KJ∕mol), ($\Delta S°$) is standard entropy (J∕mol. K), (T) is the temperature (K). ($\Delta G°$) is the standard Gibbs free energy (KJ∕mol) .

Thermodynamic parameters $\Delta G°$, $\Delta H°$ and $\Delta S°$ are indicators of the possible nature of adsorption. The negative or positive value of ($\Delta H°$) is an indicator that either the adsorption reaction is exothermic or endothermic respectively. Also, a negative value of ($\Delta S°$) represents a decrease in the entropy, in contrast the increasing in the entropy is presented by positive value. The degree of spontaneity of an adsorption process is indicated by ($\Delta G°$), a negative value represents energetically desirable adsorption, while the positive value of ($\Delta G°$) indicates non-spontaneous adsorption.

1.4.6 Adsorption Kinetics

Kinetics is the study of chemical processes that explains the rate of adsorbate uptake as well as other factors that may have an impact on rates. This rate help to controls the time of adsorbate at a solid- liquid interface which was studied by using two main kinetic models: The pseudo- first- order model and the Pseudo-second order model.

1.4.7 Optimum Condition of Adsorption

1.4.7.1 Effect of pH

The pH is very important because it directly affects the surface charge of adsorbents and structure of adsorbates by controlling the degree of ionization and dissociation of functional group,[39] since both adsorbates and adsorbents may have functional groups that can be protonated or deprotonated to produce different surface at different pH, so electrostatic interaction between the charged adsorbates and adsorbents may occur[40]. This effect can be observed through the competition for (OH^-) and (H^+) ions and their overlapping with adsorbate or adsorbent surface or the solvent. The degree of ionization of a species is affected by pH (for example, a weak basis or a weak acid) which in turn affects adsorption. As the result of this interaction, the varying extent of adsorption either decreases, increases, or remains unchanged according on the adsorbate functional groups [41].

Generally, the adsorption decreases with increasing pH for anionic dyes [40 42] while it increases with increasing pH for cationic dyes [43-45].

1.4.7.2 Effect of Adsorbent Dosage

The dosage of the adsorbent is an important parameter for determining the capacity of the adsorbent for a given quantity of adsorbate under operating conditions[46]. The conditions to be properly considered when choosing an adsorbent supported the following subsequent criteria : low cost ,readily available, acceptable mechanical properties, high physical strength (not disintegrating) in the solution ,long life and regenerative ability if necessary [32].

1.4.7.3 Effect of Contact Time

Contact time can be defined as the longest time when the adsorption process complete and the balance or change is slight. The time required for the adsorption processes to reach equilibrium and depends on the surface nature and the available adsorption sites. The contact time between adsorbent and adsorbate has a major impact on the adsorption capacity. Commonly, the speed of adsorbate removal increases to a specific degree with arise in time to an extent, further increase the time wouldn't increase the uptake, because of the buildup of the adsorbate on the present adsorption sites, this time is termed as an equilibrium time, which represents the utmost adsorption capacity of the adsorbate on the adsorbent [46].

1.4.7.4 Effect of Temperature

Another important factor is the temperature. Temperature greatly affects the equilibrium condition of the adsorption mechanism and changes the parameters of thermodynamics. Regulation the temperature of the system regulates the adsorption rate of the contaminant. The adsorption rate of endothermic reactions and desorption rates of exothermic reactions could be increased by high temperatures[34]. Adsorption process is usually exothermic, it is a study of the temperature dependence to adsorption reactions which gives valuable information about the entropy changes during adsorption [47] .

1.4.7.5 Effect of the Initial Concentration of Adsorbate

A defined mass of adsorbent can only adsorb a set amount of dye, which is why the initial concentration of dye within the effluent is one among the important factors to be studied. The effect of the increase within the initial dye concentration would increase the loading capacity of the adsorbent by decreasing the available adsorption sites, this result decrease within the performance removal of dye or other

contaminants. Therefore, the share of dye removal relies on the initial concentration [34] .

1.4.7.6 Effect of Ionic Strength

The presence of salts (NaCl) as might screen the attractive forces between opposite charges in the adsorbent and adsorbate molecules, hence lowering the adsorbate uptake. On the contrary, adsorbate dissociation may be facilitated by the presence of foreign ions with an overall improvement in dye adsorption [48].

1.5 Adsorbents

1.5.1 Carbonaceous Nanomaterials

Carbonaceous means any organic material with high carbon content. The "carbon" is stands for the periodic table's sixth element[49].There are countless different ways that carbon can be found , the two allotropes of carbon that are most common are graphite and diamond.
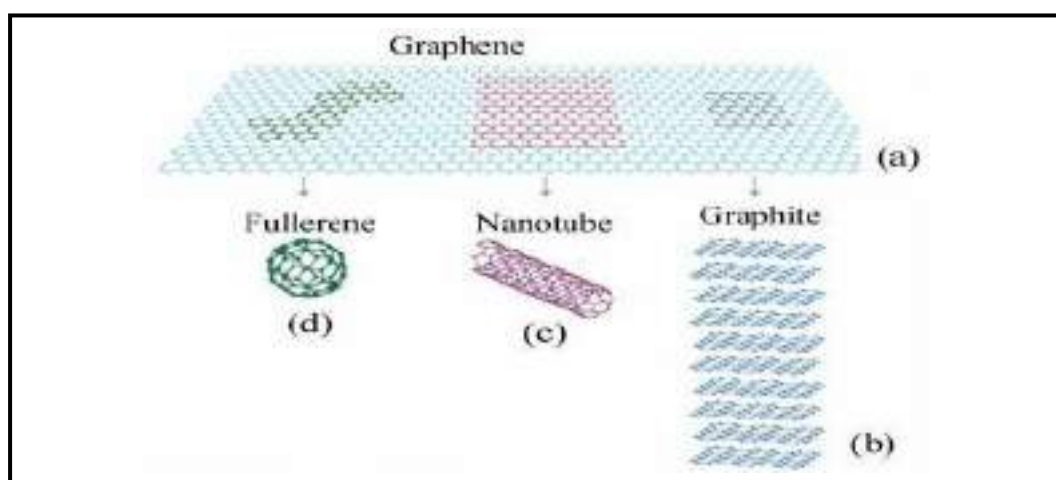
Fig. (1-3): Different dimensions of carbon-based nano adsorbent [50]

Graphite is made of stacked hexagonal carbon sheets that have undergone sp^2 hybridization. When carbon undergoes sp^3 hybridization, a metastable form of

carbon, it creates a tetrahedral lattice diamond[32].Nano technology has been used to develop sort of carbonaceous materials whose dimensions aren't greater than nanoscale (100 nm) with new properties and capacities that qualify them to be used as an activate adsorbent. In comparison to activated charcoal, carbonaceous nano-adsorbents can be manufactured for less money and have an overly large reactive surface, effective adsorption rates with the least amount of materials, and so on[49]. Numerous nano adsorbents are divided into groups according to their types and dimensions (D) for the removal of dyes. Nanoparticles can be categorized as 0D, 1D nanofibers and nanotubes, 2D nanosheets, and 3D nanoflowers.

Graphene-based nano adsorbents, carbon nanotubes (CNTs), fullerenes are examples of carbonaceous nanomaterials in several dimensions that are used as adsorbents for water treatment. As described above, nanostructured adsorbents provide a wide extent with an optimum adsorption power. This adsorption potential either physically or chemically is improved by surface functionalization, and therefore the porosity available is promoted [46].Beside to the environmental treatment, the carbonaceous nanomaterials have widespread interest in several applications relying on their outstanding of thermal and electrical conductivity, also the mechanical strength (high flexibility and high tensile strength) properties, including medical domain as drug delivery, catalysis, super capacitors, air filtration etc.[49] .

1.5.1.1 Graphene Oxide (NGO) Nano-Sheets

Graphene is a 2D substance made from graphite (3D),graphene is a honeycomb structure made up of sp^2 hybridized linked carbon atom lattice, with high specific surface area[41].NGO can be made in various ways, including brodie's and hummer's methods [51] as shown in fig ,pure NGO with numerous hydroxyl (−OH), carbonyl (−CO), epoxy (−COC), and carboxyl (−COOH) groups

can be synthesized by oxidizing graphite .
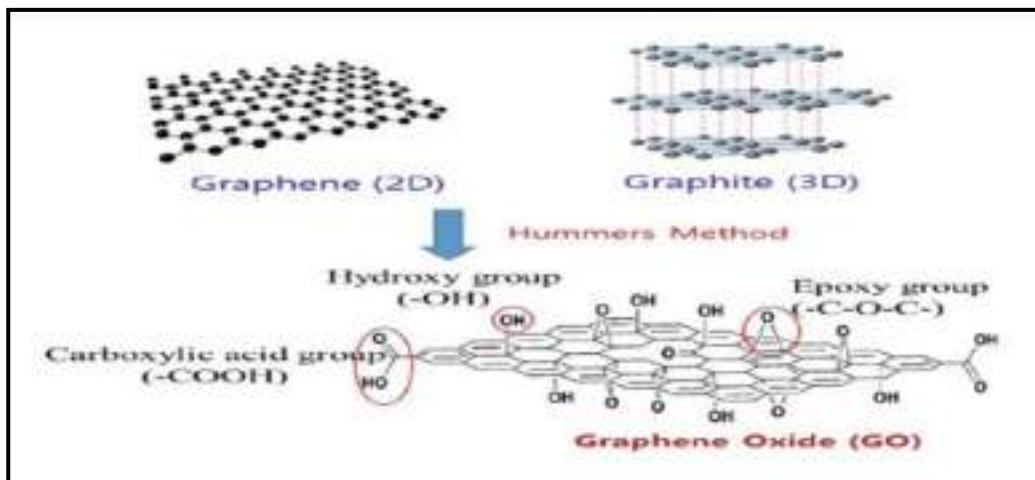
Fig. (1-4): Mechanism of graphene oxide synthesis[52]

Graphene oxide presents a high adsorption capacity because of its particular properties: high specific surface area, rich oxygen functional sites with both hydrophilic and hydrophobic groups and good thermal and chemical stability[39]. Thus, graphene oxide can be used in the decontamination of wastewater due to its adsorption properties, having the ability to remove one or more toxic compounds, NGO has attractive electrical, optical, and chemical capabilities because of its graphene skeleton and oxygen content These oxygen groups can bind metal ions,[51] and positively charged organic compounds, through coordination and electrostatic interaction. However, like other negatively charged adsorbents, NGO exhibits low affinity for anionic dyes, due to the strong electrostatic repulsion between them[53].

1.5.2 Chitosan (CS)

Chitosan, a copolymer of β[1,4]-linked 2-acetamido-2-deoxy-D-glucopyranose and 2-amino-2-deoxy-D-glucopyranose, is generally obtained by deacetylation of chitin, one of the most natural polymers on earth a major

component of the shells of crustacea such as crab, shrimp, and crawfish and the second most abundant natural biopolymer after cellulose[54].
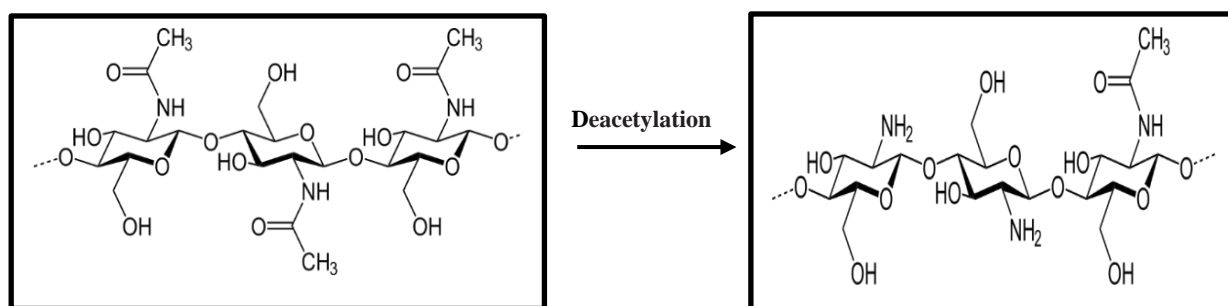
Fig. (1.5): Conversion of chitin to chitosan by deacetylation

Where chitin is N-deacetylated to such an extent that it becomes soluble in dilute aqueous acetic acid[55] The degree of deacetylation (%DD) generally dictates the physicochemical and biological properties of CS. Chitosan with its higher deacetylation degree, carries more positive charges, it exhibits better performance in removing pollutants by adsorption, coagulation, or bacteriostasis than agents of a lower deacetylation degree [56] . Chitosan has free hydroxyl groups and amino groups on its backbone, which can be easily modified by many organic reactions.[57] Application of chitosan is limited due to its poor solubility in common organic solvents. Again in biological fields its applications are limited because it is insoluble in water and can only be dissolved in acids [58,59]. Chitosan that is used as an adsorbent has drawn attentions due to its high contents of amino and hydroxy functional groups showing high potentials of the adsorption of dyes, the free amino–hydroxyl groups enable CS such properties as antibacterial, heavy metal chelation, protein affinity [42].

As mentioned in other reviews and articles, several important reasons make chitosan -based material a good adsorbent:

(1) Chitosan is an abundant, cheap resource, which makes it economically viable

(2) With abundant amino and hydroxyl groups, chitosan has a good adsorption capacity for many pollutions [60].

(3) Chitosan can be easily modified through physical or chemical methods for more versatile applications.

(4) As a biodegradable polymer, chitosan is non-toxic and environmental friendly[61].

1.5.3 Nano Graphene Oxide-Chitosan (NGO-CS) Composite

NGO exhibits low affinity for anionic dyes, due to the strong electrostatic repulsion between them [53], besides, nano graphene oxide, tend to aggregate in a layer-by-layer mode due to strong interplanar interactions. As a result, when these 2D sheets are made into powder, a considerable part of their surface area will be lost. Using the dispersion of single-layered NGO as an absorbent allows one to utilize the surface area to the utmost extent, but these NGO sheets are difficult to collect from water. Thus, how to make use of the surface area of NGO is another issue one should consider when developing NGO-based adsorbents. [62-64] the incorporation of CS can provide NGO–CS composite hydrogels with the ability of adsorbing anionic dyes. In fact, our study demonstrates that NGO-CS composite hydrogel have large adsorption capacity towards both cationic and anionic dyes, as well as metal ions. The adsorption capacities of the hydrogel towards different adsorbates can be adjusted by changing the composition of the hydrogel, and the adsorption process the NGO-CS hydrogel can be easily collected from the water by filtration or decantation. Moreover, we will further show that the NGO-CS hydrogel can be used as column packing, to fabricate a column for water purification by filtration.

1.6 Desorption Studies

Through the economy perspective, researchers has put monumental efforts in designing novel adsorbents that can be regenerated and also present long-term stability for continuous and sustainable operation of wastewater treatment plants[39]. Desorption studies help to explain adsorbate and adsorbent recovery, and the adsorption mechanism. Since the regeneration of the adsorbent makes the treatment process economical, desorption studies were performed to regenerate the spent adsorbent[65] . The process of adsorbent regeneration is a complex task, as the desorption depends on the adsorbent, the adsorbate (different types of dyes ionic nature), and the adsorption process. In adsorption–desorption studies, it is essential to examine the reusability of the adsorbent. Between dye removals, the adsorbent should be cleaned and regenerated to ensure that it can continue to be used and the water treatment can be reproduced. There are different desorption methods as using acetone, acetonitrile and ethanol etc. Equation (1.8) using to determine desorption %.

$$\% \text{ Desorption} = \frac{C_d - V_d}{q_e \times W}$$ .... (1.8)

Where: C_d, V_d, W, and q_e are the desorbed dye concentration (mg L^{-1}), volume of desorption solution (L), mass of dye loaded adsorbent (g), and adsorption capacity (mg g^{-1}), respectively[39].

1.7 Membrane Filtration

The membrane filtration technique has drawn more attention than other treatment technologies for water purification. Membrane technique is considered

an effective and economical approach in many fields of wastewater treatment, its performance significantly depends on the selectivity and permeability of the membrane materials. High energy consumption caused by membrane fouling and other problems limited the wide application of this technique. The technique suffers from high capital cost and has a risk of clogging. Frequent membrane replacement is one more disadvantage of this process. This method is suitable, if the effluent contains a low concentration of dyes. Membrane filtration has the ability to work in combination with other effluent treatments. This method is not only restricted to organic contaminants and microorganisms present in wastewater but to salts membrane filtration, used for color removal, BOD reduction, salt reduction, polyvinyl acetate (PVA) recovery, and latex recovery, among others. The method is resistant to temperature, the membrane filtration can be detrimentally influenced by microbes. The remaining.

The common membrane filtration types are Micro-Filtration (MF), Ultra-Filtration (UF), Nano-Filtration (NF), and Reverse Osmosis (RO). The choice of the membrane process is influenced by the required quality of the final effluent [66].

Considerable studies have reported that incorporation of carbonaceous nanomaterials into membranes make it possible to improve the selectivity permeability and fouling resistance of membranes. Microporous membranes with a pore size about 0.1–5 μm can only be used for filtering particles with 1–10 μm, which limits their applications in water purification. Meanwhile, nano porous membranes exhibited high performance for water purification. They can filter most of the pollutants (1–10 nm) such as metallic ions, organic molecules, salts, and microbes from wastewater[67]. To design high performance nano-porous membranes for water purification, many kind of inorganic, organic, and inorganic-organic hybrid materials have been utilized. For instance, the water desalination by using nano porous single-layer graphene[68] .

1.7.1 Types of Nano-porous Membranes

Nano-porous membrane for water purification can generally be divided into three types based on their material composition[69]:

1-inorganic membranes.

2- organic membranes.

3-inorganic-organic hybrid membranes.

Inorganic membranes are mainly made of ceramics (Al_2O_3, TiO_2, ZrO_2, SiO_2, TiO_2-SiO_2, TiO_2-ZrO_2, Al_2O_3-SiC), graphene[70], and carbon nanotubes (CNTs) Organic membranes are mainly made of polymeric materials such as polyvinyl alcohol (PVA), polyimide (PI), polypropylene (PP), polyethersulfone (PES), cellulose acetate (CA), cellulose nitrates, polysulfone (PSU), polyvinylidene fluoride (PVDF), polyacrylonitrile (PAN), polytetrafluoroethylene (PTFE), and biomacromolecules. Inorganic-organic hybrid membranes are usually made by introducing inorganic materials (metals, metal oxide, or carbon-based materials) into a polymeric matrix system[71].

1.8 Literature Survey

1- (Pand & Subrata et al. 2016) studied the interaction of graphene oxide (GO) with amino acids bearing variable charge, by using isothermal titration calorimetry. To explore the effect of lateral size and degree of oxidation in GO. The results show that the interactions of GO with amino acids are mainly governed by electrostatic and π−π interaction with variable enthalpy and entropy values[72].

2-(Shahzad & Asif et al. 2017) synthesized Ethylenediaminetetraacetic acid (EDTA)-functionalized magnetic chitosan (CS) graphene oxide (GO) nanocomposites (EDTA-MCS/GO) were using a reduction precipitation method

and applied to the removal of heavy metals, such as Pb^{2+}, Cu^{2+} and As^{3+}, from aqueous solutions. The influence of various operating parameters, such as pH, temperature, metal ion concentration, and contact time on the removal of the metal ions, was investigated. Studied Langmuir and Freundlich isotherms and kinetic[73].

3- (Hossein & Hossein et al. 2018) synthesized magnetic chitosan/graphene oxide nanocomposite (MCGON) .The magnetic MCGON with a high specific surface area of (132.9 m^2 g^{-1}), large pore volume (4.03 cm^3 g^{-1}), small particle size (15 nm) and strong saturation magnetization (3.82 emu g^{-1}) was used as an efficient adsorbent for the removal of Cu^{2+} ions from wastewater[74].

4- (Sarkar & Amit et al. 2019) developed biopolymeric GO with magnetic activity, namely, cl–CS–p(MA)/Fe_3O_4NPs. has been and used for the removal cationic dye in significant quantity, e.g., methylene blue (MB), which is used as a model water pollutant [75].

5- (Sohni & et al. 2019) synthesized magnetic chitosan-graphene oxide composite (Cs-GO) has been and used for the removal of two common textile dyes; acid red-17 (AR-17) and bromophenol blue (BPB). The effect of various parameters including pH, time, adsorbent dosage, initial dye concentration, as well as temperature. Present work revealed fast adsorption kinetics with removal efficiency of around 79 and 97% for AR-17 and BPB, respectively, were studied using Langmuir and Freundlich models. Thermodynamic analysis uncovered the spontaneous and endothermic nature of dye-composite interaction [39].

6- (Fathy & Mahmoud et al. 2020) prepared nanostructure reduced graphene oxide by using catalytic acid spray (CAS) method in the existence of cobalt silicate nanoparticles. The structure characterized by a number of modern techniques like

FTIR, transmission electron microscopy, X-ray diffraction, and Raman characterizations [76]**.**

7- (Sahli & Mohd Kamari et al. in 2020) studied of chitosan-graphene oxide (CS-GO) nanocomposites, namely CS-GO 1% (w/ w), CS-GO 2% (w/w) and CS-GO 3% (w/w) as water-solubilizing agents for rotenone pesticide was evaluated for the first time. The interaction of nanocomposites with rotenone was investigated through adsorption study involving several experimental parameters such as solution pH, initial concentration and contact time. Additionally, the adsorption kinetic data were best described by the pseudo-first order equation while the adsorption equilibrium data were correlated well with the Langmuir isotherm model. Based on Langmuir isotherm model, CS-GO 3% (w/w) exhibited the highest adsorption capacity for rotenone. The CS-GO 1% (w/w), CS-GO 2% (w/w) and CS-GO 3% (w/w) nanocomposites were able to increase the solubility of rotenone in water by 34.40%, 38.80% and 46.30%, respectively [77]**.**

8-(Jin & Xiaoheng et al. in 2021) Graphene oxide (GO)-based materials have demonstrated promising potential for adsorption and purification applications, due to its amphiphilic nature, GO offers the possibility of removing various kinds of contaminants, including heavy metal ions and organic pollutants from aqueous environments[78].

9-(Samhan & Sahar et al. in 2021) The graphite oxide GO-450 nm was prepared by oxidation-reduction reaction (Hummer's method) and studied the removal of bromophenol blue dyes (BPB), The structure was confirmed by SEM and FTIR spectroscopy. And studied the effect of several factors such as pH, adsorbent dose, contact time, initial dye concentration and temperature on the adsorption of BPB dye on GO particles was investigated. The adsorption isothermal (Langmuir

isotherm model, the Freundlich model). The kinetic data for adsorption process obeyed a pseudo-second-order rate equation. The thermodynamic parameters such as ΔG, ΔH and ΔS[79].

1.8 Aims of the study

1- Synthesis and characterization of three nano-graphene oxide composites

- Nano graphene oxide‑Chitosan (NGO-CS).

- Nano graphene oxide- Methionine (NGO-M).

- Nano graphene oxide-Cysteine (NGO-C).

2- Using (NGO-CS, NGO-M, NGO-C) composites as adsorbents for water treatment, to remove some organic pollutants from water, such as bromophenol blue dye (BPB), and finding the optimal conditions for adsorption for each composite.

3- Synthesis and characterization five membranes (NGO, CS, NGO-CS, NGO-M, NGO-C), find out their efficiency to separate the organic pollutants such as BPB dye and inorganic pollutants such as trace heavy metals (Ni^{2+}, Cd^{2+}, Co^{2+}, Cu^{2+} and Pb^{2+} ions) from water.
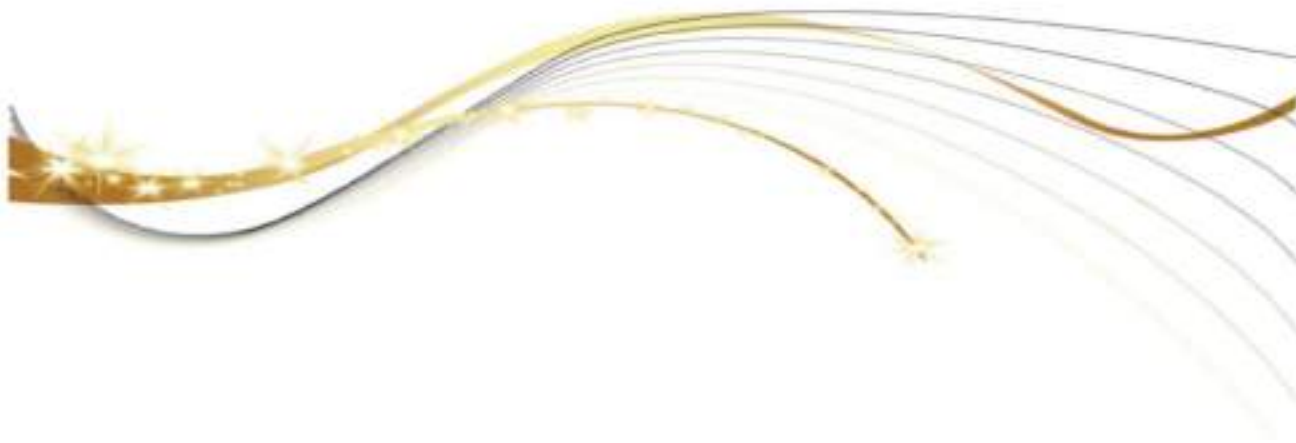
Chapter two

EXPERIMENTAL

2.1 Instruments and Chemicals

The instruments used in the present study and their models, companies and origin are listed in Table (2-1), the chemicals listed in Table (2-2) respectively.

Table (2-1): Instruments used in study and their models, companies, origin and laboratory location.

Ser	Devise	Company	Origin	Laboratory
1	Flame Atomic Absorption Spectroscopy, Al -1200	Aurora	Canada	Misan University/ College of Science/ Chemistry Dep.
2	UV-Vis. Spectrophotometer, UV-1800	Shimadzu	Japan	Misan University/ College of Science/ Chemistry Dep.
3	FT-IR Spectrophotometer, FT-IR-8400S	Shimadzu	Japan	BPC Analysis Center Yarmouk/ Baghdad
4	X-Ray Diffraction (XRD), PW1730	Philips	Holland	Tehran / Iran
5	Zeta Potential, SZ-100	Horiba scientific	Jabanese	Tehran / Iran
6	Zeta potential analyzer, Zeta Plus	Brookhaven	USA	The Science & Technology Ministry/ Water & Environment Dep.
7	Probe Ultrasonicator, FSFJY92-IIN	Sino Sonics	China	Misan University/ College of Science/ Biology Dep.
8	Field Emission Scanning Electronic Microscope (FESEM), inspect f 50	Fei	Holland	Al-Khora Company Yarmouk/ Baghdad
9	Ultrasonic Bath Sonicator, WHC-A10H	Daihan Scientific	China	Misan University/ College of Science/ Chemistry Dep.
10	Vacuum Pump	Value	China	Misan University/ College of Science/ Chemistry Dep.
11	pH-meter, pH 7110	Inolab	Germany	Misan University/ College of Science/ Chemistry Dep.

Table (2-2): Chemicals used and their chemicals formula, purities, companies and origin

Ser.	Chemicals	Chemical Formula	Company	Origin
1	Sulphuric acid	H_2SO_4	ChemLab.	UK
2	Potassium permanganate	$KMnO_4$	GCC	UK
3	Graphite	C	CDH	India
4	Sodium nitrate	$NaNO_3$	Thomas beaker	India
5	Hydrogen peroxide	H_2O_2	Panreac applab	Spain
6	Chitosan polymer	$(C_6H_{11}NO_4)_n$	Alpha chemical	India
7	Cellulose nitrate membrane filters	$(C_6H_{11}N_2O_{10})_n$	Fiscger	India
8	Sodium chloride	NaCl	Thomas beaker	India
9	(L-) Methionine	$C_5H_8N2O_2S$	S. d. line. CHEM Limited	India
10	(L-) Cysteine	$C_6H_{12}N_2O_4S_2$	S. d. line. CHEM Limited	India
11	Dimethyl Formamide (DMF)	$HCON(CH_3)_2$	Thomas beaker	India
12	Bromo phenol blue indicator	$C_{19}H_{10}O_5S\ Br_4$	CDH	India
13	Hydrochloric acid	HCl	Applichem	USA
14	Sodium hydroxide	NaOH	ChemLab.	UK
15	Acetic acid	CH_3COOH	ChemLab.	UK
16	Copper sulphate pentahydrate	$CuSO_4.5H_2O$	Pubchem	China
17	Cadmium sulphate octahydrate	$CdSO_4.8H_2O$	Pubchem	China
18	Lead nitrate	$Pb\ (NO_3)_2$	Merck	UK
19	Cobalt sulphate heptahydrate	$CoSO_4.7H_2O$	Merck	UK
20	Nickel sulphate hexahydrate	$NiSO_4.6H_2O$	Merck	UK

2.2 Synthesis of Nano Graphene Oxide (NGO)

Nano graphene oxide synthesized by modified Hummer's method [80][51] Added 0.60 g graphite and 0.50 g sodium nitrate, dissolved in 23 mL cooled (0 ºC) concentrated sulphuric acid in beaker onto ice bath, stirring for 15 min. Added 3.0 g potassium permanganate gradually to the suspension (black color), continuous stirring to keep the reaction temperature below 20 ºC onto ice bath for 30 min. The reaction beaker placed in stirring water bath at 35 ºC for 2 hrs. (the suspension changed to dark brown). Added 50 ml deionized water gradually (by dropper) into the suspension over a hot plate magnetic stirrer, the temperature kept below 98 ºC, for 15 min, added 100 mL of warm deionized water, added 10 mL of hydrogen peroxide 30% gradually (by dropper) for 15 min. The suspension separated by centrifuge (4000 rpm for 5 min), the precipitate washed with warm hydrochloric acid (5% v/v) to remove sulphate ions (test by $BaCl_2$), the precipitate washed with deionized water until the pH of washing solution became 7.0. The product (graphene oxide) dried in oven at 60 ºC for 1 hr. Added 0.5 g of Graphene oxide to 50 mL of N, N-di methyl formamide and sonicated by Probe ultrasonicator for 30 min, the suspension separated by centrifuge (4000 rpm for 10 min) the separated residue dried in oven at 60 ºC for 1 hr. as shown in Fig(2-1) and Fig(2-2).

Fig. (2-1): (A) Oxidation of graphite in stirring water bath, (B) Synthesis of nano graphene oxide by Probe ultrasonicator
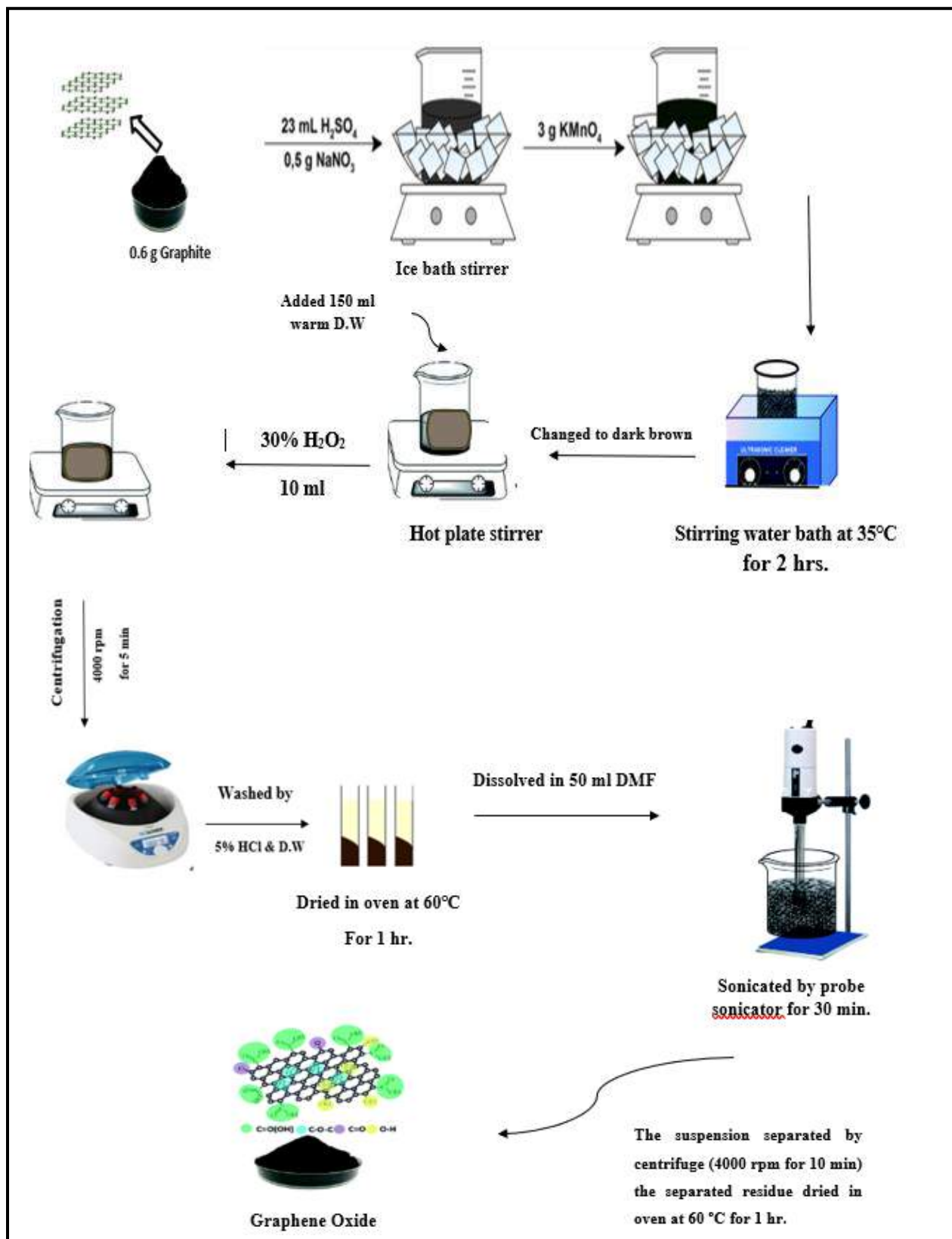
Fig.(2-2):The flow chart of the synthesis nano graphene oxide

2.3 Synthesis Composites From Nano Graphene Oxide

2.3.1 Synthesis of Nano Graphene Oxide-Chitosan Biopolymer Hydrogels Composite (NGO-CS) [81]

Dissolved 1.0 g of chitosan polymer in 50 mL of (1%) v/v acetic acid[60,82] stirred until became homogeneous solution. Nano graphene oxide 5 mg added to a few distilled water, sonicated by bath sonicator for 2 min. for dispersion, the NGO suspension gradually added to the chitosan solution, stirred for 10 min. The mixture was sonicated for 30 min. to remove bubbles. The NGO-CS solution was injected by syringe needle (60 drops/min), 10 cm above sodium hydroxide solution 500 ml (0.5 mol/L) ,the resulting NGO-CS microspheres kept stirred slowly in the solution for 4 hrs., filtered by Buechner funnel with aluminum foil sheet, washed with (D.W) until the pH became neutral, dried for 48 hrs. at room temperature, brown beads formed[83] as shown in Fig.(2-3) and Fig.(2-4)

| (A) | (B) | | (C) | (D) |
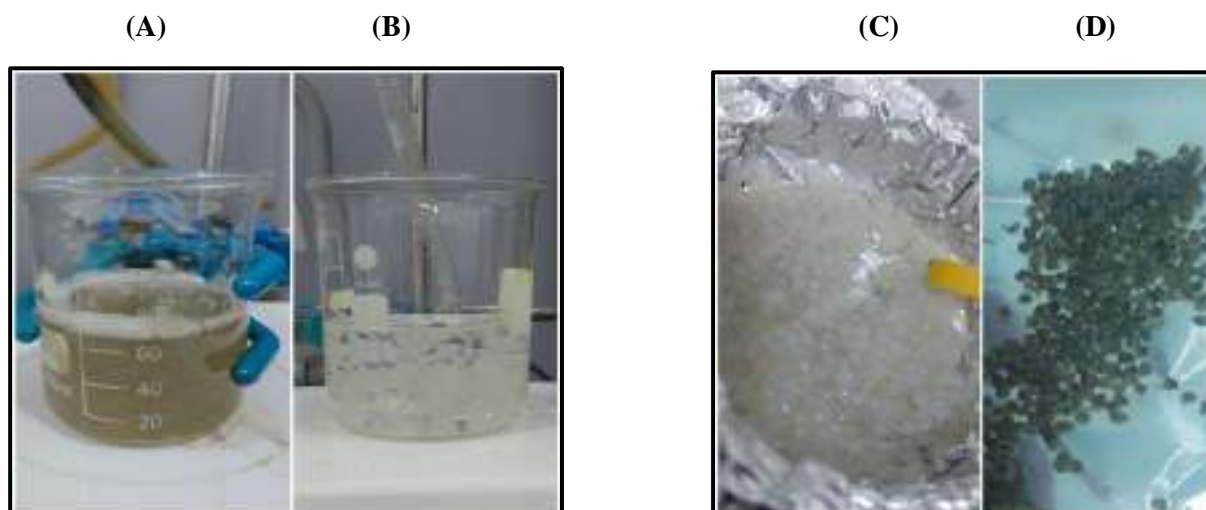
Fig. (2-3): Synthesis of NGO-CS composite, (A) Chitosan Polymer solution, (B) hydrogel
NGO-CS microspheres in NaOH solution, (C) hydrogel NGO-CS microspheres
on Buechner   funnel with aluminum foil sheet, (D) NGO-CS brown beads
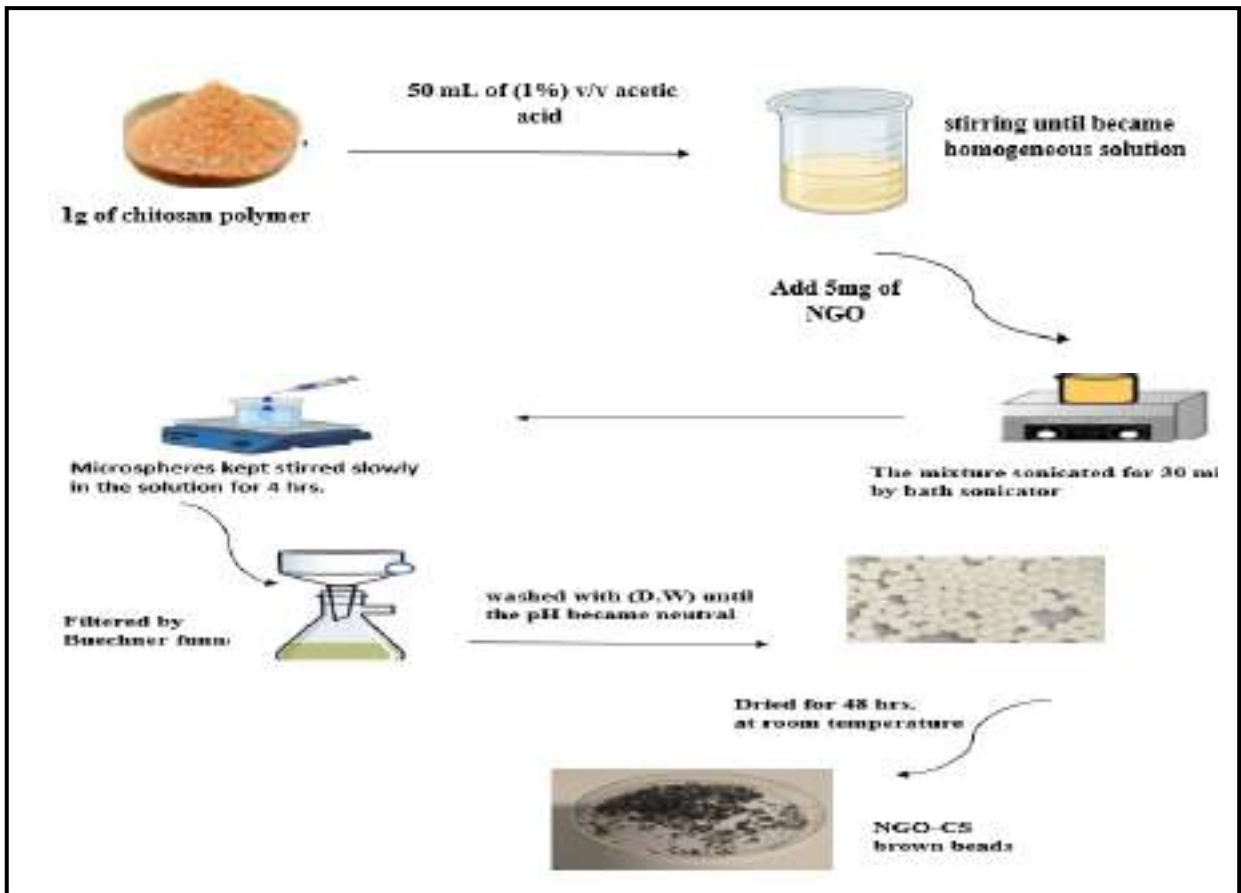
Fig.(2-4):The flow chart of the synthesis of (NGO-CS) composite
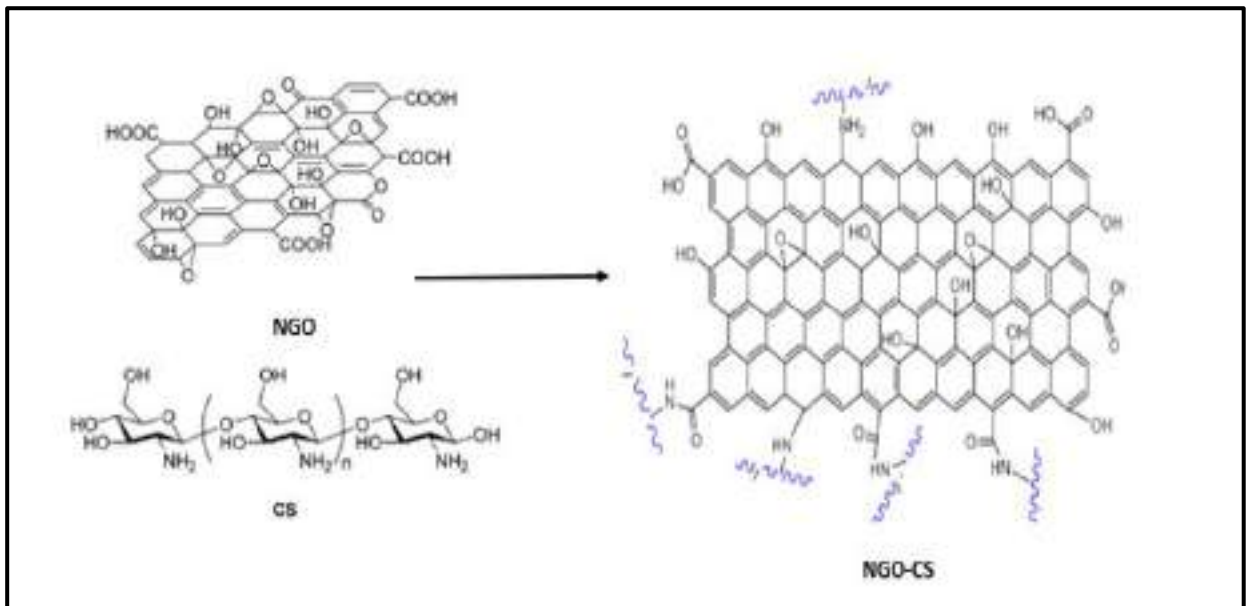
Fig.(2-5): Equation of composite (NGO-CS) synthesis

In addition, NGO-CS film prepared by dissolved 1.0 g of chitosan polymer in 50 mL of (1%) v/v acetic acid[82], stirred until became homogeneous solution. Nano graphene oxide 5 mg added to a few distilled water, sonicated by bath sonicator for 2 min. for dispersion, the NGO suspension gradually added to the chitosan solution, stirred for 10 min. the mixture was sonicated for 30 min. to remove bubbles, Chitosan-graphene oxide solutions subsequently poured into a plastic petri dish, dried at room temperature for 48 hrs. to form film [81], as show in Fig. (2-6).

Fig. (2-6): (A) NGO-CS solution poured into a plastic Petri dish (B) the NGO-CS film after dry

2.3.2 Synthesis of NGO-M Composite

In a beaker 0.5 g of NGO added to 50 ml DMF, ultra-sonicated for 30 min.,1.5 g of Methionine added, ultra-sonicated for 30 min. In a microwave, the suspension was heated for 30 min. (140 W), the suspension washed with 200 mL anhydrous ethanol several times, followed by distilled water and ethanol, until black powder formed NGO-M, dried at 70°C for 6 hrs. [83][84], as shown in Fig. (2-7).
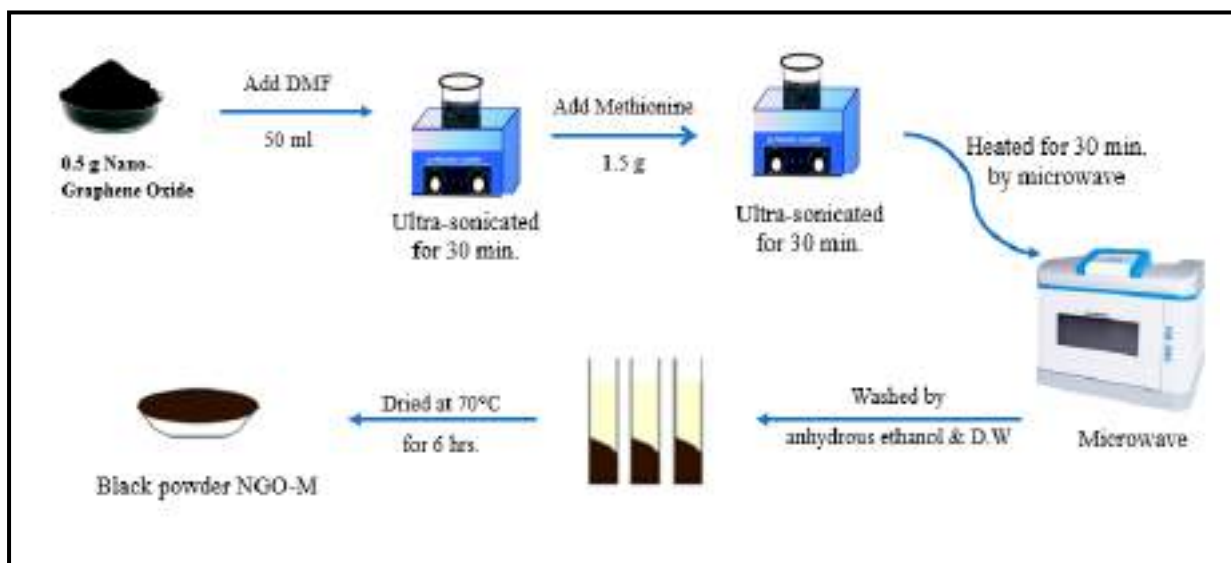
Fig.(2-7): The flow chart of the synthesis of NGO-M composite
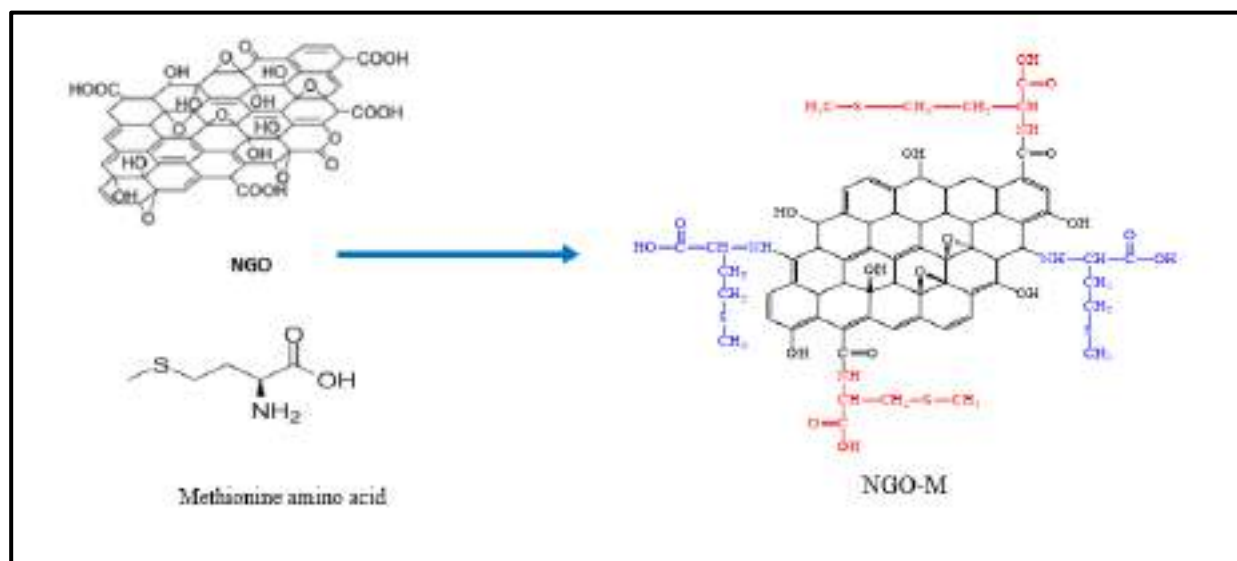
Fig.(2-8): Equation of composite (NGO-M) synthesis

2.3.3 Synthesis of NGO-C Composite

In a beaker 0.5 g of NGO added to 50 ml DMF, ultra-sonicated for 30 min., 1.21 g of cysteine added, ultra-sonicated for 30 min. In a microwave, the suspension was heated for 30 min. (140 W), the suspension washed with 200 mL anhydrous ethanol several times, followed by distilled water and ethanol, until black powder formed NGO-M, dried at 70°C for 6 hrs. [84, 85],
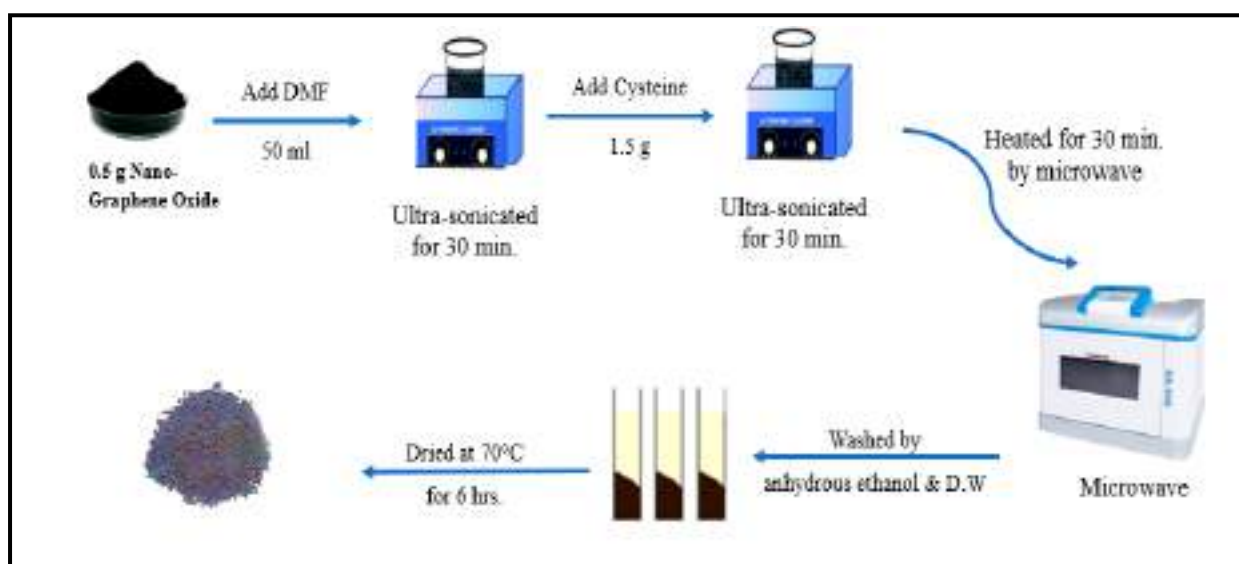
Fig.(2-9): The flow chart of the synthesis of NGO-C composite
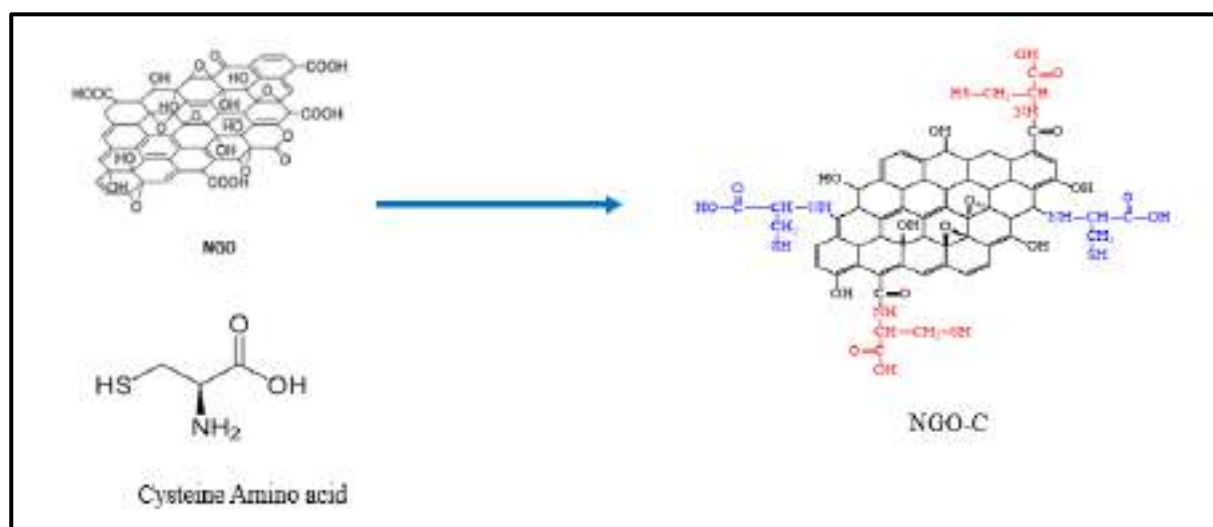
Fig.(2-10): Equation of composite (NGO-M) synthesis

2.4 Preparation of Solutions

2.4.1 Stock Solution of Bromophenol Blue Indictor (1000 mg.L^{-1})

A stock solution of 3′,3″,5′,5″tetrabromophenolsulfonphthalein (BPB) (M_{wt} = 669.98 g/mol) was prepared by dissolving 100 mg of the BPB dye in deionized water into beaker, transferred quantitatively to volumetric flask (100 mL), filled up to the mark with deionized water. The working standard solutions were prepared by serial dilution of stock solution.

2.4.2 Stock Solution of Nickel (II) (1000 mg.L^{-1})

Nickel sulphate $NiSO_4.6H_2O$ (0.4476 gm) dissolved in a small volume of (5% HCl) into beaker (50 ml), transferred quantitatively to volumetric flask (100 mL) filled up to the mark with deionized water. The working standard solutions were prepared by serial dilution of the stock solution.

2.4.3 Stock Solution of Copper (II) (1000 mg.L^{-1})

Copper sulphate $CuSO_4.5H_2O$ (0.3927 gm) dissolved in a small volume of (5% HCl) into beaker (50 ml), transferred quantitatively to volumetric flask (100 mL) filled up to the mark with deionized water. The working standard solutions were prepared by serial dilution of the stock solution.

2.4.4 Stock Solution of Cadmium (II) (1000 mg.L^{-1})

Cadmium sulphate $CdSO_4.8/3H_2O$ (0.2281 gm) dissolved in a small volume of (5% HCl) into beaker (50 ml), transferred quantitatively to volumetric flask (100 mL) filled up to the top mark with deionized water. The working standard solutions were prepared by serial dilution of the stock solution.

2.4.5 Stock Solution of Lead (II) (1000 mg.L^{-1})

Lead nitrate $Pb (NO_3)_2$ (0.1598 gm) dissolved in a small volume of (5% HCl) into beaker (50 ml), transferred quantitatively to volumetric flask (100 mL) filled up to the mark with deionized water. The working standard solutions were prepared by serial dilution of the stock solution.

2.4.6 Stock Solution of Cobalt (II) (1000 mg.L^{-1})

Cobalt sulphate $CoSO_4.7H_2O$ (0.4769 g) dissolved in a small volume of (5% HCl) into beaker, transferred quantitatively to volumetric flask (100 mL) and filled up to the top mark with deionized water. The working standard solutions were prepared by serial dilution of stock solution.

2.5 Optimum Conditions for BPB dye Adsorption

2.5.1 Effect of pH [38, 31]

Beaker contains 20 ml of BPB dye (10 mg.L^{-1}), the pH of solution was set by using (0.1M HCl) and (0.1M NaOH) at pH values (1,2,3,4,5,6,7,8,9,10,11 and

12) by using pH-meter. The absorbance measured by using UV-Vis. spectrophotometer at λ_{max}=437 nm or λ_{max}=590.5 nm. according to the pH of the solutions, added 10 mg of (NGO-CS) composite to each solution, left in an incubator shaker for 60 min. at room temperature to oscillation. After adsorption process, the adsorbent remained at the bottom of the conical flask, separated by centrifuge (4000 rpm 10 min.), the absorbance of the residual dye solution measured at the same wavelengths. The pH effect on the NGO-M and NGO-C composites studied at the same method at pH range (0.5,1, 1.5,2,2.5,3 and 3.5).
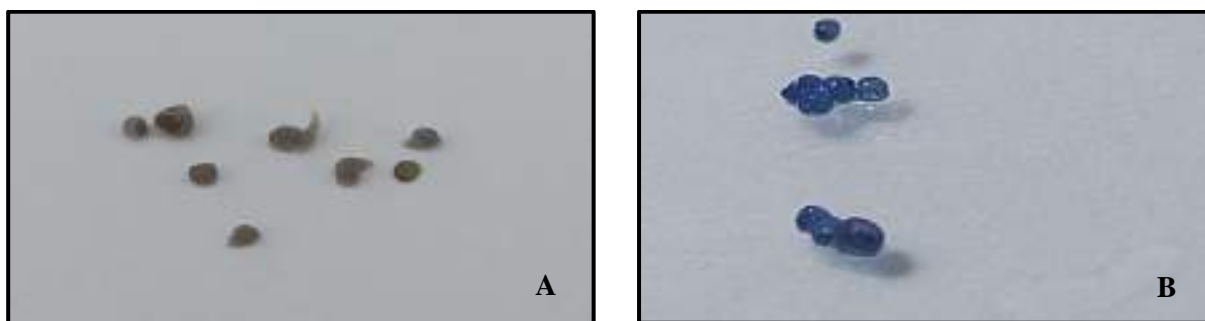
Fig. (2-11): Show NGO-CS composite beads (A) before (B) after adsorption BPB dye

2.5.2 Effect of Adsorbent Dosage [38, 31]

In several conical flasks included 20 mL of BPB dye (10 mg.L^{-1}) at pH =2 the absorbance of the solutions measured at λ_{max}= 437 nm. different amount of the NGO-CS composite (2,4,6,8,10,12,14 mg) added respectively, left in an incubator shaker for (60 min) at room temperature, after adsorption process, the adsorbent remained at the bottom of the conical flask, separated from the adsorptive by centrifugation (4000 rpm 10 min.), the absorbance of the residual dye solution measured at the same wavelength. The dosages effect on the NGO-M composite at pH =3 and NGO-C composite at pH =1 was studied at the same method.

2.5.3 Effect of Contact Time and Study Kinetic of Adsorption [38,31]

Three conical flasks used each one containing 20 mL aqueous solution of BPB dye (10 mg.L^{-1}), the first solution set at pH = 2 , the second solution at pH=3 and the third at pH=1, the absorbance measured for each solution by using UV-Vis. spectrophotometer at λ_{max} = 437 nm, added 2.0 mg of each NGO-CS, NGO-M and NGO-C composite to the three conical flasks respectively, kept in incubator shaker for (15, 30, 45, 60, 75 , 90 and 105 min.) at room temperature, after adsorption process, the adsorbent remained at the bottom of the conical flask, separated from the adsorptive by centrifugation (4000 rpm 10min.), the absorbance of the each residual dye solution measured at the same wavelengths. In order to find out the best adsorption kinetic description, different models were applied on the experimental data.

2.5.4 Effect of Temperature[38, 45]

The effect of the temperature on the adsorption process, 20 mL aqueous solution of BPB dye (10 mg.L^{-1}) on each NGO-CS, NGO-M and NGO-C composite was studied at (15,25,35,45,55,65 and 75 °C) on the optimum conditions, pH, composite weight and contact time for each composite.

2.5.5 Effect of Initial Concentration of BPB dye[38, 45]

The effect of the initial concentration of the BPB dye on the adsorption capacity of the NGO-CS composite was studied by preparing series concentrations of the BPB dye (5, 10, 15, 20, 25, 30 mg.L^{-1}) at the optimum conditions: pH =2,

weight of 2 mg of composite, contact time =75 min. and temperature = 45℃. The adsorption capacity was calculated for each concentration and the optimum initial concentration was determined. The same steps was repeated for the NGO-M and NGO-C composites at the optimum conditions for each composite.

2.5.6 Effect of Ionic Strength[38 ,45]

The effect of ionic strength on the adsorption capacity for the NGO-CS, NGO-M and NGO-C composites studied by preparing several solutions of BPB dye 20 ml (10 mg.L^{-1}), contains different concentrations of NaCl (0%, 5% 10%, 15%, 20%, 25%, and 30%) respectively, at the optimum conditions: pH, weight of composite, contact time, temperature and concentration of dye, for each composite.

2.6 Adsorption Isotherm [38, 45]

Adsorption isotherms were studied of NGO-CS composite by preparing the following concentrations (5, 10, 15 and 20 mg.L^{-1}) of the BPB dye at different temperatures (15,25,35 and 45℃) respectively, 20 ml of BPB dye, at the optimum conditions: pH =2, weight = 2 mg of composite and contact time =75 min., after the adsorption process for each solution. The Freundlich and Langmuir isotherm models were applied to the experimental data to evaluate which the best description adsorption isotherm. The same steps was repeated for the NGO-M and NGO-C composites at the concentrations (5, 10, 15, 20 ,25 and 30 mg.L^{-1}) of the BPB dye, temperature (15,25,35,45 and 55℃) at the optimum contact time and pH for each composite.

2.7 Desorption study[39]

The desorption of the NGO-CS composite was studied, after completing the adsorption process for BPB dye 20 mL (10 mg.L^{-1}), at optimum conditions: pH =2, weight of 2 mg of composite, contact time =75 min and temperature = 45°C, that were previously determined. The NGO-CS composite beads filtered by Buechner funnel with aluminum foil sheet, the beads dried at room temprature, weighted, poured to 5 ml of acetone [39], left at room temperature for 24 hrs., the absorbance of the filtered acetone was measured at λ_{max}=322 nm, the percentage of desorption calculated by Equation(1.8).

2.8 Membranes Preparation

2.8.1 NGO Membrane

NGO membrane (100 mg.L^{-1}) was prepared by adding 5 mg of NGO powder to 50 ml deionized water, sonicated by bath sonicator (30 °C for 2 min.) for dispersion, filtered by using a vacuum pump (-15 psi) with cellulose nitrate membrane filter as a substrate (pores 0.22 μm), as shown in Fig. (2-12) (A).

2.8.2 CS Membrane

CS membrane (100 mg.L^{-1}) prepared by dissolve 5 mg of chitosan polymer in 50 ml of 1% acetic acid[82],filtered by vacuum filtration (-15 psi) with cellulose nitrate membrane filter as a substrate (pores 0.22 μm), as shown in Fig. (2-12) (B).

2.8.3 NGO-CS Membrane

NGO-CS membrane (100 mg.L^{-1}) prepared by dissolve 2.5 mg of chitosan polymer in 50 ml of 1% acetic acid [82], 2.5 mg of nano graphene oxide added, sonicated by ultrasonic bath (30 °C for 2 min.), filtered by vacuum filtration with cellulose nitrate membrane filter as a substrate (pores 0.22 μm), as shown in Fig. (2-12) (C).

2.8.4 NGO-M Membrane

NGO-M membrane (100 mg.L^{-1}) was prepared by adding 5 mg of composite to 50 ml of deionized water, sonicated by ultrasonic bath (30 °C for 2 min.) for dispersion, filtered by vacuum filtration (-15 psi) with cellulose nitrate membrane filter as a substrate with pores 0.22 μm), as shown in Fig. (2-12) (D).

2.8.5 NGO-C Membrane

NGO-C membrane (100 mg.L^{-1}) was prepared by adding 5 mg of composite to 50 ml of deionized water, sonicated by ultrasonic bath (30 °C for 2 min.) for dispersion, filtered by vacuum filtration (-15 psi) with cellulose nitrate membrane filter as a substrate (pores 0.22 μm), as shown in Fig. (2-12) (E).
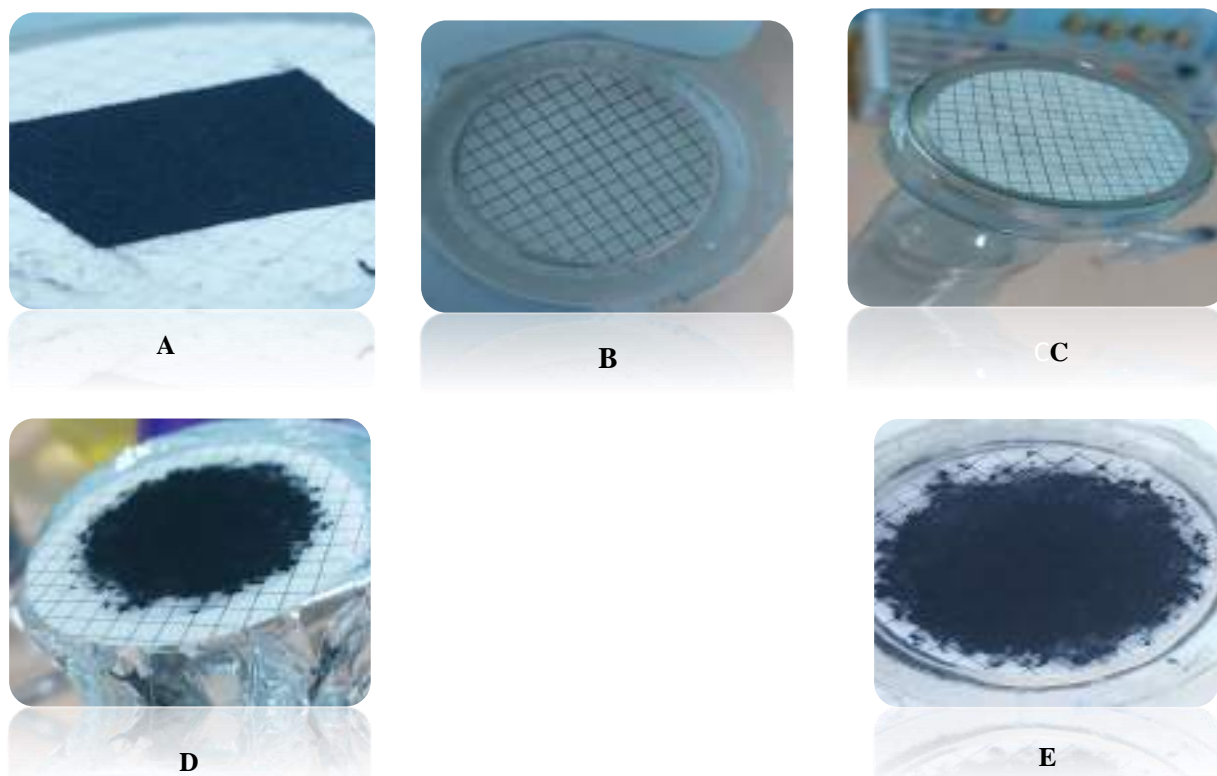
Fig. (2-12): (A) NGO membrane (B) CS membrane, (C) NGO-CS membrane, (D)NGO-M membrane, (E) NGO-C membrane on substrate (cellulose nitrate)

2.9 Applications of Membranes

2.9.1 Separation of BPB Dye by (NGO, NGO-CS, NGO-M, NGO-C and CS) Membranes

Prepared 10 mg.L^{-1} of BPB dye in 100 mL as standard solution, absorbance at λ_{max}= 590.5 nm measured by using UV-Vis Spectrophotometer. Added 10 ml of BPB dye solution to each membrane (NGO, CS, NGO-CS NGO-M and NGO-C) filtered by using the vacuum measured at the same wavelength.

(A)

(B)

(C)
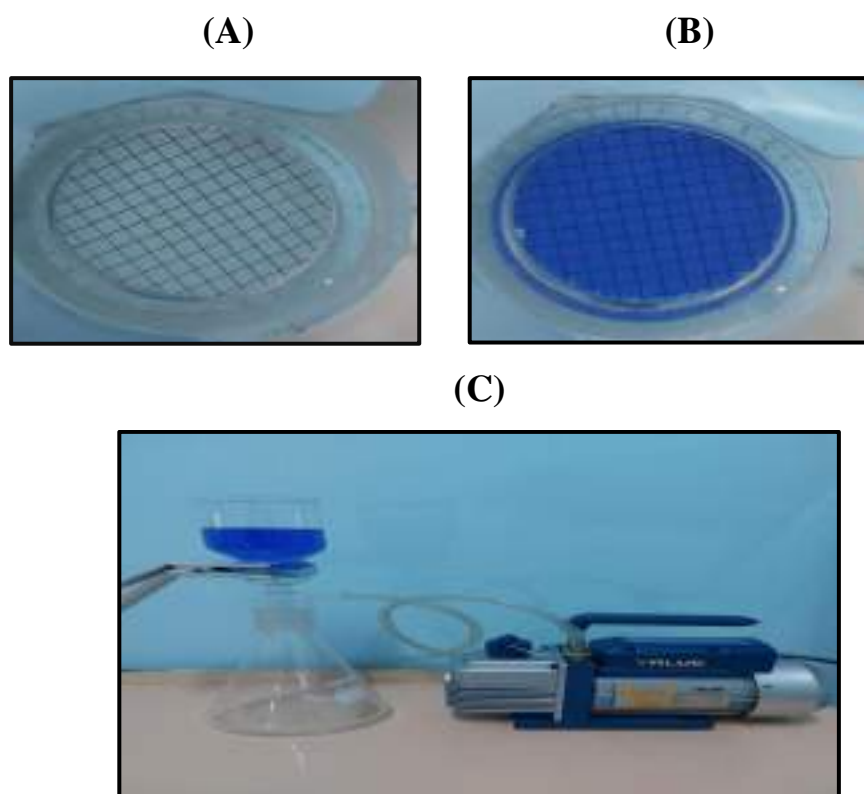
Fig. (2-13): CS membrane (A) before, (B) after separation of BPB dye

(C) Vacuum filtration pump

2.9.2 Separation of Ni^{2+}, Cd^{2+}, Co^{2+}, Cu^{2+} and Pb^{2+} Ions by (NGO, NGO-CS, NGO-M, NGO-C and CS) Membranes

Standard solutions 20 ml (10 mg.L^{-1}) of each element (Ni^{2+}, Cd^{2+}, Co^{2+}, Cu^{2+} and Pb^{2+}) prepared, added to each membrane (NGO, CS, NGO-CS NGO-M and NGO-C) filtered by using the vacuum filtration (-15 psi). The concentration of each metal filtrate ions measured by flame atomic absorption spectroscopy, after calibration the device according to the conditions suitable each metal ions shown in Table (2-3).

47

Table (2-3): The analytical conditions for determination of metal ions by FAA

Ser.	Ion	(λ_{max}) nm	Detection limit $(mg.L^{-1})$	Working rang $(mg.L^{-1})$	Silt width (nm)	Flame
1	Co^{2+}	240.7	0.015	2-10	0.2	Air / Acetylene (99%)
2	Ni^{2+}	232.0	0.01	2-10	0.2	Air / Acetylene (99%)
3	Cu^{2+}	324.7	0.004	2-10	0.2	Air / Acetylene (99%)
4	Cd^{2+}	288.8	0.0022	2-10	0.2	Air / Acetylene (99%)
5	Pb^{2+}	217.0	0.014	2-10	0.2	Air / Acetylene (99%)

Chapter three

RESULTS AND

DISCUSSION

3.1 Spectral Characterization of NGO, NGO-CS, NGO-M and NGO-C composites
3.1.1 Fourier Transform Infrared Spectroscopy (FT-IR)

The FT-IR spectrum of nano graphene oxide (NGO) as shown in Fig. (3-1) broad band observed at 3000-3700 cm^{-1} represents the stretching vibration of-OH in carboxylic and alcohol groups[51], while the band at 3124.68 cm^{-1} refer to aromatic C-H stretch of NGO. Peaks appeared at 1712.79 cm^{-1} and 1678.07 cm^{-1} which can be assigned to vibration stretching C=O of carboxylic groups and C=C on the basal plan of NGO sheets respectively. The peaks appeared 1516.05 cm^{-1} refers to epoxy group C-O-C, as shown in Table (3-1).
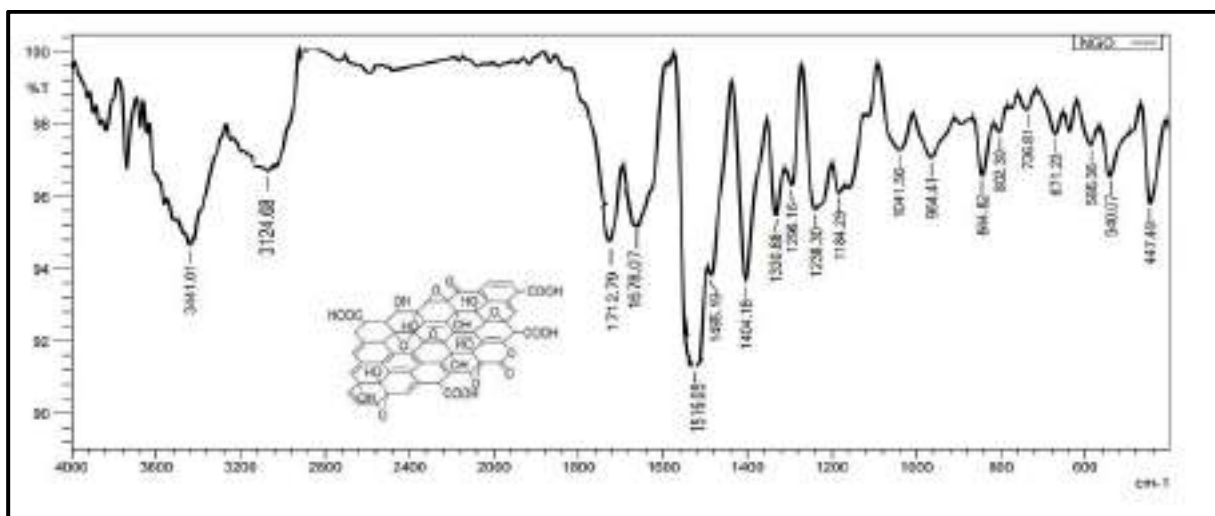
Fig. (3-1): FT-IR spectrum of NGO

Table (3-1): The major peak bands of NGO

Functional Group	Wavenumber (cm^{-1})	Functional Group	Wavenumber (cm-1)
O-H	3300-3700	C=C	1678.07
C-H (Ar)	3124.68	C-O-C	1516.05
C=O	1712.79		

The FT-IR spectrum of nano graphene oxide-chitosan composite (NGO-CS) as shown in Fig. (3-2), appeared peak refers to carbonyl of amides group(-NHC=O) at 1651.07 cm^{-1} (This observation can be related to reaction of carboxyl groups of NGO with amino groups of CS). Band at 1543.05 cm^{-1} could be attributed to C-N of NH II groups formed due to reaction between amino groups of CS and epoxy groups of NGO[77]. Peak observed at 2893.22 cm^{-1} attributed to C-H aliphatic of CS while, discernible peak at 3112.32 cm^{-1} can be ascribed to aromatic C-H stretch of NGO, the broad peak of OH groups at 3000-3700 cm^{-1} might be due to formation of hydrogen bonding during interaction of NGO and CS, as shown in Table (3-2).

Fig. (3-2): FT-IR spectrum of NGO-CS composite

Table (3-2): The major peak bands of NGO-CS composite

Functional Group	Wavenumber (cm^{-1})	Functional Group	Wavenumber (cm-1)
O-H, N-H	3000-3700	-NHCO	1651.07
C-H (Alph.)	2893.22	C=C	1633.12
C-H (Ar)	3112.32	C-N	1543.05

The FT-IR spectrum of nano graphene oxide-methionine composite (NGO-M) as show in Fig. (3-3), the broad band observed at 3000-3700 cm^{-1} can be attributed to the stretching vibration of O-H groups which is overlapped with N-H, while the band at 3055.15 cm^{-1} and 2915.47 cm^{-1} corresponds to the asymmetric stretching vibrations of aromatic C-H of NGO and aliphatic C-H for the amino acid (methionine), respectively. While the sharp peak at 1712.79 cm^{-1} corresponds to C=O of carboxylic groups. Tow peaks appeared at 1654.92 cm^{-1} and 1612.49 cm^{-1} the first peak represents C=O stretching vibrations of -NHCO results from the interaction of the COOH group of NGO with the -NH$_2$ of methionine, while the second peak represents C=C mode of the sp^2 carbon skeletal network of NGO. Appeared band at 1516.05 cm^{-1} could be attributed to C-N of NH II groups formed due to reaction between amino groups of methionine and epoxy groups of NGO, as shown in Table (3-3).
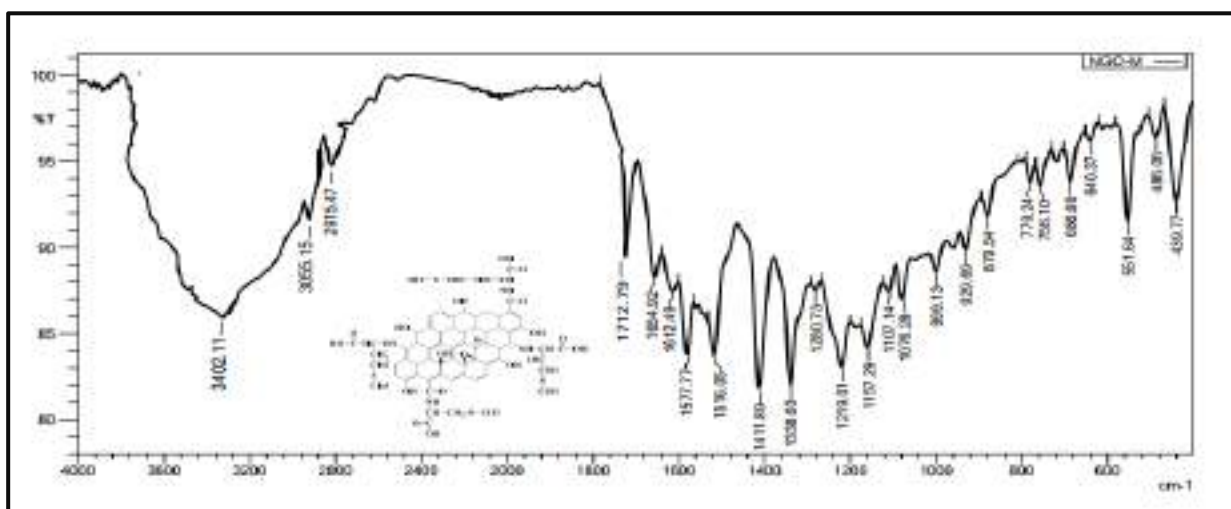
Fig. (3-3): FT-IR spectrum of NGO-M composite

Table (3-3): The major peak bands of NGO-M composite

Functional Group	Wavenumber (cm^{-1})	Functional Group	Wavenumber (cm-1)
O-H, N-H	3402.11	C-N	1577.77
C=O	1712.79	-NHCO	1654.92
C-H $_{(Alph.)}$, C-H $_{(Ar)}$	2915.47, 3055.15	C=C	1612.49

The FT-IR spectrum of nano graphene oxide-cysteine composite (NGO-C) as show in Fig. (3-4), The band observed at 3000-3700 cm^{-1} can be attributed to the stretching vibration of O-H groups which is overlapped with N-H stretching vibration, while the band at 3108.80 cm^{-1} and 2958.80 cm^{-1} corresponded to the asymmetric stretching vibrations of aromatic C-H of NGO and aliphatic C-H for amino acid (cysteine), respectively. While the sharp peak at 1711.22 cm^{-1} corresponds to C=O of carboxylic groups. absorption band appeared at 1647.21 cm^{-1} represents C=C stretching mode of the sp^2 carbon skeletal network of NGO, while the peak at 1550.77 represents to C-N of NH II groups formed due to reaction between amino groups of cysteine and epoxy group of NGO. The S-H group of cysteine has a sharp peak at 3201.83 cm^{-1}, as shown in Table (3-4).
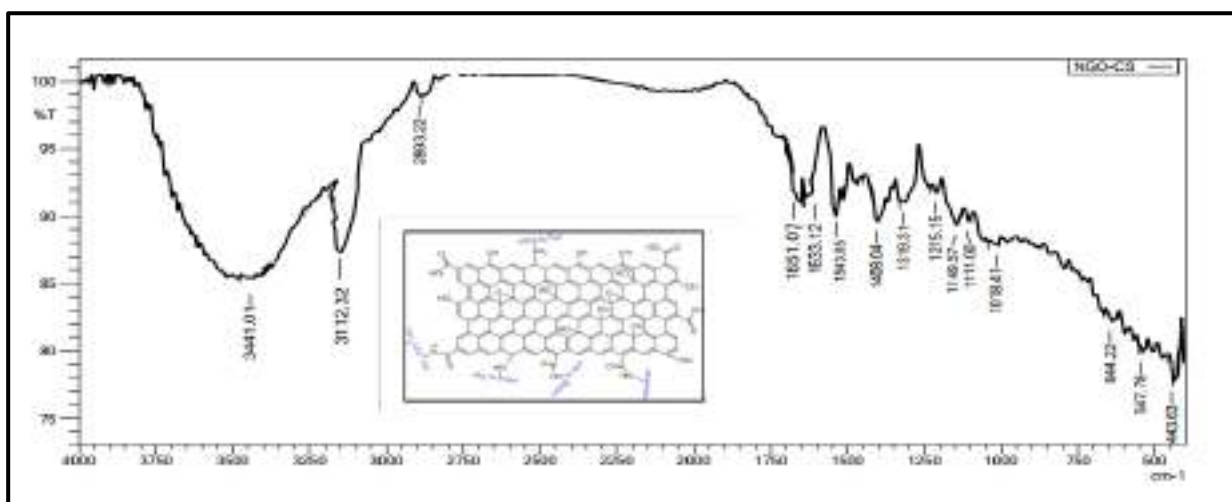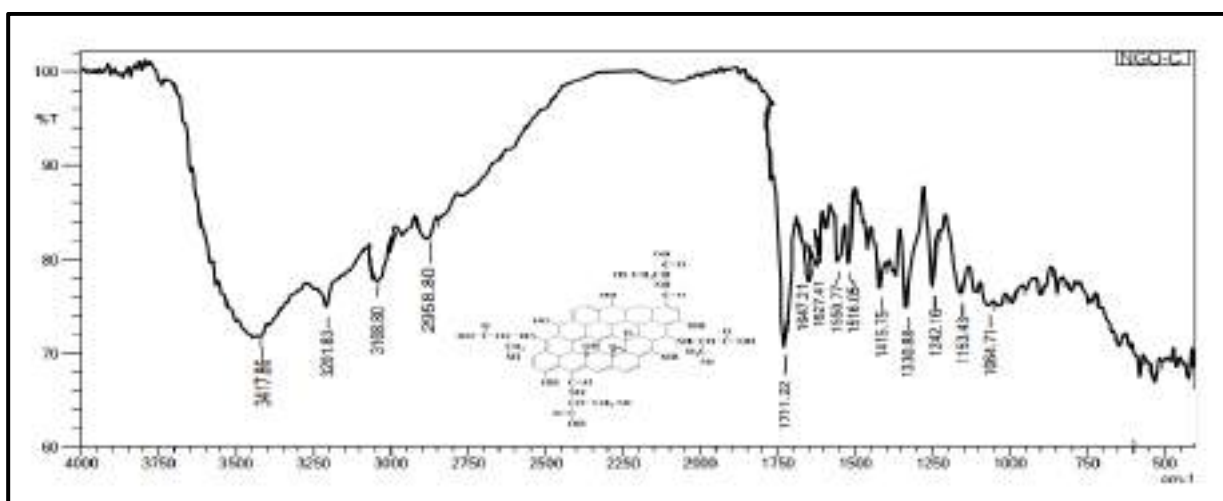

Fig. (3-4): FT-IR spectrum of NGO-C composite

Table (3-4): The major peak bands of NGO-C composite

Functional Group	Wavenumber (cm^{-1})	Functional Group	Wavenumber (cm-1)
O-H, N-H	3000-3700	C-N	1550.77
C=O	1711.22	C=C	1647.21
C-H $_{(Ar.)}$	3108.80	S-H	3201.83
C-H $_{(Alph.)}$	2958.80	-NHCO	1647

51

3.1.2 X-Ray Diffraction Spectroscopy (XRD)

The XRD spectrum measured in a range (5°-80°) of 2θ at 0.154 nm (copper source). The XRD peaks of NGO appeared at ($2\theta=11.1297°$) high intensity corresponding to interlayer spacing of (d=7.94350A°), ($2\theta= 42.4972°$) low intensity with interlayer spacing of (d=2.12546 A°) and ($2\theta= 9.1074°$) low intensity with interlayer spacing of (d=9.70232 A°), as shown in Fig. (3-5), The obtained results agree with the previous studies[86,87].

As for NGO-CS composite appeared at ($2\theta=20.3255°$) high intensity corresponding to interlayer spacing of (d=4.36929 A°) and ($2\theta= 35.4690°$) low intensity with interlayer spacing of (d=2.53092 A°) as shown in Fig. (3-6), the main peaks of NGO are disappeared by react with chitosan (CS) proved the presence pure phase of the synthesized NGO-CS composite so the results agree with the previous studies[87].

The NGO-M composite appeared at ($2\theta= 34.02°$) high intensity corresponding to interlayer spacing of (d=2.63 A°), ($2\theta = 38.80°$) medium intensity with interlayer spacing of (d=2.36 A°), ($2\theta= 48.86°$) medium intensity with interlayer spacing of (d=1.86 A°), ($2\theta= 54.73°$) low intensity with interlayer spacing of (d=1.67 A°) and ($2\theta= 55.35°$) low intensity with interlayer spacing of (d=1.56 A°) as shown in Fig. (3-7).

NGO-C composite appeared at ($2\theta= 34.05°$) medium intensity corresponding to interlayer spacing of (d=2.63 A°), ($2\theta= 38.80°$) low intensity with interlayer spacing of (d=2.36 A°), ($2\theta= 48.86°$) low intensity with interlayer spacing of (d=1.86 A°), ($2\theta= 54.73°$) low intensity with interlayer spacing of (d=1.67 A°), ($2\theta= 55.35°$) low intensity with interlayer spacing of (d=1.56 A°), ($2\theta= 62.15°$) low intensity with interlayer spacing of (d=1.49 A°) and ($2\theta= 65.24°$) low intensity with interlayer spacing of (d=1.43 A°) as shown in Fig. (3-8).

52

The peaks Appearance at several angles compared to the NGO, and this indicates that methionine and cysteine were successfully attached to the NGO surface during the modification[83].The particle size calculated by Debye-Scherrer Equation(3.1)[88].

$$D = \frac{K\lambda}{\beta \cos \theta} \ .... \ (3.1)$$

Where: D particle size, K Scherrer's constant equal 0.9, λ wave length of x-ray radiation source, β full width at half maximum (FWHM), θ X-ray diffraction angle in radians.

The average particles size of synthesized NGO, NGO-CS, NGO-M and NGO-C composites are (7.4, 10.8, 16.83 and 19.52 nm) respectively, as shown in Table (3-5)
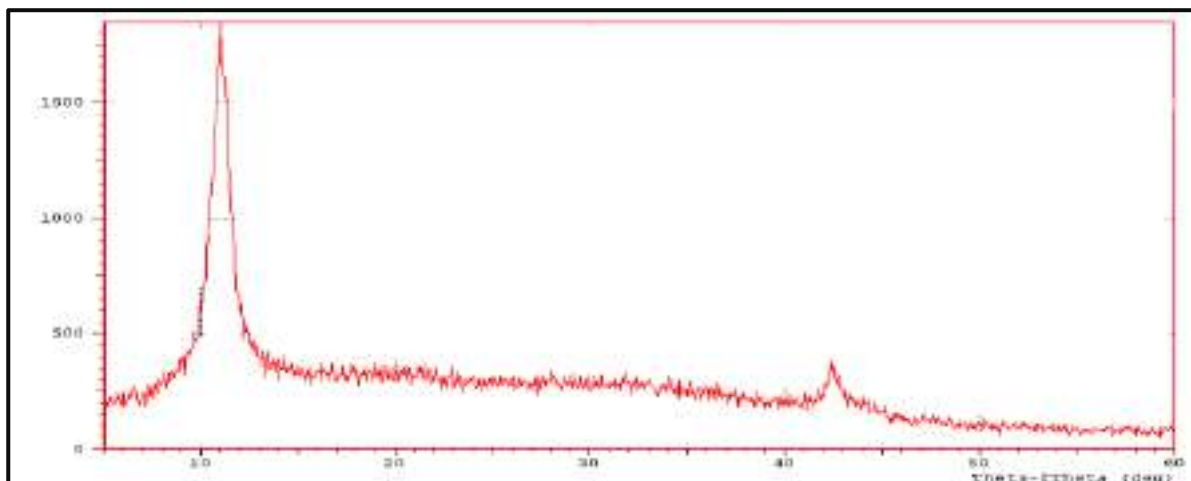
Fig. (3-5): XRD pattern of NGO
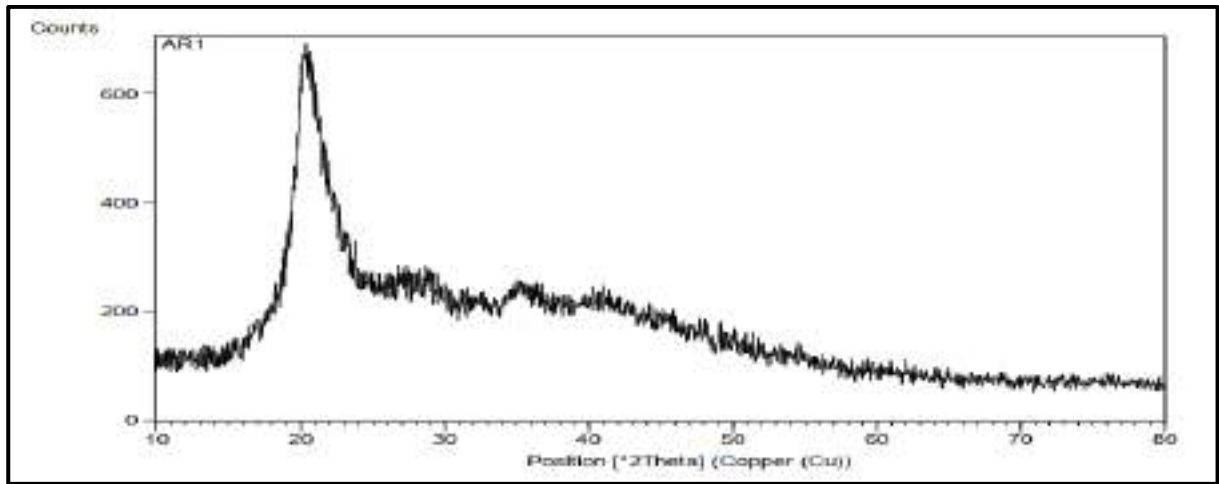
Fig. (3-6): XRD pattern of NGO-CS composite
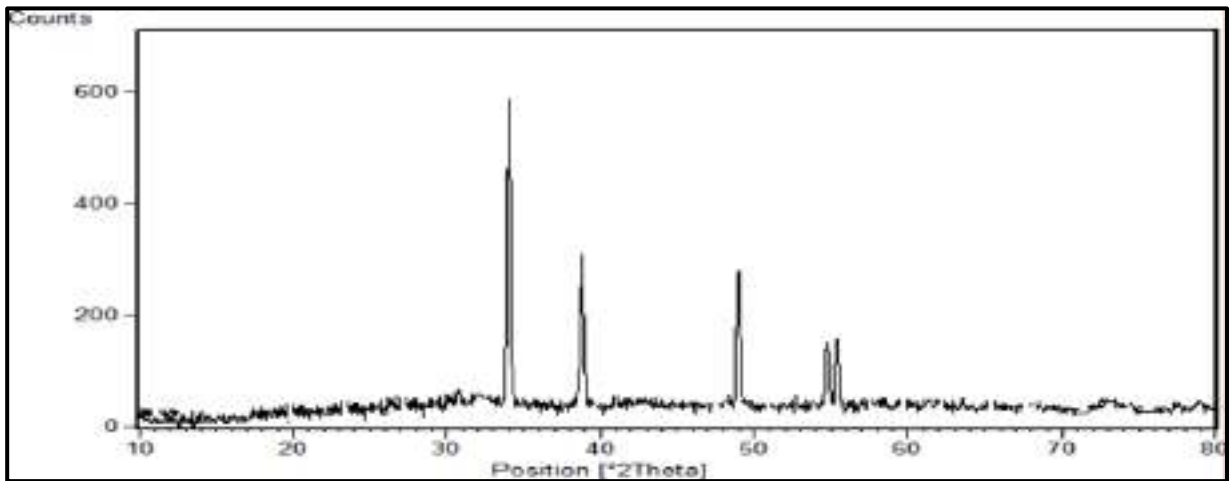
Fig. (3-7): XRD pattern of NGO-M composite
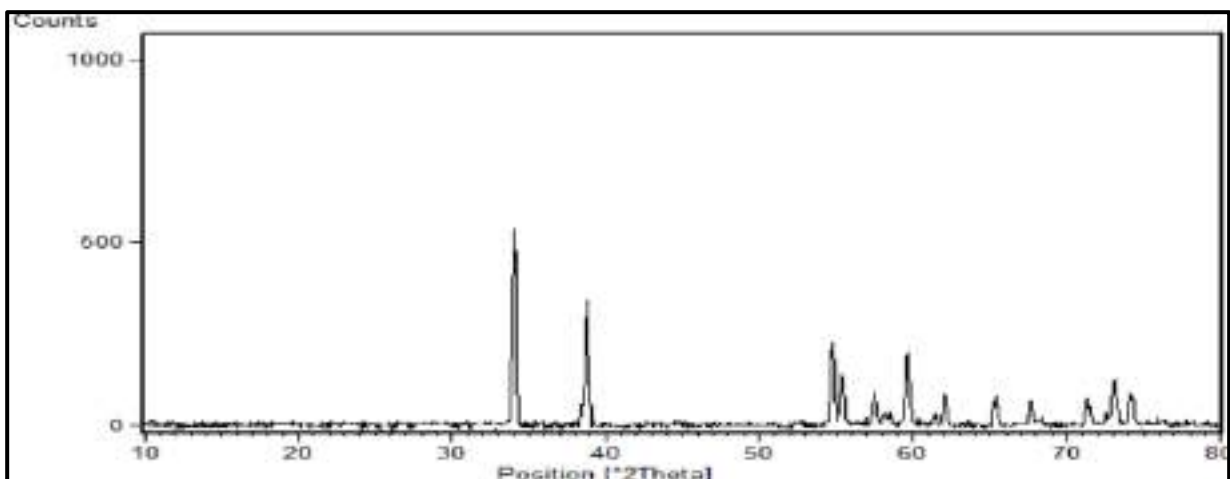
Fig. (3-8): XRD pattern of NGO-C composite

Table (3-5): Values of 2θ and d-spacing of NGO, NGO-CS, NGO-M, NGO-C

Compound	particles size (nm)	2θ (degree)	d-spacing (A⁰)
NGO	7.4	11.1297	7.94350
		42.4972	2.12546
		9.1074	9.70232
NGO-CS	10.8	20.3255	4.36929
		35.4690	2.53092
NGO-M	16.83	34.02	2.63
		38.80	2.63
		48.86	1.86
		49.51	1.83
		54.73	1.67
		55.35	1.65
NGO-C	19.52	34.05	2.63
		38.80	2.32
		54.72	1.67
		55.35	1.65
		58.43	1.57
		62.15	1.49
		65.24	1.43

3.1.3 Field Emission Scanning Electron Microscopy Analysis (FESEM)

The FESEM used to study the surface morphology of NGO, CS membranes, as well as NGO-CS, NGO-M and NGO-C composites membranes, where the corrugation shape is observed of nano sheets. The NGO membrane contain a high porosity[69], pores size (52.31-613.2) nm at different scales, as shown in Fig.(3-9).
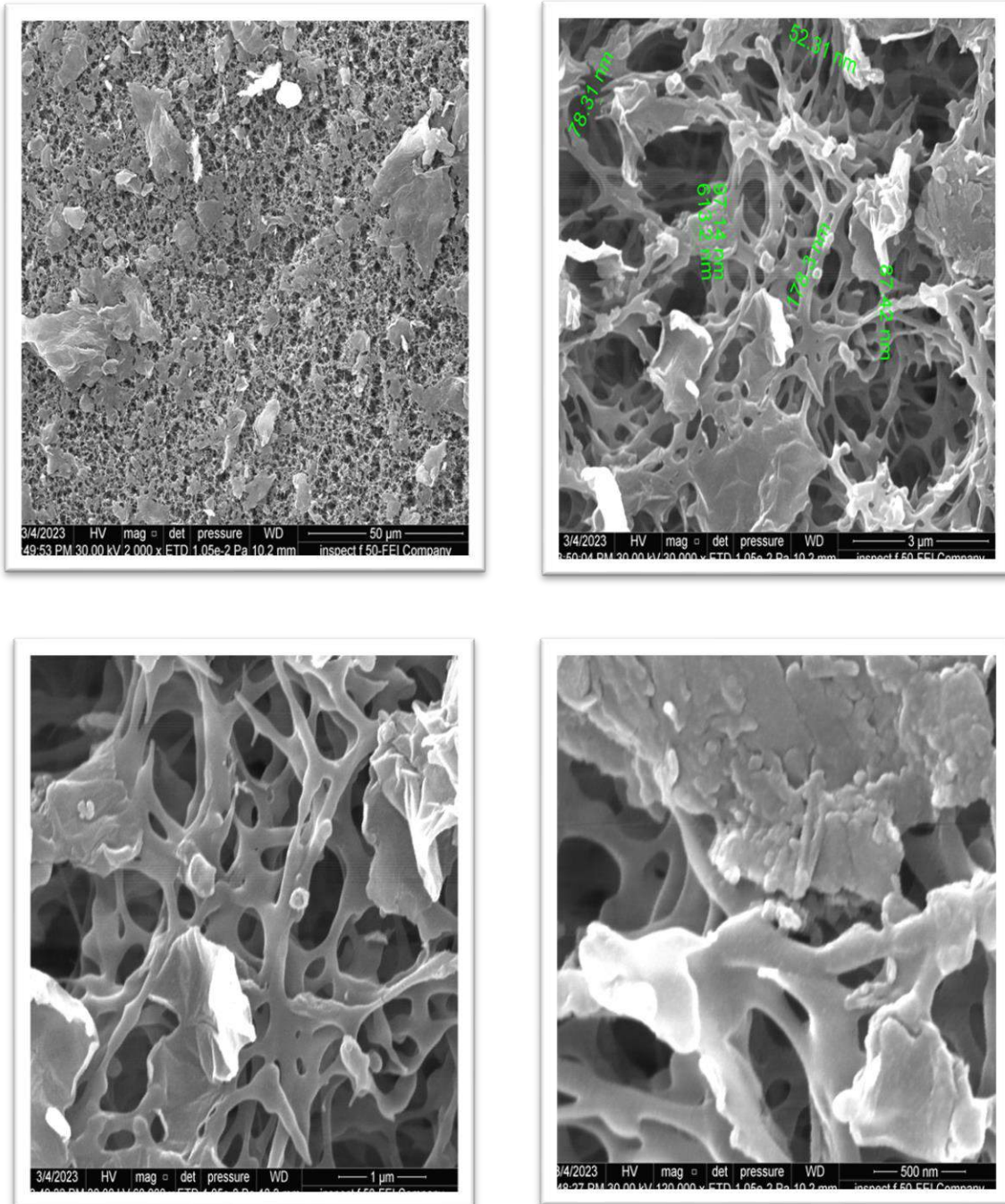
Fig. (3-9): FESEM images of NGO membrane at (50μm, 3μm, 1μm and 500 nm) scales
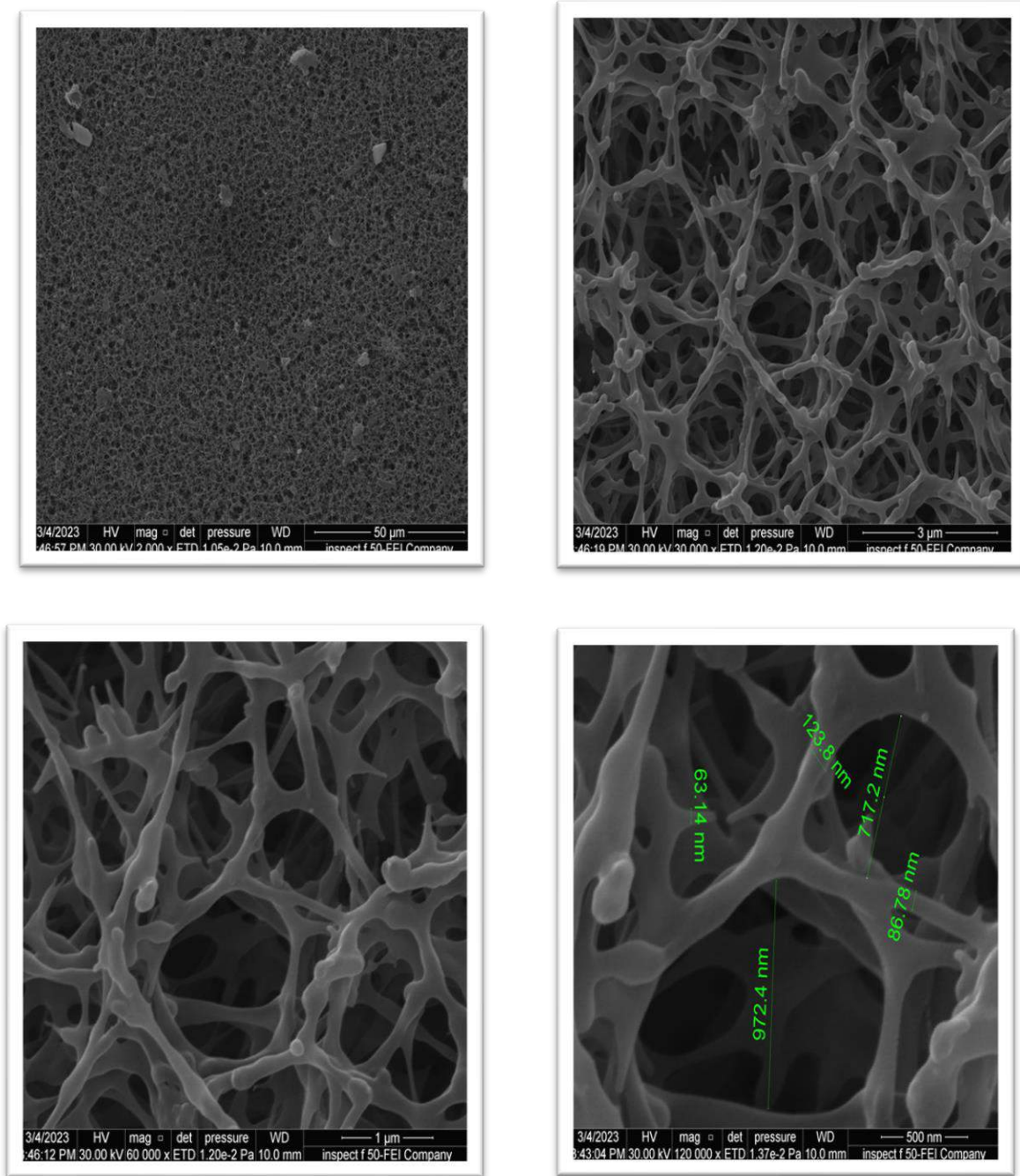
Fig. (3-10): FESEM images of CS membrane at (50 μm, 3 μm, 1μm, 500 nm) scales

The CS membrane contain a high porosity, the range of pores size (63.14-972.4) nm at different scales as shown in Fig. (3-10).
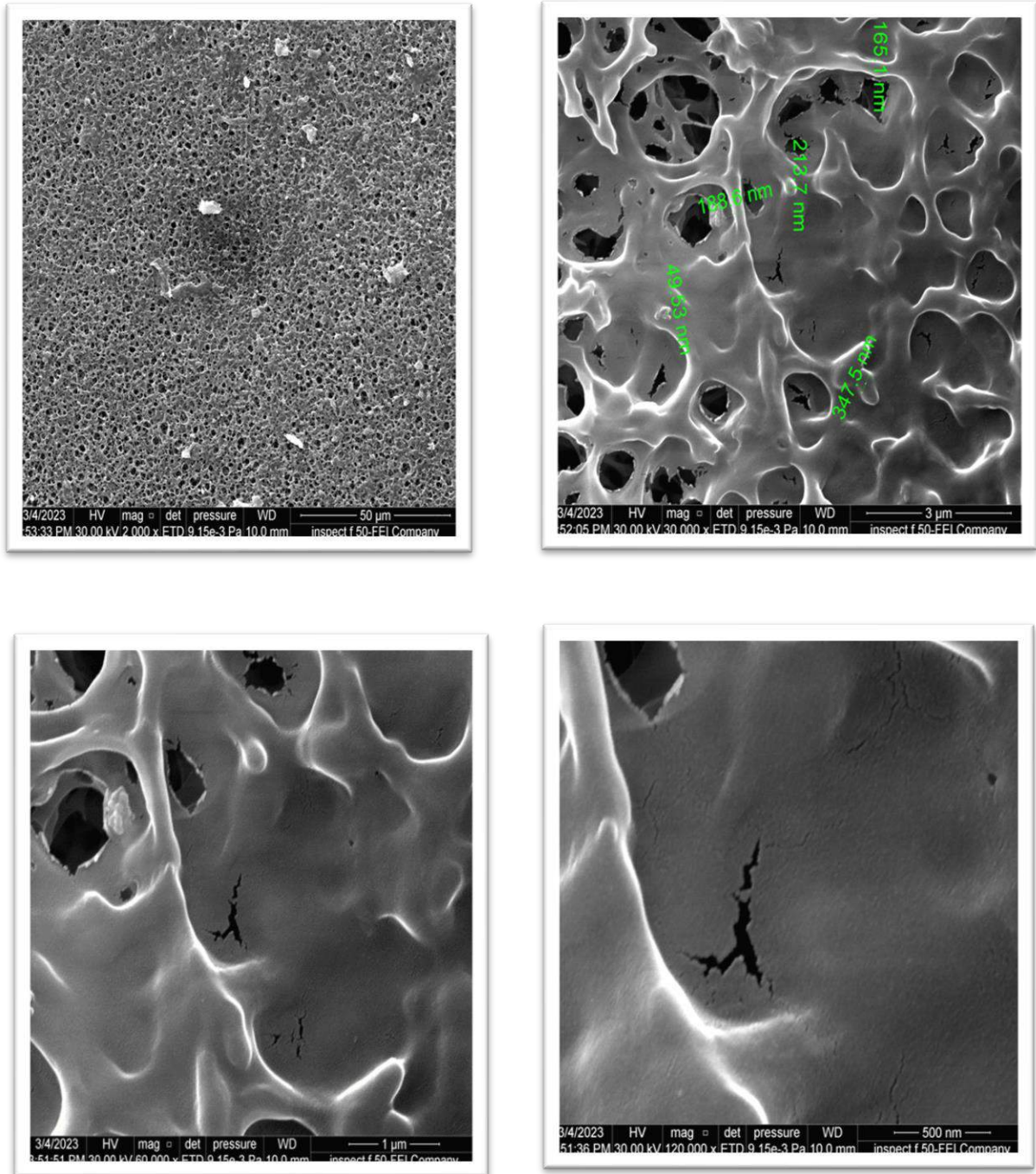
Fig. (3-11): FESEM images of NGO-CS membrane at (50 μm, 3 μm, 1μm and 500 nm) scales

No obvious CS particles are found in FESEM images of NGO-CS composite, indicating a uniform distribution of NGO sheets in CS [89]. The interconnected pores enable the diffusion of solute throughout the composite, pores size (49.53-347.5) nm at different scales as shown in Fig. (3-11).
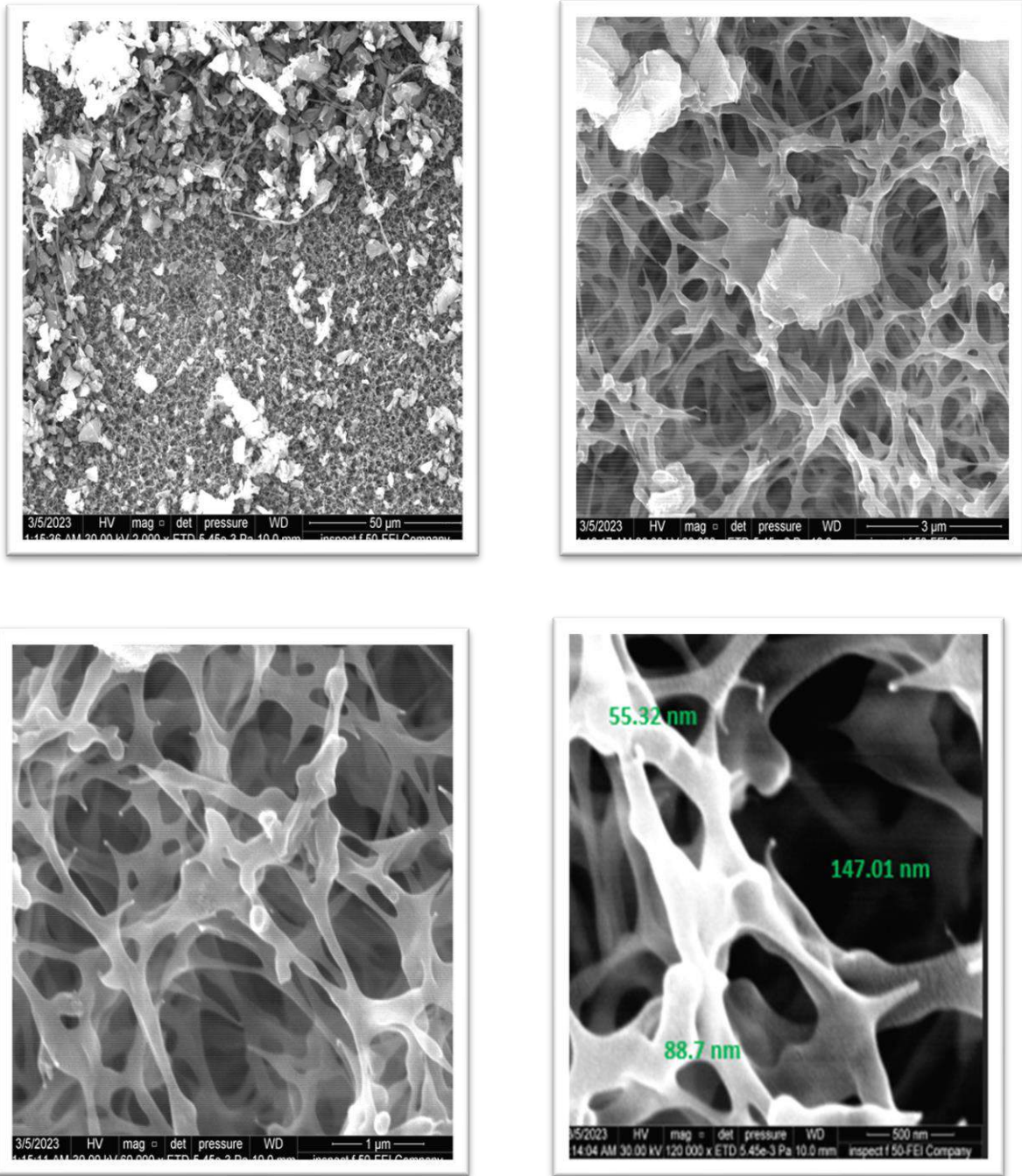
Fig. (3-12): FESEM images of NGO-M membrane at (50 μm, 3 μm, 1μm and 500 nm) scales
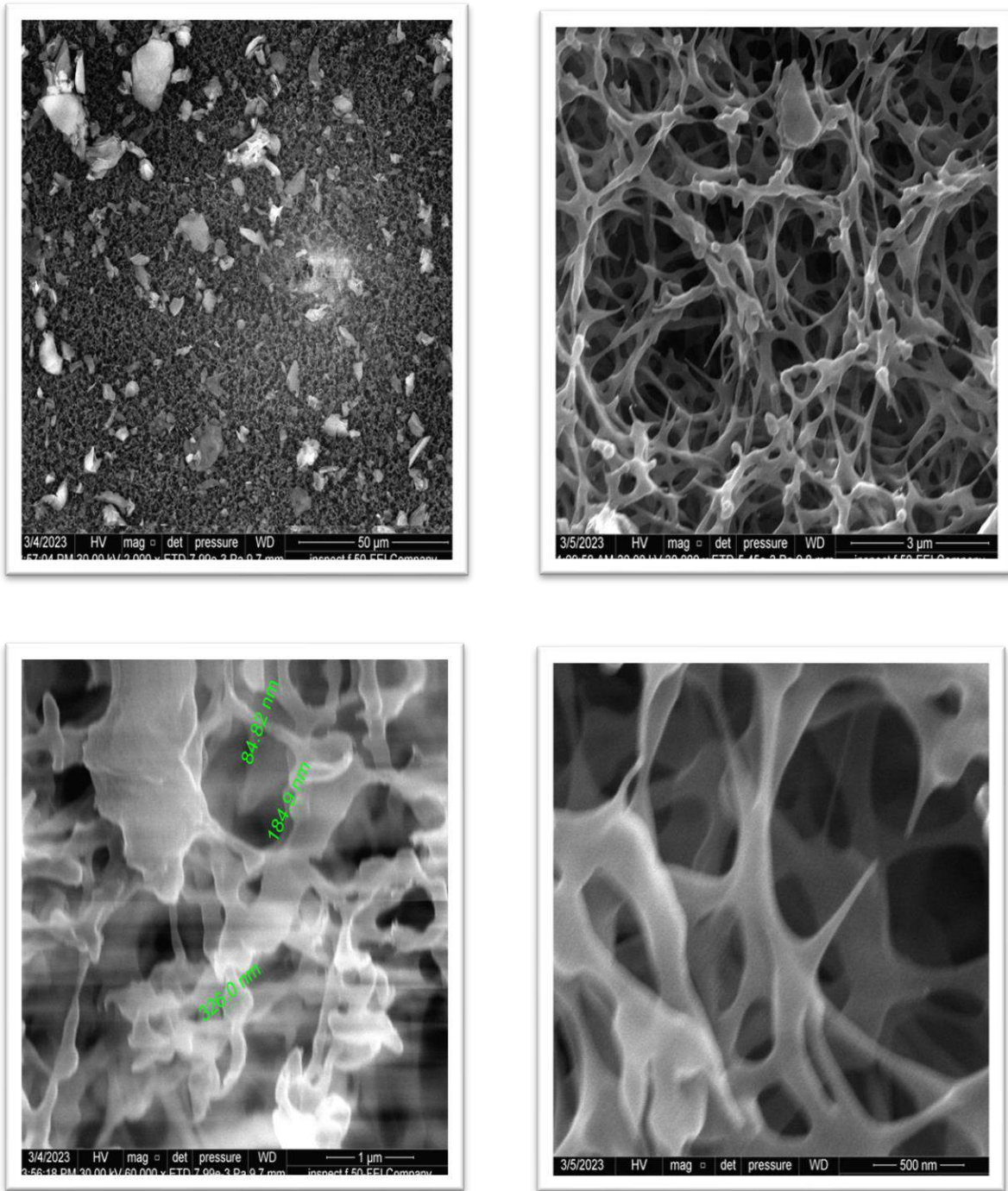
Fig. (3-13): FESEM images of NGO-C membrane at (50 μm, 3 μm, 1μm, 500 nm) scales

The NGO-M and NGO-C membranes contain a high porosity, the pores size (84.8-326.0) nm and (55.32-147.01) respectively at different scales, as shown in Fig. (3-12) and Fig. (3-13). Low wrinkled above nano sheets surfaces, has more sensitive and show better recovery ability [90].

Table (3-6): Summary range pores size of NGO, CS, NGO-CS, NGO-M, NGO-C membranes

Membranes	Pores size (nm)	
	Min.	Max.
NGO	52.31	613.2
CS	63.14	972.4
NGO-CS	49.53	347.5
NGO-M	84.8	326.0
NGO-C	55.32	147.01

It was concluded the distribution of pores in the membranes are irregular and the size of the pores are heterogeneous, and some pores size located within nanoscale (< 100 nm).

3.1.4 Zeta Potential Analysis

Zeta potentials study the surface charge of a particle which affects the nanomaterial agglomeration and adsorption of ions onto nano surface[91]. Mobility and zeta potential analyzed for NGO, NGO-CS, NGO-M, NGO-C by electrophoresis light scattering (ELS) method .The values of mobility and zeta potential shown in Table (3-7).

Table (3-7): Values of mobility and zeta potential for NGO, NGO-CS, NGO-M, NGO-C

Comp.	Zeta potential (mV)	Mobility (cm²/V. s)	Charge
NGO	-17.17	-0.000134	Negative
NGO-CS	-17.5	-0.000135	Negative
NGO-M	-15.33	-0.000126	Negative
NGO-C	-14.36	-0.000115	Negative
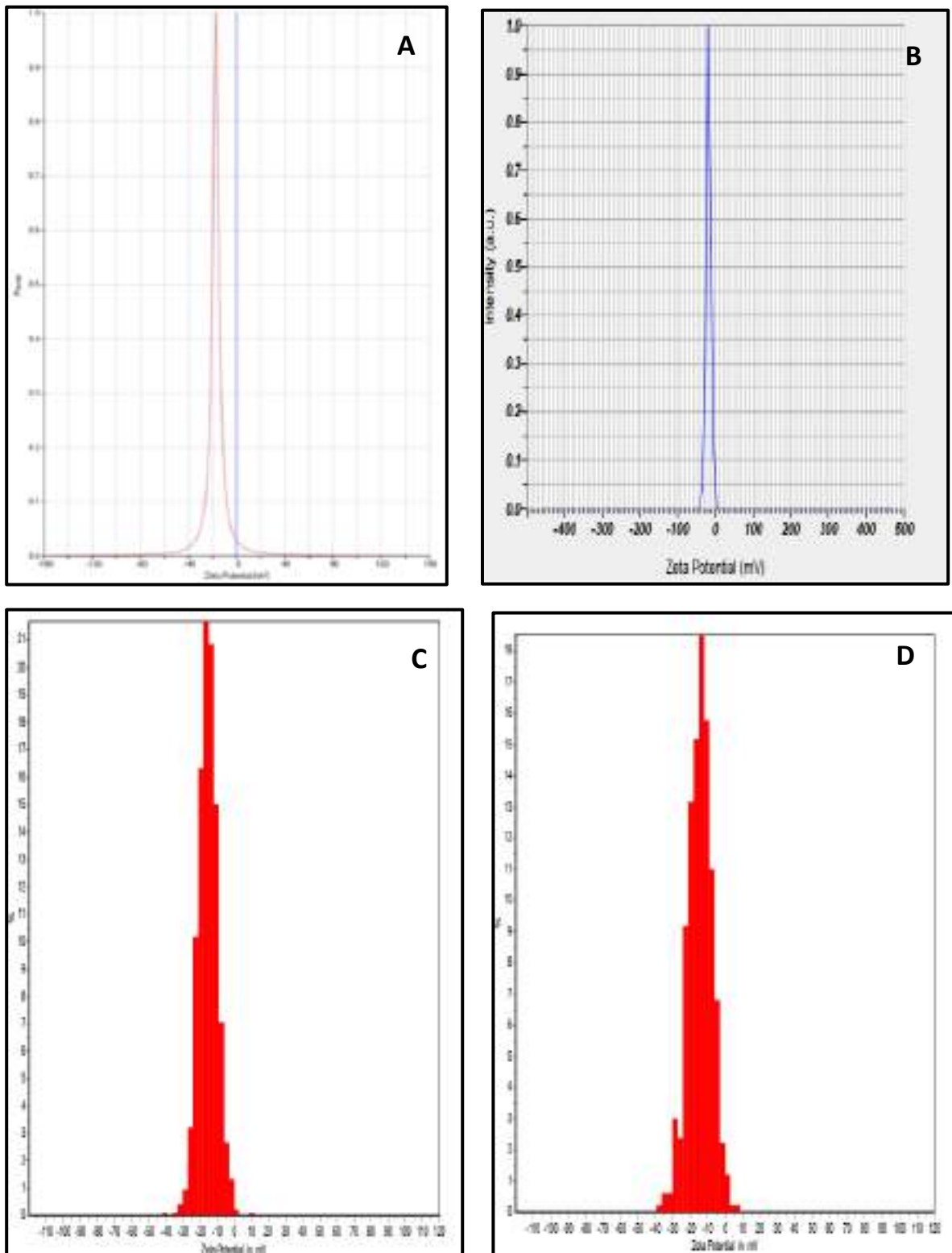
Fig. (3-14): Zeta potential of (A)NGO, (B)NGO-CS, (C)NGO-M, (D)NGO-C composites

3.1.5 Flame Atomic Absorption Spectroscopy

3.1.5.1 Determination of Calibration Curves for Metal Ions by
Flame Atomic Absorption Spectroscopy

The standard calibration curves for (Ni^{2+}, Cd^{2+}, Co^{2+}, Cu^{2+} and Pb^{2+}) bivalent ions has determined by flame atomic absorption spectroscopy (FAAS) according to the manual instructions of (Aurora AI-1200) for each analyte with the limit of detection (LOD), the lowest concentration level that can be determined to be statistically different from the blank, gives a signal above the background signal by three times of the standard deviation of the background signal, Equation (3.2).

$$LOD = 3.3 * \frac{S}{Slope} \quad .... (3.2)$$

Where: the slope of calibration curve of the analyte, Standard deviation (S) in statistics, the standard deviation is a measure of the variation or dispersion amount of a set of values as in Equation (3.3)[92].

$$S = \sqrt{\frac{\sum(xi - \bar{x})^2}{n-1}} \quad .... (3.3)$$

Where: xi absorbance values of standard solution at same concentration, $\bar{x}$ average of absorbance values, n number of absorbance values. Series of standard solutions has prepared (2,4.6.8 and 10 mg $.L^{-1}$) for each ion, the standard calibration curves of the analyte ions are shown in Fig. (3-15) to (3-19).
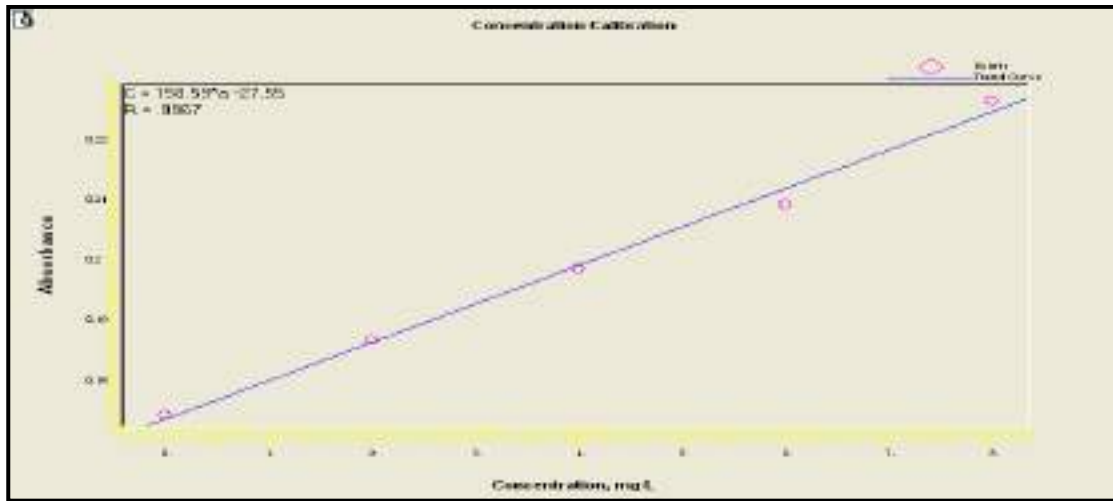
Fig. (3-15): Calibration curve of Lead (Pb^{2+})

Fig. (3-16): Calibration curve of Nickel (Ni^{2+})
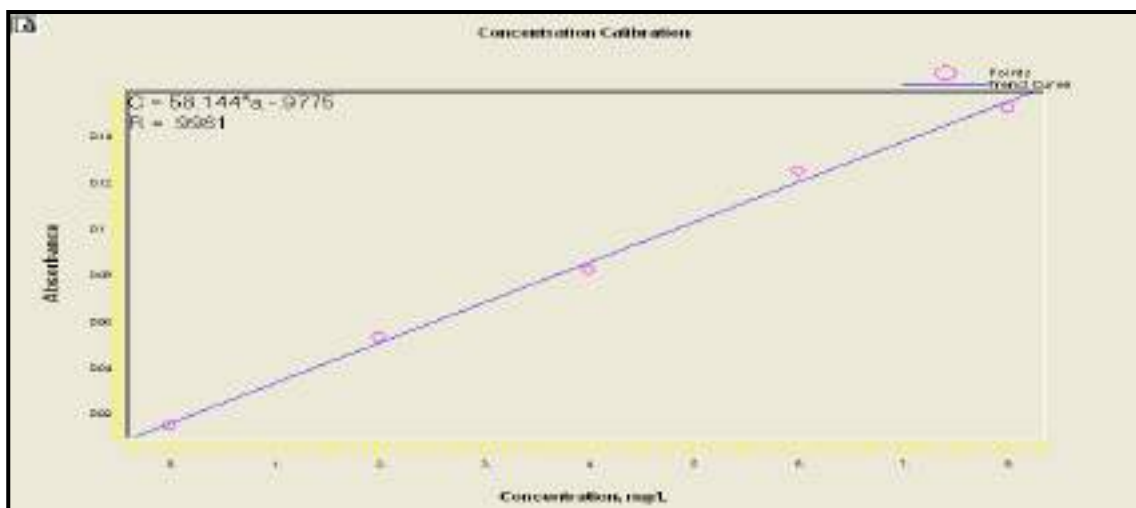
Fig. (3-17): Calibration curve of Cobalt (Co^{2+})
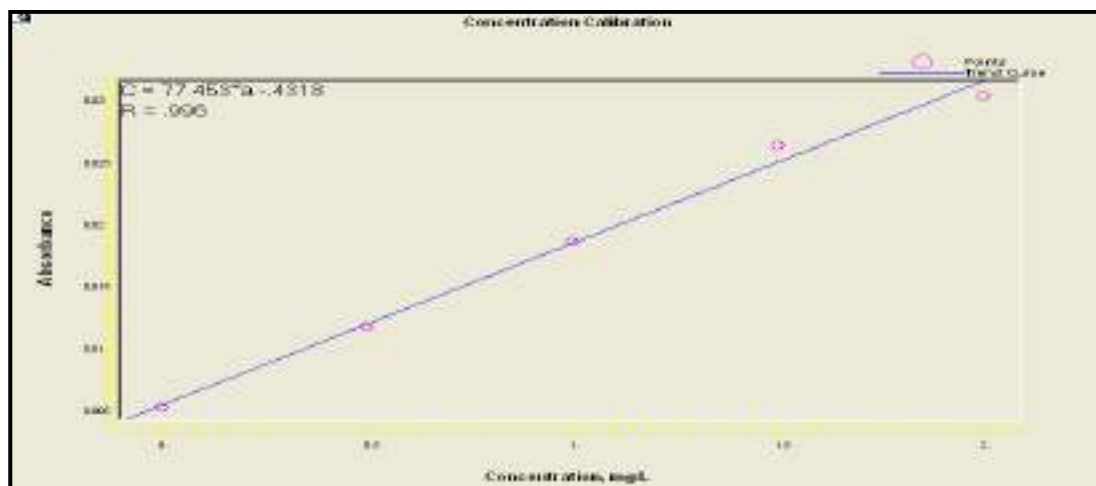
Fig. (3-18): Calibration curve of Cadmium (Cd^{2+})
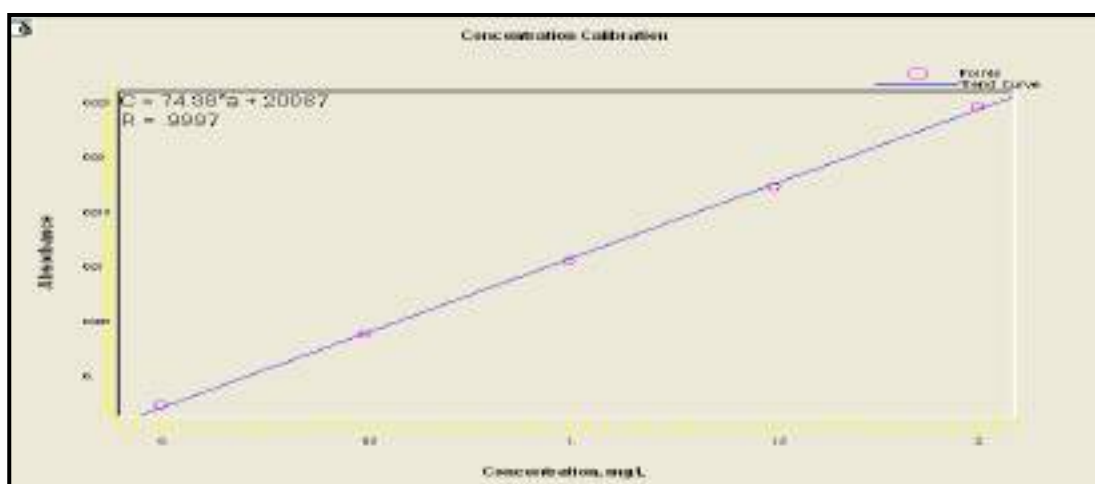
Fig. (3-19): Calibration curve of Copper (Cu^{2+})

3.1.6 UV-visible Spectrophotometer

3.1.6.1 Determination wavelength maximum (λ_{max}) of BPB by UV-visible Spectrophotometer

The absorption spectrum of BPB dye ($C_{19}H_{10}Br_4O_5S$) was obtained by UV-Visible spectrophotometer as shown in Fig. (3-20) and (3-21).
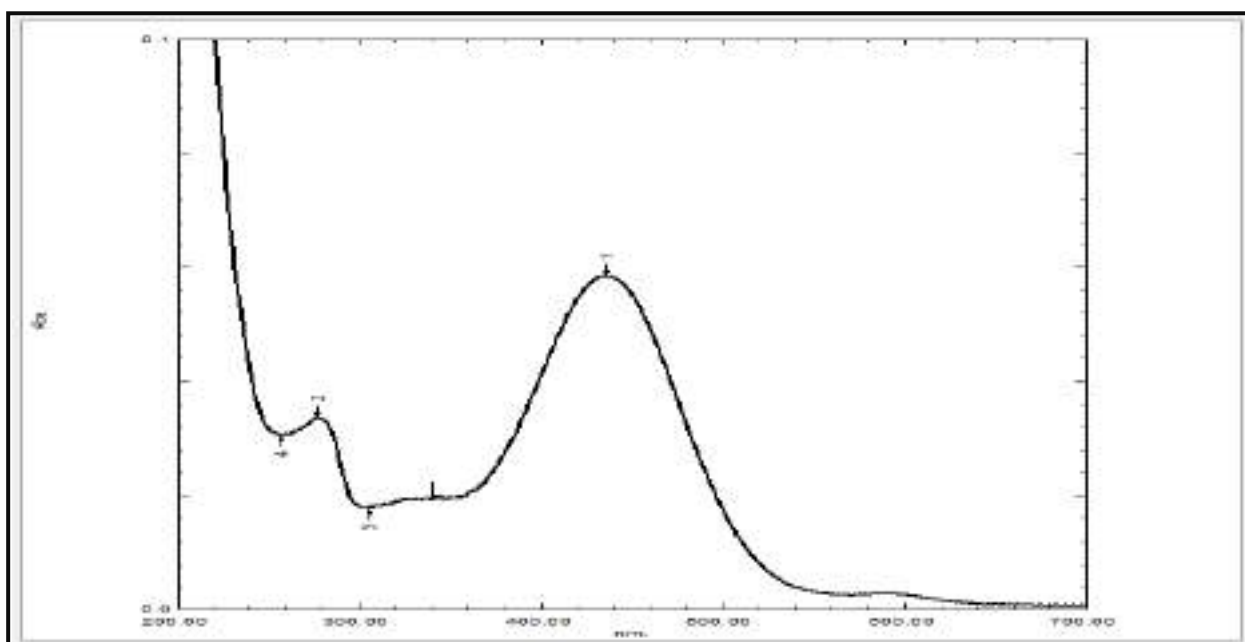
Fig. (3-20): Absorption spectrum of BPB dye in acidic media
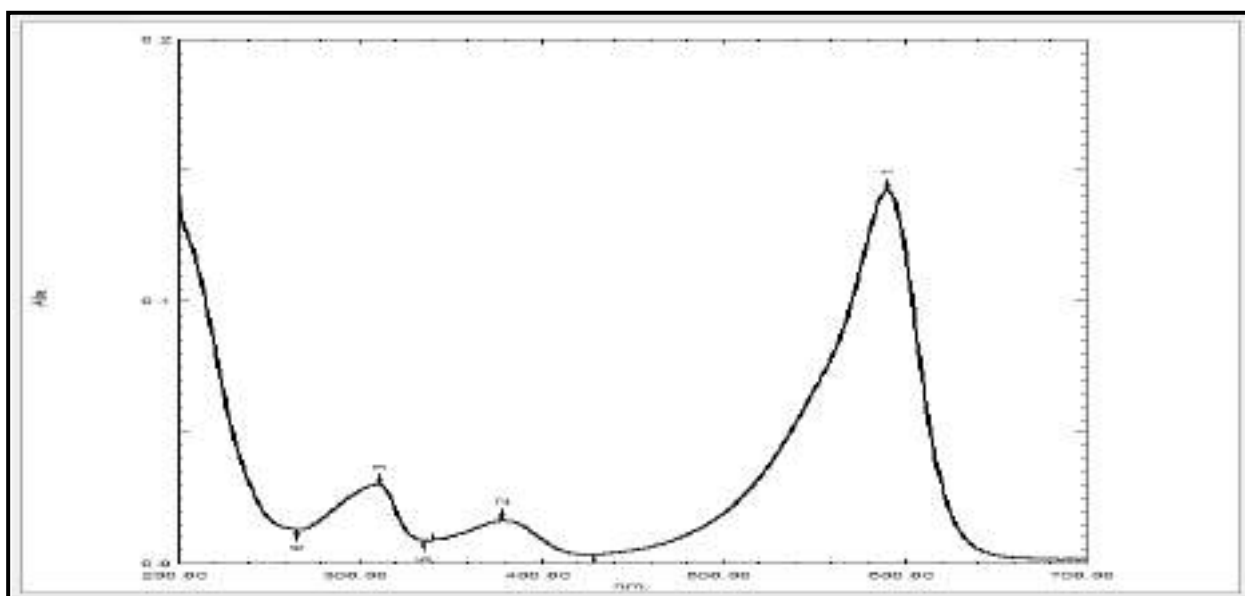
Fig. (3-21): Absorption spectrum of BPB dye in neutral media

The maximum absorption wavelength of BPB dye was $\lambda_{max} = 437$ nm and $\lambda_{max} = 590.5$ nm in the acidic medium and neutral medium respectively.
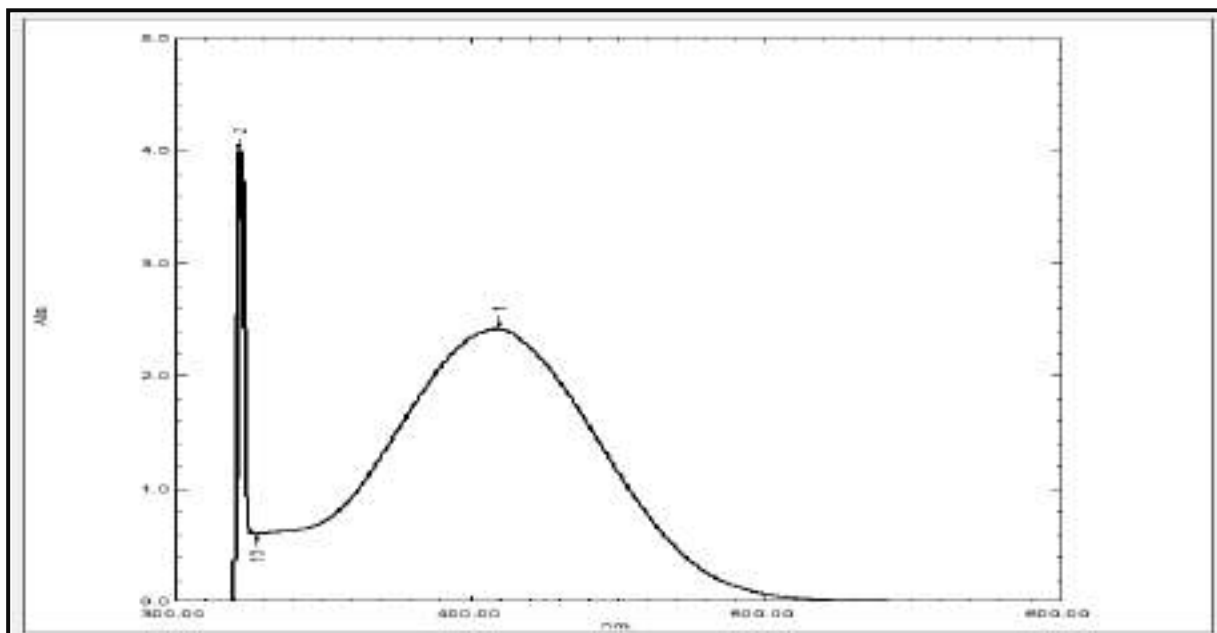
Fig. (3-21): Absorption spectrum of BPB dye in neutral media

3.1.6.2 Determination the Calibration Curve of BPB Dye by UV-visible Spectrophotometer

The calibration curve of BPB was determined by using series of standard solutions (2,4,6,8 and 10 mg.L^{-1}) of BPB dye, at λ_{max} = 437 nm. (acidic media pH< 4) and the λ_{max} =590.5 nm. (neutral media pH > 4) as shown in Fig. (3-23) and (3-24) respectively.
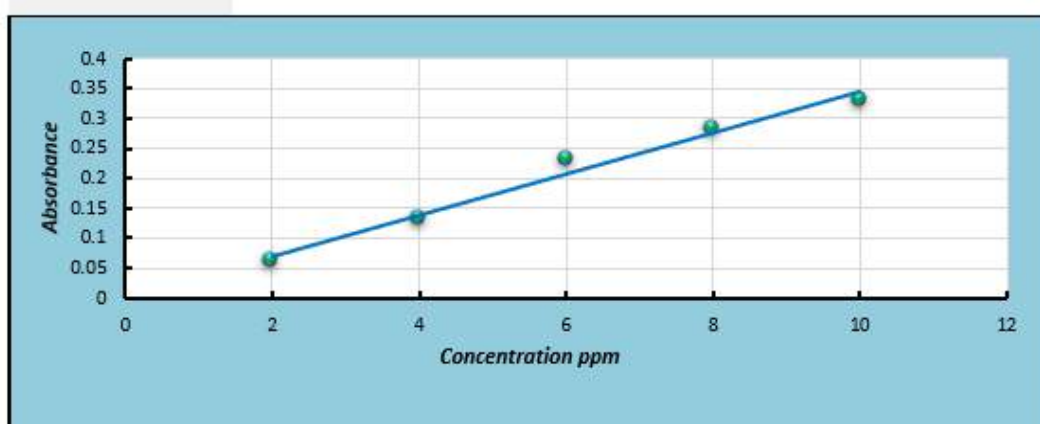
Fig. (3-23): Calibration curve of BPB dye in acidic media

67
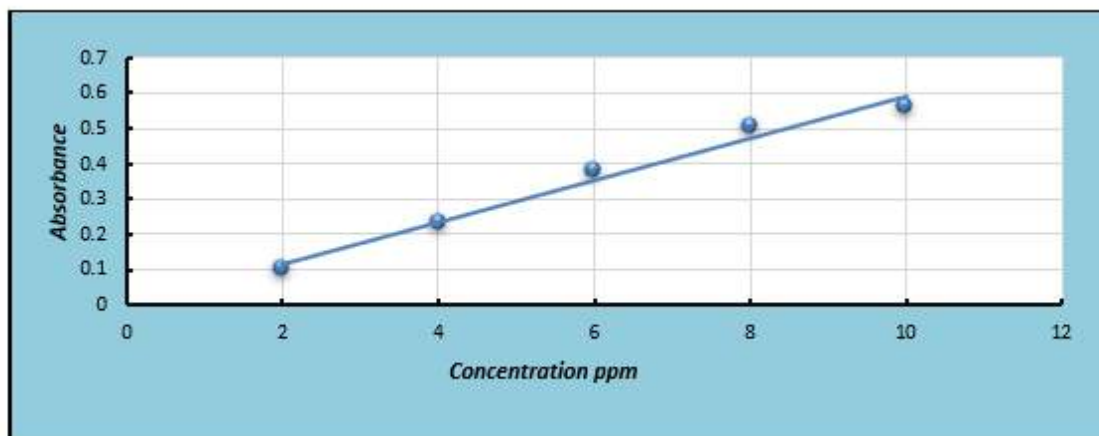
Fig. (3-24): Calibration curve of BPB in neutral media

3.2 Optimum Conditions of Adsorption

The NGO-CS, NGO-M and NGO-C composites has many functional groups, like carboxylic acids, epoxides, alcohols, amide and amine. Thus, it can interact with the organic dye like BPB dye. There are many factors can affect the adsorption mechanism, pH, dosage of composites, contact time, temperature, dye concentration, and ionic strength.

3.2.1 Effect of pH

BPB dye is an acid-base indicator, thus the degree of ionization of the functional groups of BPB dye is also affected by pH. BPB dye acts as weak acid-base system (HIn/In-), where (In⁻) form has a different color than the (In⁻) form in the aqueous solutions. In⁻ form of BPB dye absorbs red light and transmits blue color, therefore the solution of dye is blue. At low pH the (HIn) form of BPB dye absorbs ultraviolet light and transmits yellow color, so the solution of dye appears yellow color in pH < 4.0. as shown in Fig. (3-25).
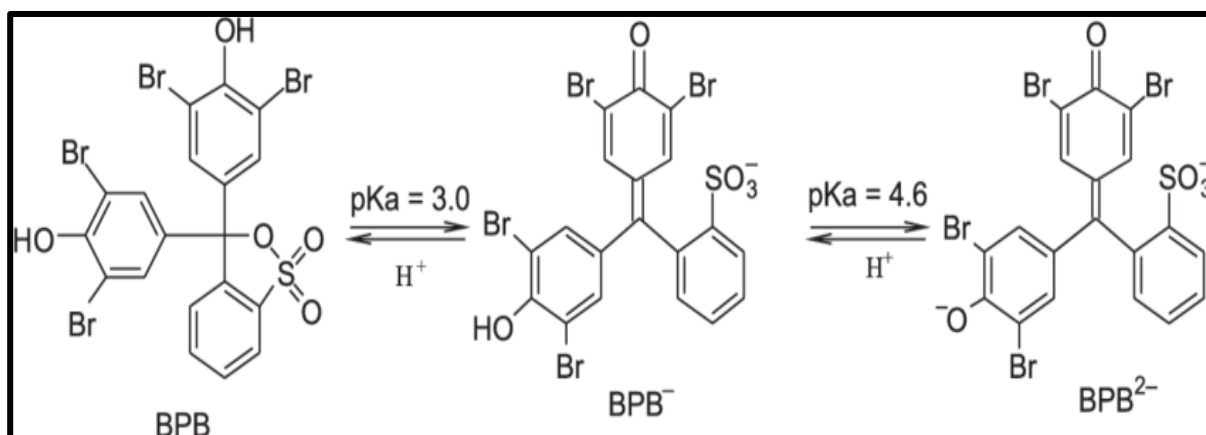
Fig. (3-25): Dissociation equilibrium of BPB dye in different pH media[93]

This can be ascribed to three types of interactions between NGO-CS, NGO-M and NGO-C composites and BPB dye [39].

(i) pi-pi interaction between aromatic ring of BPB dyes and basal plane (benzene rings) of three composites.

(ii) Hydrogen bonding.

(iii) Electrostatic attraction.

Fig. (3-26) A,B,C shown the effect of pH on the adsorption of BPB dye on NGO-CS, NGO-M and NGO-C composites respectively, the results show the maximum adsorption capacity of dye was at pH =2,3 and 1 respectively, but beyond this points a decreasing was observed. In NGO-CS, NGO-M and NGO-C the amide bond has formed, interaction of -COOH groups of NGO with -NH_2 of chitosan, methionine and cystine respectively, and NH II groups formed due to reaction between amino groups of chitosan, methionine and cystine and epoxy groups of NGO[77]. Fig. (3-27, 3-28 and 3-29) are shows the structure of the composites.
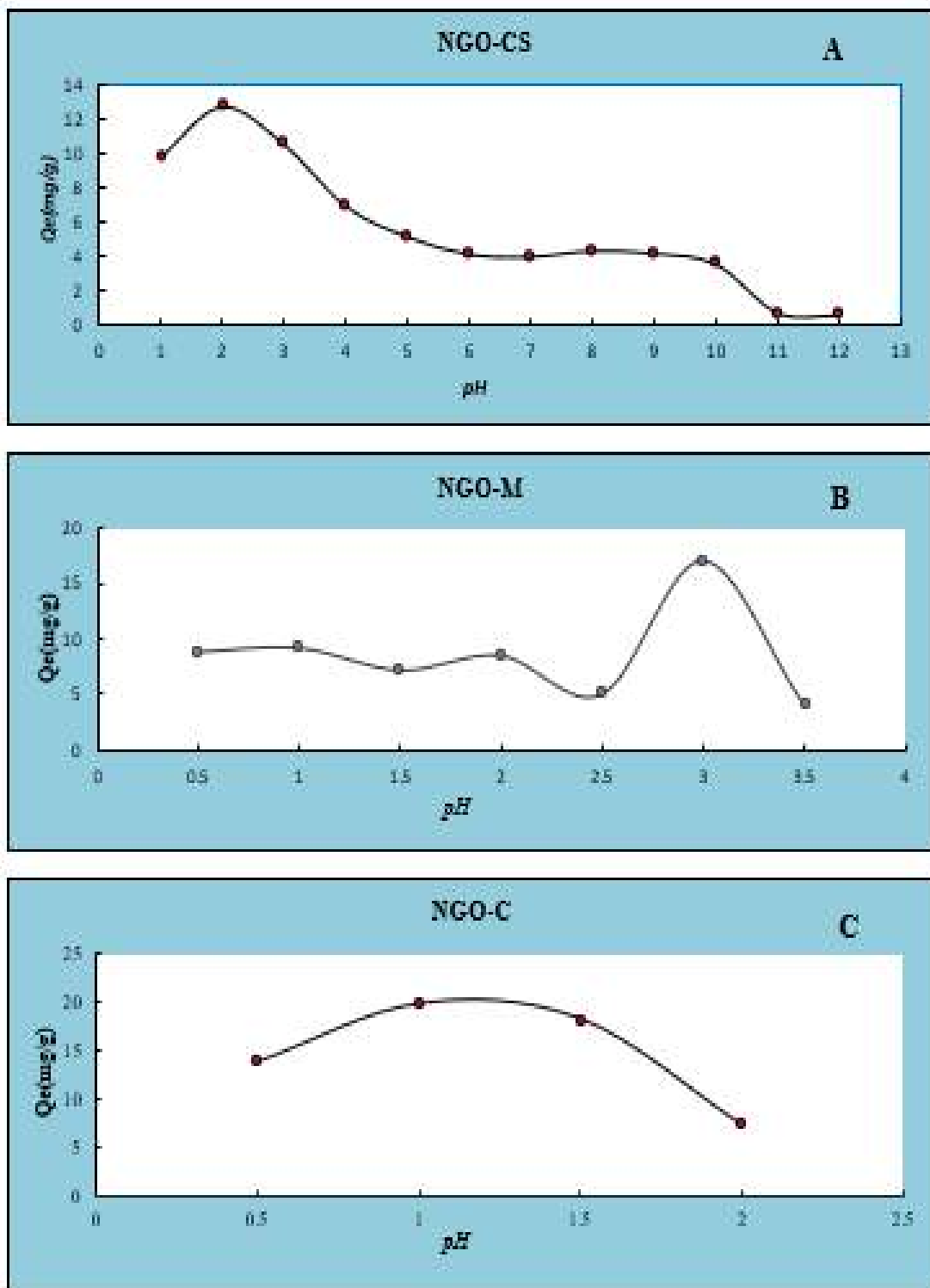
Fig. (3-26): Effect of pH on adsorption capacity of BPB at [Experimental conditions: dye conc.=10 mg.L^{-1}, composites dosage =10 mg; vol. = 20 mL, time = 60 min. room temperature]. (A) NGO-CS composite, (B) NGO-M composite, (C) NGO-C composite
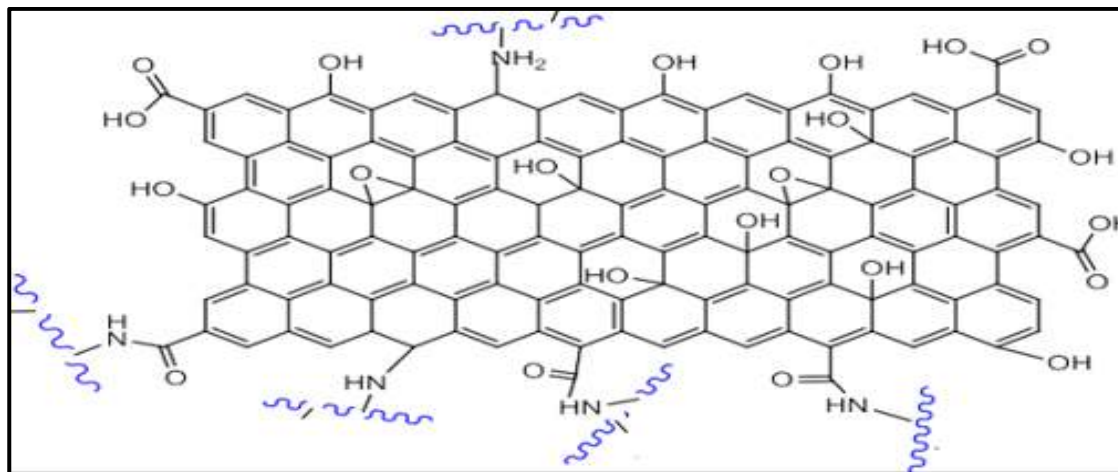
Fig. (3-27): Structure of NGO-CS composite [87]
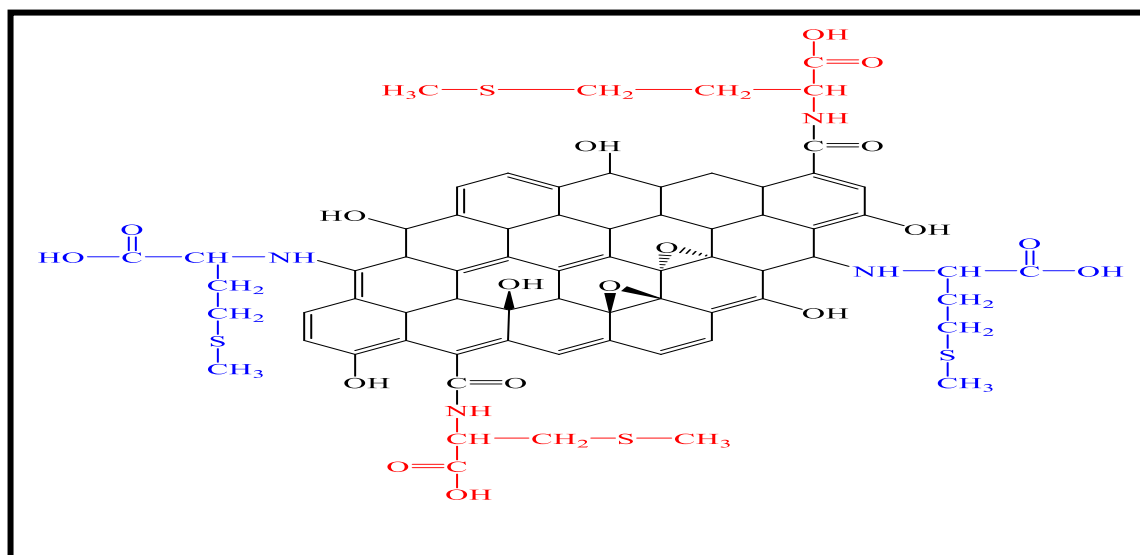
Fig. (3-28): Structure of NGO-M composite
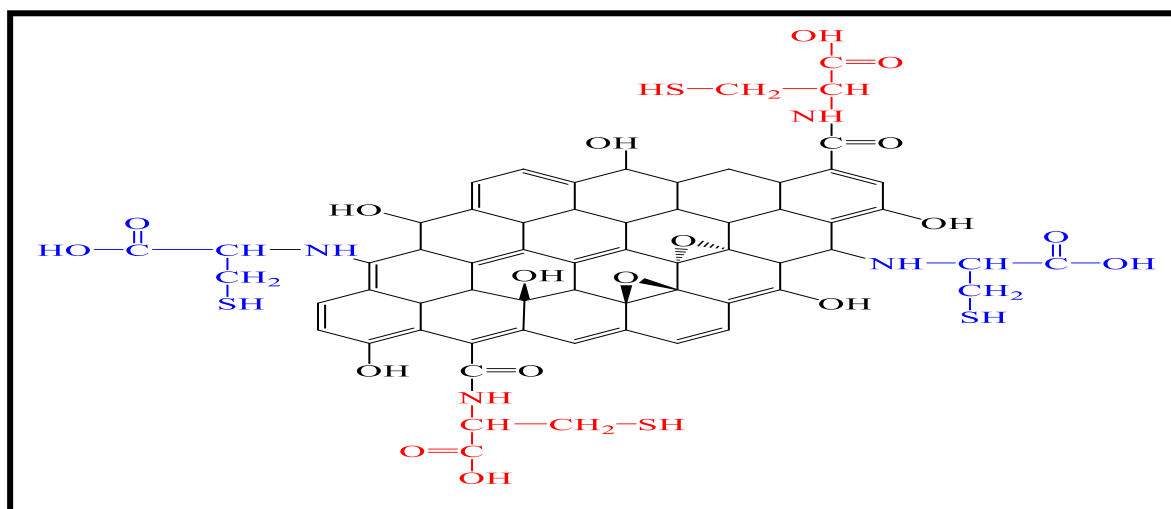
Fig. (3-29): Structure of NGO-C composite

71

In aqueous solutions, the amide and NH II groups can be protonated or deprotonated depending on the pH of the solution, which affect the charge surface of composites. At low pH, the protonation of amide groups and NH II groups of composites forms a positive charge on the surface of the composites, increasing the binding of BPB dye toward composites, but increasing the pH decline the adsorption capacity attributed to the mutual repulsion between anionic dye and negatively charged surface of the composites. Notably, NGO of NGO-CS remains fairly negatively charged in a wide pH range because of ionization of–COOH and phenolic -OH on the NGO sheets[39].Generally, the adsorption decreases with increasing pH for anionic dyes , while it increases with increasing pH for cationic dyes [43,44].

3.2.2 Effect of Adsorbent Dosage

The effect of the dosage of NGO-CS, NGO-M and NGO-C composites on the adsorption of BPB dye was studied by using different weights of composites (2, 4, 6, 8.10, 12,14 and 16 mg). Fig. (3-30) shown the adsorption capacity (mg/g) of the dye on NGO-CS, NGO-M and NGO-C composites were decreased with increase the adsorbent dosage, because of the inversely relationship can be seen Equation (1.1), so the best dosage was 2 mg. The reason for this is attributed to the agglomeration of composite surface particles, causes many pores and active sites are not available [94]. When the dosage of the composite is low, it will spread more in the solution, which leads to the exposure of the great number of active sites for adsorption.
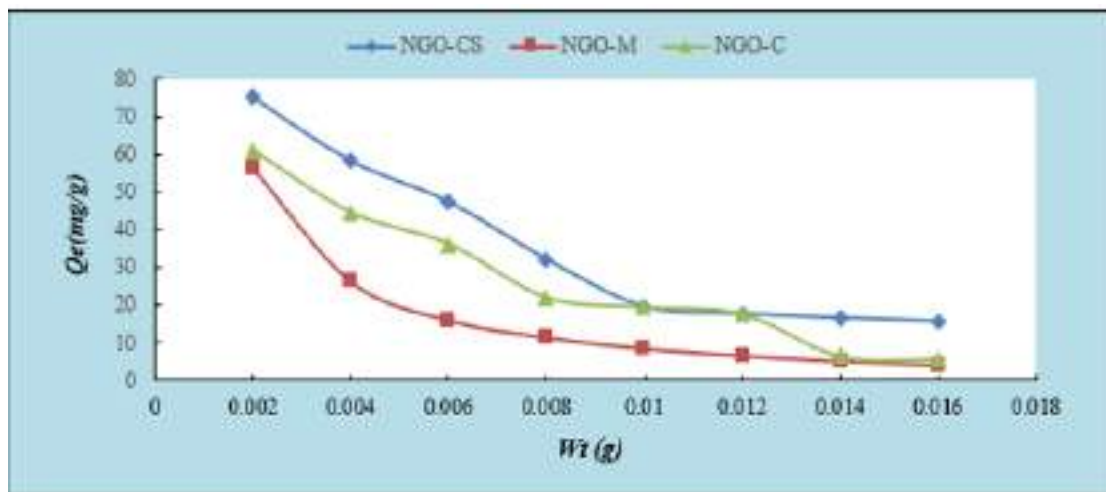
Fig. (3-30): Effect of Adsorbent dosage on adsorption capacity of BPB on NGO-CS, NGO-M and NGO-C composites at pH=2,3 and 1 respectively. [Experimental conditions: dye conc.=10 mg.L^{-1}, composites dosage (2, 4, 6, 8.10, 12,14 and 16 mg); vol. = 20 mL; time =60 min. and room temperature]

3.2.3 Effect of Contact Time

Equilibrium time is an essential parameter. The adsorption of BPB dyes onto NGO-CS, NGO-M, NGO-C composites, was studied as a function of contact time to determine the adsorption equilibrium time as show in Fig.(3-31). The results shows the adsorption capacity gradually increasing contact time, [95]
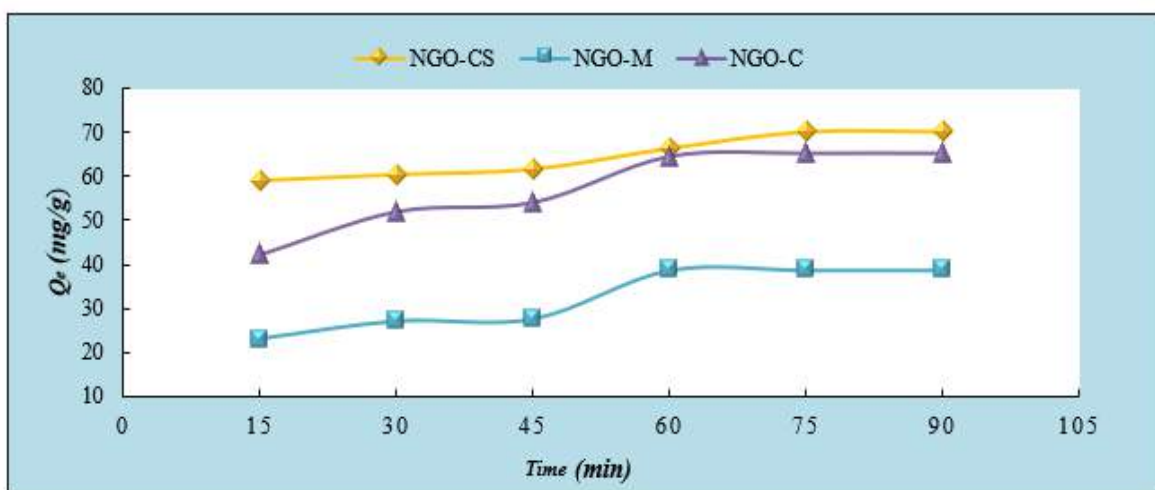
Fig. (3-31): Effect of contact time on adsorption capacity of BPB for NGO-CS, NGO-M and NGO-C composites at pH=2,3 and 1 respectively. [Experimental conditions: dye conc.=10 mg.L^{-1}, composites dosage=2 mg; volume = 20 mL, time = (15-90 min room temperature]

73

The maximum adsorption capacity was a about 75 min for NGO-CS composite and 60 min for NGO-M and NGO-C composites respectively. Therefore, these times were chosen as an optimum contact time or equilibrium time, the adsorption was fast at the beginning and speed up with the increasing time until reaching the equilibrium state. The rapid adsorption at the beginning attributed to the available of the active sites, but after that will be occupied.

3.2.4 Effect of Temperature

It is very important to know the effect of temperature on the efficiency of adsorption or desorption on a solid surface[36]. The adsorption capacity of BPB dye onto NGO-CS, NGO-M, NGO-C composites, increasing with the rising of temperature as show in Fig. (3-32), the maximum adsorption capacity of dye was at T= 45°C for NGO-CS and NGO-C composites and T= 55°C for NGO-M composite.
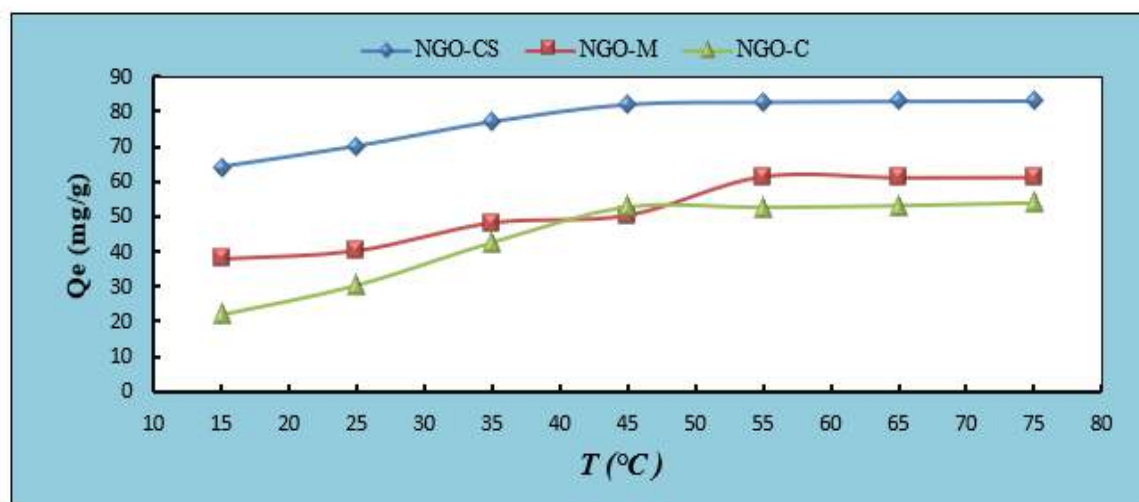
Fig. (3-32): Effect of temperature on adsorption capacity of BPB for NGO-CS, NGO-M, NGO--C composites at pH=2,3,1 respectively. [Experimental conditions: dye conc.=10 ppm, composites dosage= 2mg, volume = 20mL; range temperature =15-90 °C].

3.2.5 Effect of The Initial Concentration of Adsorbate

Studying the effect of the initial concentration of BPB dye on the adsorption onto NGO-CS, NGO-M and NGO-C composites, at the beginning the adsorption capacity was gradually increased with increasing concentration of the BPB dye until reaches the equilibrium state, at the concentrations (40,25 and 25 mg.L^{-1}) respectively as shown in Fig. (3-33).
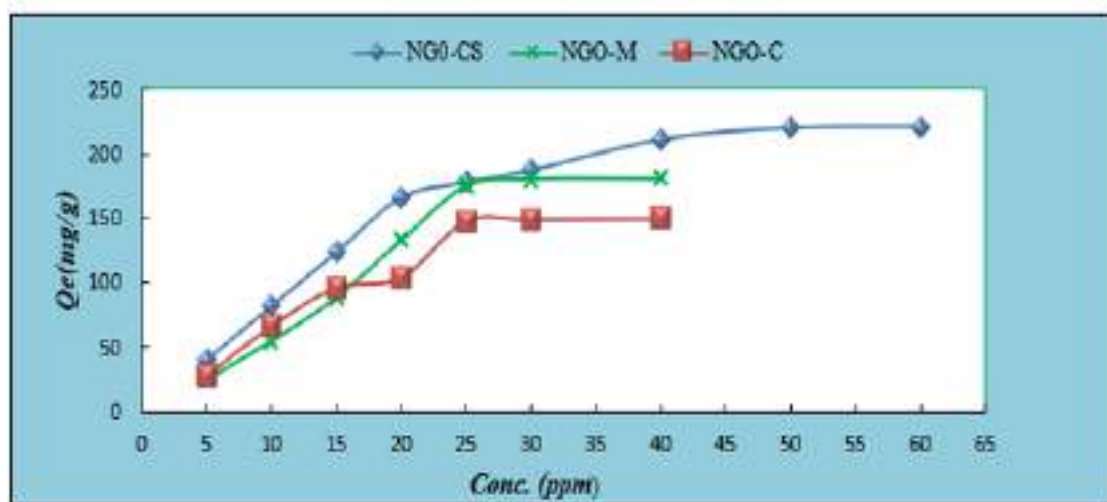
Fig. (3-33): Effect of Initial Concentration of BPB dye on adsorption capacity for NGO-CS,

NGO-M and NGO-C composites at pH=2,3and 1, temperature =45,55 and 45°C respectively. [Experimental conditions: dye concentration=5-50 mg.L^{-1}, composites dosage=2mg; volume = 20mL]

3.2.6 Effect of Ionic Strength

The ionic strength has influence on the nature and extent of electrostatic interactions between NGO-CS, NGO-M, and NGO-C composites with BPB dye, it is very important to investigate the influence of foreign electrolytes (in particular, NaCl) on the interaction between dye molecules and the composites. Increasing concentration of NaCl causes a decrease in capacity adsorption as show in Fig.(3-34) by increasing the ionic strength, more Na$^+$ and Cl$^-$ ions can occupied the charged sites of the adsorbents, leading to suppress the electrostatic interaction (reduction the electrostatic attraction and repulsion) [96].The increased ionic strength causes

75

competition between the species in the solution, the cationic species Na$^+$ interacts with the anionic dye causing the reduction of its adsorption capacity onto the composites surface, the adsorption capacity can also be attributed to the competition of the Cl$^-$ species with the anionic BPB dye on the charged site of composites. According to these ionic competition interactions, the adsorption was decreased with increasing of ionic strength[31].
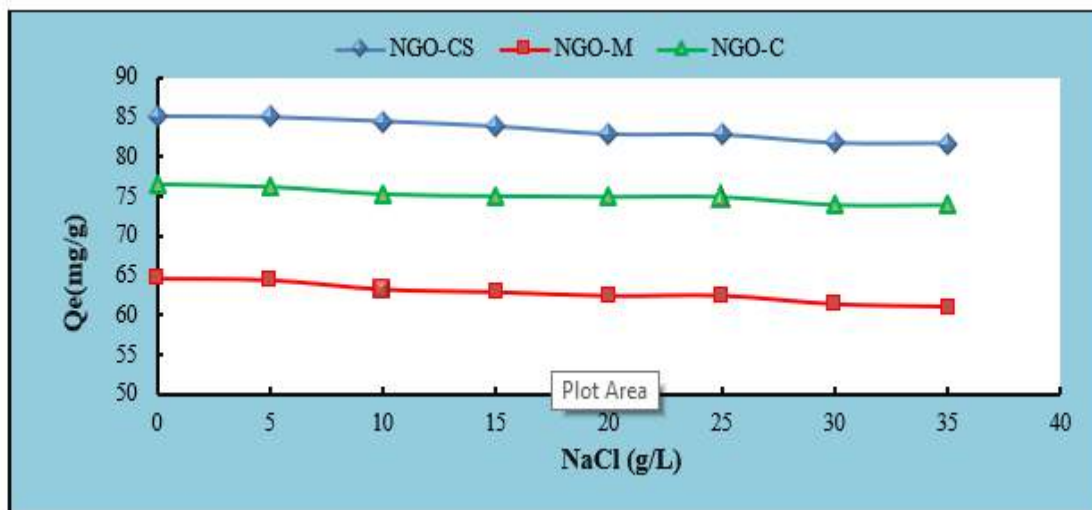
Fig. (3-34): Effect of ionic strength on adsorption capacity of NGO-CS, NGO-M and NGO-C composites at optimal conditions

Table (3-8): Summary optimum condition of adsorption on NGO-CS, NGO-M and NGO-C Composites

	pH	Dosage of composite (mg)	Contact time (min.)	Temperature (°C)	Initial Concentration of BPB dye (mg.L^{-1})
NGO-CS	2	2	75	45	40
NGO-M	3	2	60	55	25
NGO-C	1	2	60	55	25

3.3 Adsorption Isotherm Models

There is a relationship between the amount of adsorbate on a certain solid surface (Qe) and the concentration of the adsorbent at equilibrium (Ce) at constant temperature. *Giles* shows that the adsorption isotherms from a solution classified into four Main classes depending on the form of the initial slope of the isotherms (S, L, H, C) as show in Fig. (3-35).
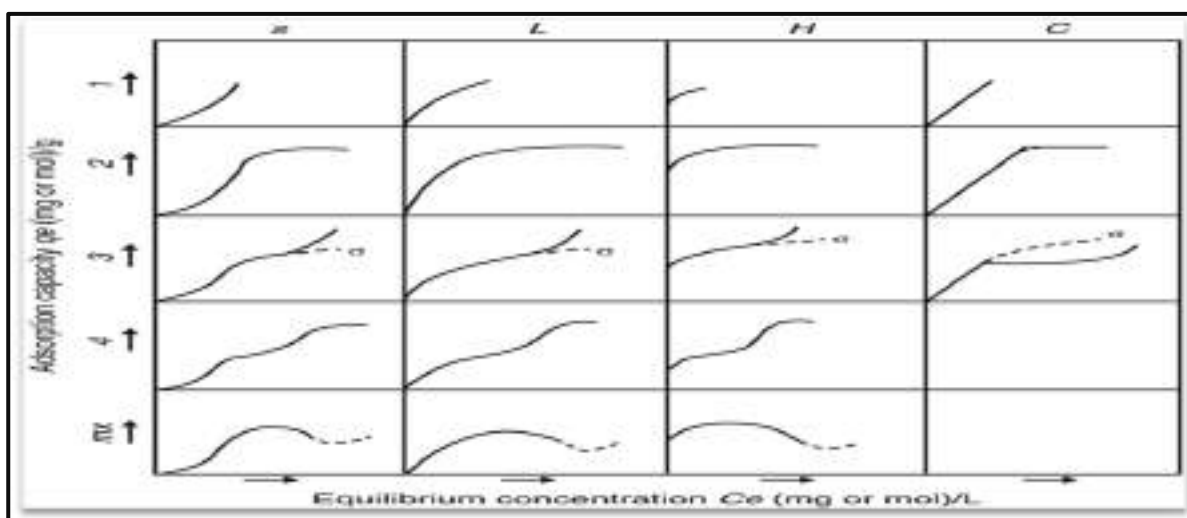
Fig. (3-35): Giles classification of adsorption isotherm[97]

In the Fig. (3-36), (3-37) and (3-38) it is clear that the adsorption of a BPB dye on on NGO-CS, NGO-M and NGO-C composites according to the Gilles classification, follows a pattern **S₃** the isotherm takes the form of (S-type), meaning that the adsorbate molecules on the adsorbent surface are oriented obliquely or vertically, which show that the amount of adsorbate at 288 K is the least, and then it changes about Slightly at 298K, then the amount of adsorption increases at the rest of the temperatures. In general, when the amount of adsorption increases with increasing temperature, this means that the process is endothermic, and this indicates that the goodness of the porous surface contributes significantly to the occurrence of adsorption.

Table (3-9): Qe and Ce values for the adsorption of BPB dye on the surface of NGO-CS composite at different temperatures

T (K)	288		298		308		318	
C_i ppm	Ce ppm	Q mg/g	Ce ppm	Q mg/g	Ce ppm	Q mg/g	Ce ppm	Q mg/g
5	1.821	31.784	1.611	33.884	1.225	37.74	0.909	40.90
10	3.592	64.079	2.991	70.087	2.280	77.19	1.780	82.19
15	4.905	100.94	4.099	109.009	3.205	117.9	2.476	125.2
20	7.011	129.88	5.366	146.337	4.081	159.1	3.119	168.8
25	8.625	163.7	6.511	184.880	4.762	202.37	3.511	214.8
30	9.962	200.3	7.716	222.835	4.871	251.2	4.711	252.8
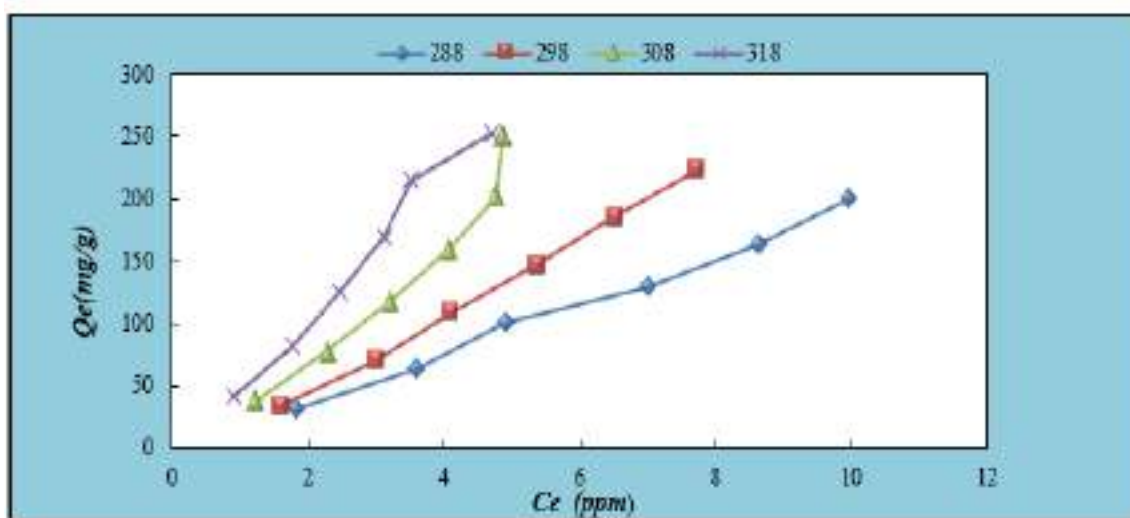
Fig. (3-36): Adsorption isotherm of BPB dye on NGO-CS composite

Table (3-10): Qe and Ce values for the adsorption of BPB dye on the surface of NGO-M composite at different temperatures

T (K)	288		298		308		318		328	
C_i ppm	Ce ppm	Q mg/g	Ce ppm	Q mg/g	Ce ppm	Q mg/g	Ce ppm	Q mg/g	Ce ppm	Q mg/g
5	3.311	16.88	3.2757	17.242	2.736	22.633	2.405	25.942	2.218	27.81
10	6.211	37.88	5.9757	40.242	5.173	48.263	4.961	50.386	3.8507	61.49
15	10.119	48.80	9.5720	54.27	8.662	63.374	6.505	84.942	5.9068	90.93
20	14.811	51.88	13.021	69.798	12.593	74.063	11.05	89.494	9.9005	100.9
25	18.511	64.88	16.920	80.798	14.762	102.37	11.97	130.23	9.0905	159.0
30	23.611	63.88	21.720	82.798	19.576	104.23	16.70	132.94	13.850	161.4
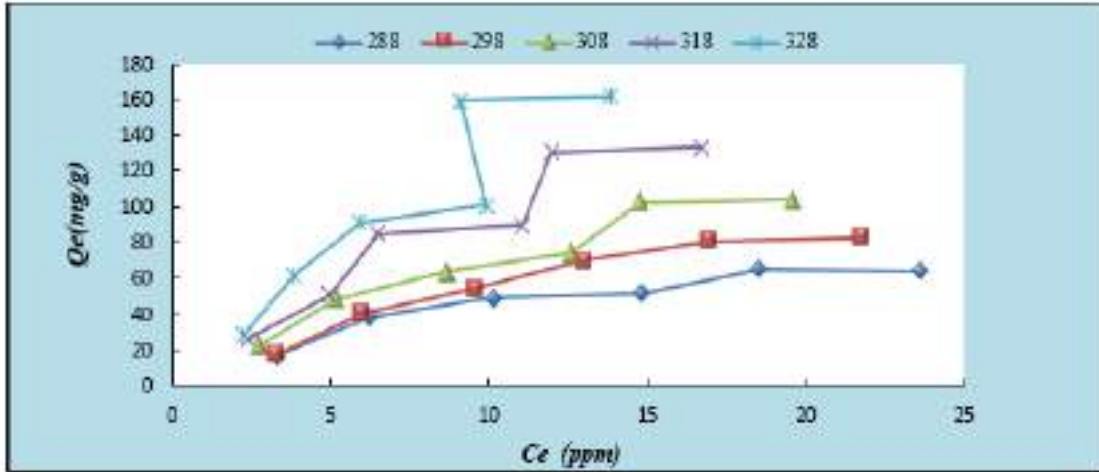
Fig. (3-37): Adsorption isotherm of BPB dye on NGO-M composite

Table (3-11): Qe and Ce values for the adsorption of BPB dye on the surface of NGO-C composite oxide at different temperatures

T (K)	288		298		308		318	
Ci ppm	Ce ppm	Q mg/g	Ce ppm	Q mg/g	Ce ppm	Q mg/g	Ce ppm	Q mg/g
5	3.934	10.658	3.690	13.098	2.986	20.130	2.3761	26.238
10	7.793	22.065	6.957	30.427	5.736	42.633	4.731	52.686
15	11.003	39.965	9.9572	50.427	8.5792	64.207	6.5057	84.942
20	14.811	51.880	12.902	70.979	11.059	89.4063	7.050	129.494
25	17.91193	70.880	15.7092	92.907	13.0762	119.237	8.0761	169.238
30	21.01193	89.880	18.0201	119.798	14.762	152.374	8.9576	210.423
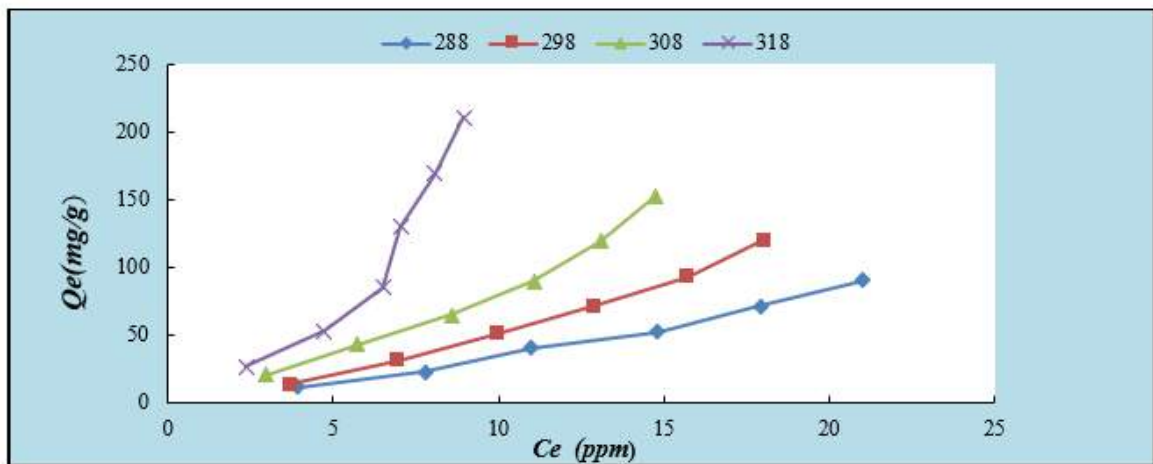
Fig. (3-38): Adsorption isotherm of BPB dye on NGO-C composite

3.3.1 Langmuir Isotherm Model

The Langmuir adsorption model suggest a single molecular layer adsorption, has been applied to the surfaces. The three composites NGO-CS, NGO-C and NGO-M were expressed according to Equation (1-3) at different temperatures drawing the relationship between C_e/Q_e versus C_e, where the slope represents a/K_L either intercept $1/K_L$.

3.3.2 Freundlich Isotherm Models

Freundlich equation was applied for the adsorption of the BPB dye on the NGO-CS, NGO-C and NGO-M composites. The isotherm was expressed according to Equation (1.6), there is a linearity between log Q_e versus log C_e, (1/ n) intersection, in order to calculate K_f.

Table (3-12) Langmuir and Freundlich parameters for the adsorption of the BPB on NGO-CS

C_i ppm	Langmuir isotherm			Freundlich isotherm		
	K_L (L.mg^{-1})	R_L	R^2	K_F	$1/n$	R^2
5	-11.5089	-0.0176	0.999	39.950	-0.359	0.9842
10	-8.49994	-0.0119	0.999	101.868	-0.352	0.9828
15	-8.45	-0.0079	0.999	167.9143	-0.3129	0.9836
20	-6.66097	-0.0075	0.999	5.08E+08	-5.29137	0.9304
25	-6.57174	-0.0061	0.999	1.22E+09	-5.51637	0.9355
30	-6.08812	-0.0579	0.999	4.67E+08	-5.110393	0.9115

Table (3-13) Langmuir and Freundlich parameters for the adsorption of the BPB on NGO-C

Ci ppm	Langmuir isotherm			Freundlich isotherm		
	K_L (L.mg^{-1})	R_L	R^2	K_F	$1/n$	R^2
5	-0.67242	-0.42336	0.999	113.7545	-1.67678	0.98
10	-0.56088	-0.21697	0.999	642.8397	-1.60290	0.9745
15	-0.637	-0.1168	0.999	1060.339	-1.3396029	0.9794
20	-0.75521	-0.0709	0.999	7.75E+20	-15.390597	0.9386
25	-0.81783	-0.05143	0.999	2.34E+20	-14.868290	0.9456
30	-0.89305	-0.03877	0.999	1.29E+20	-14.575068	0.9461

Table (3-14): Langmuir and Freundlich parameters for the adsorption of the BPB onto NGO-M composite.

Ci ppm	Langmuir isotherm			Freundlich isotherm		
	K_L (L.mg^{-1})	R_L	R^2	K_F	$1/n$	R^2
5	-1.20029	-0.19994	0.999	75.73087	-1.2398	0.9908
10	-1.3695	-0.07877	0.999	230.2888	-0.97101	0.9851
15	-0.915	-0.07857	0.999	643.745	-1.0961723	0.9878
20	-0.44815	-0.12558	0.999	1.74E+15	-10.852581	0.9270
25	-0.60971	-0.07021	0.999	9.09E+20	-15.390542	0.9728
30	-0.31874	-0.11679	0.999	1.89E+21	-15.644966	0.9702

The $R_L < 1$ for all samples, which indicate the adsorption of BPB dye on three composites are irreversible [98]. Table (3-12), (3-13) and (3-14) shows that $1/n < 1$ of the Freundlich isotherm for the three composites, $1/n$ values are less than one which shows much of heterogeneity as a result of diversity within the shapes and sizes of the adsorbent pores[98].

3.4 Adsorption Thermodynamics

The temperature influence of BPB dye adsorption on NGO-CS, NGO-C and NGO-M composite surfaces were studied at temperature, 288, 298, 308, 318, and 328 k. The thermodynamic parameters provide details about the intrinsic energy modifications which related to the adsorption. The parameters, free energy ($\Delta G°$), enthalpy ($\Delta H°$) and entropy ($\Delta S°$) of the adsorption were estimated by following Equations[98].

$$\ln K_{eq} = \frac{\Delta S°}{R} - \frac{\Delta H°}{R} * T \text{ .... (3.4)}$$

$$K_{eq} = Q_e / C_e \text{ .... (3.5)}$$

$$\Delta G° = \Delta H° - T\Delta S° \text{ .... (3.6)}$$

Where:

T is the absolute temperature (K)

K_{eq} is the ability of adsorbate to retain and a measure of its movement within the solution

R is the general gas constant (8.314 J. $K^{-1}mol^{-1}$)

Q_e is the equilibrium capacity of adsorption (mg/g).

(ΔH) and (ΔS) can be calculated from the slope and the intercept by drawing Van't Hoff plot (ln K) versus (1/T)

Where:

Slope = $-\Delta H/R$

Intercept = $\Delta S /R$.

The estimated thermodynamic data for the adsorption of BPB dye on NGO-CS, NGO-C and NGO-M composites are shown in Table (3-15, 3-16 and 3-17) and from Fig. (3-39) to Fig. (3-56).The adsorption capacity increased with rising

temperature, that means the process was endothermic, $\Delta H°$ was positive, all value of $\Delta H < 40$ KJ/mol, so the adsorption of BPB dye on three composites is physical. while the entropy $\Delta S°$ was positive describe increasing in randomness.The ΔG was negative of the adsorption BPB dye for the three composites, confirmed spontaneously of the adsorption processes, ΔG values also determine the rate of the adsorption reaction, $\Delta G < 0$ indicates physisorption process and indicated the dominate adsorption too[99].

Fig. (3-39): Van't Hoff plot for adsorption of (5mg.L^{-1}) BPB dye on NGO-CS composite

Fig. (3-40): Van't Hoff plot for adsorption of (10 mg. L^{-1}) BPB dye on NGO-CS composite

Fig. (3-41): Van't Hoff plot for adsorption of (15 mg.L $^{-1}$) BPB dye on NGO-CS composite

Fig. (3-42): Van't Hoff plot for adsorption of (20 mg.L $^{-1}$) BPB dye on NGO-CS composite

Fig. (3-43): Van't Hoff plot for adsorption of (25mg.L $^{-1}$) BPB dye on NGO-CS composite

Fig. (3-44): Van't Hoff plot for adsorption of (30 mg.L $^{-1}$) BPB dye on NGO-CS composite

Table (3-15): Thermodynamic parameters for adsorption of BPB dye on NGO-CS composite

C_i mg/L	ΔH (KJ/mol)	ΔS (J/K.mol)	ΔG (KJ/mol)			
			288 K	298 K	308 K	318 K
5	24.43231	108.054	-6.68723	-7.76777	-8.84831	-9.9288
10	24.48201	108.739	-6.83484	-7.92223	-9.00962	-10.097
15	22.96935	104.663	-7.1736	-8.22023	-9.26686	-10.313
20	27.22778	118.8321	-6.99585	-8.18417	-9.3725	-10.56
25	29.80365	127.9129	-7.03527	-8.3144	-9.5935	-10.872
30	26.97772	118.8597	-7.25387	-8.44247	-9.631	-10.819
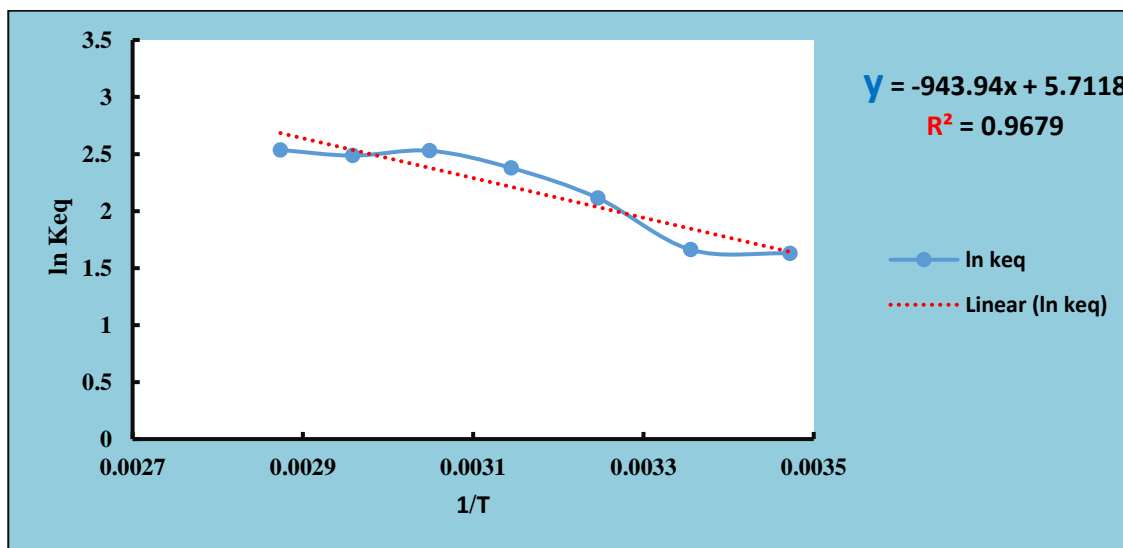
Fig. (3-45): Vanʼt Hoff plot for adsorption of (5 mg.L $^{-1}$) BPB dye on NGO-M composite
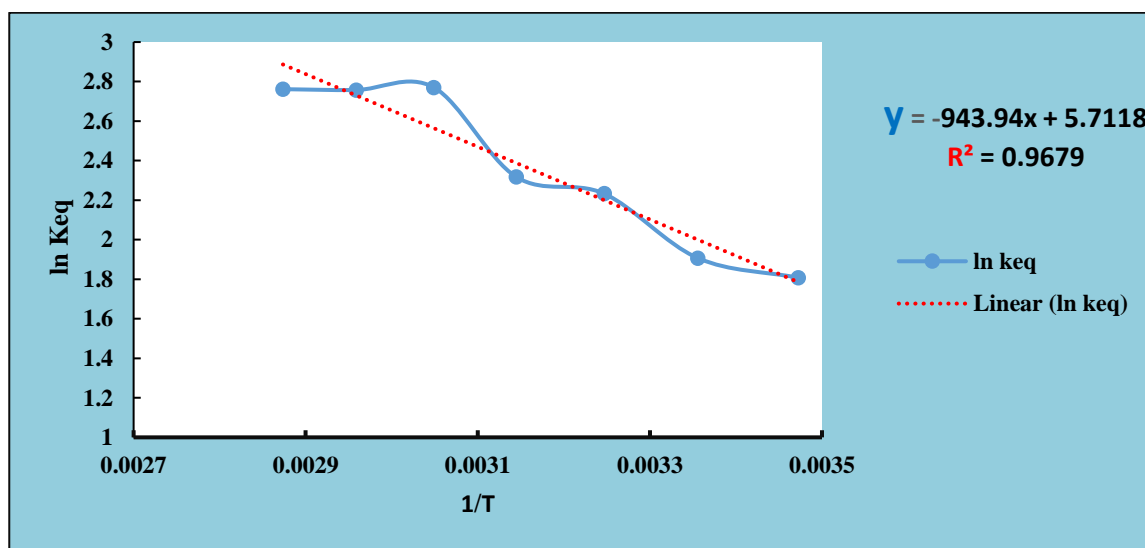
Fig. (3-46): Vanʼt Hoff plot for adsorption of (10 mg .L $^{-1}$) BPB dye on NGO-M composite
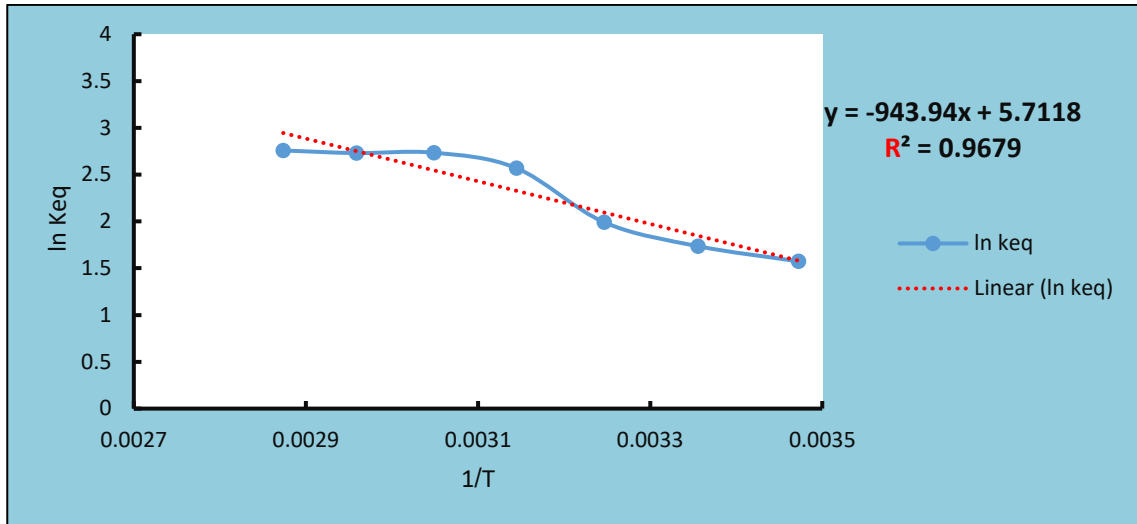
Fig. (3-47): Van't Hoff plot for adsorption of (15 mg. L^{-1}) BPB dye on NGO-M composite
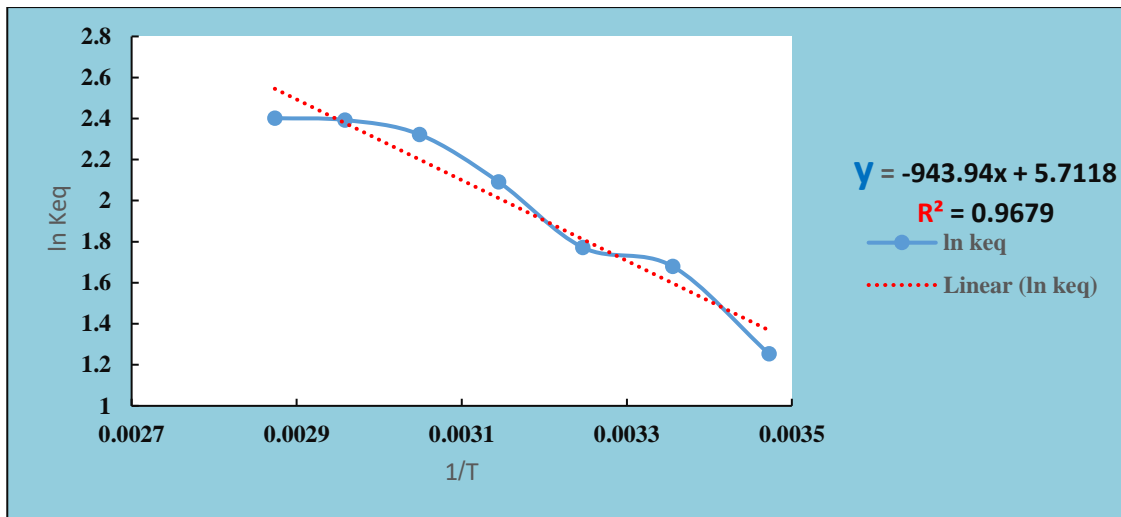
Fig. (3-48): Van't Hoff plot for adsorption of (20 mg.L^{-1}) BPB dye on NGO-M composite
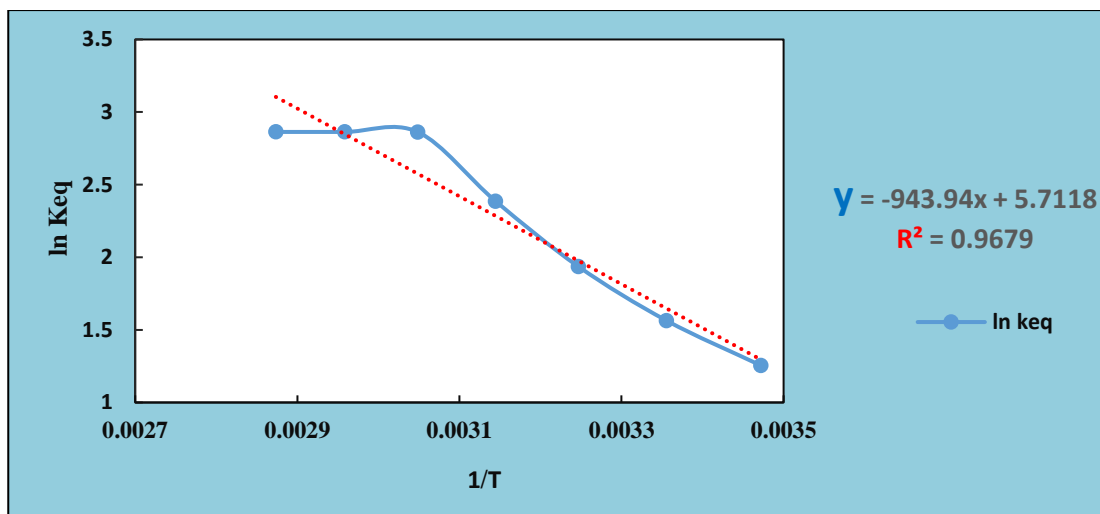
Fig. (3-49): Van't Hoff plot for adsorption of (25 mg.L^{-1}) BPB dye on NGO-M composite
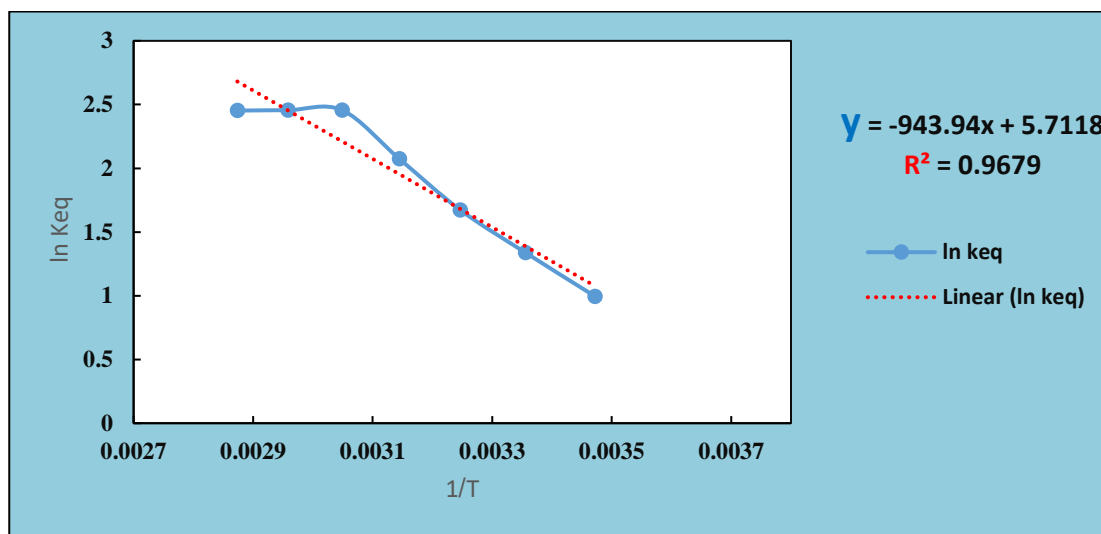
Fig. (3-50): Van't Hoff plot for adsorption of (30 mg.L $^{-1}$) BPB dye on NGO-M composite

Table (3-16): Thermodynamic parameters for the adsorption of BPB dye on NGO-M composite

Ci mg/L	ΔH KJ/mol	ΔS J/K.mol	ΔG KJ/mol						
			288 K	298 K	308 K	318 K	328 K	338	348
5	14.47	63.90	-3.9309	-4.57	-5.209	-5.984	-6.487	-7.126	-7.765
10	15.28	67.92	-4.2762	-4.95551	-5.634	-6.314	-6.993	-7.672	-8.351
15	18.94	78.91	-3.7850	-4.5742	-5.363	-6.152	-6.941	-7.730	-8.520
20	16.33	68.10	-3.2765	-3.9575	-4.638	-5.319	-6.000	-6.681	-7.363
25	25.13	98.02	-3.0999	-4.0802	-5.060	-6.040	-7.021	-8.001	-8.981
30	22.29	86.34	-2.5764	-3.43994	-4.303	-5.166	-6.030	-6.893	-7.757
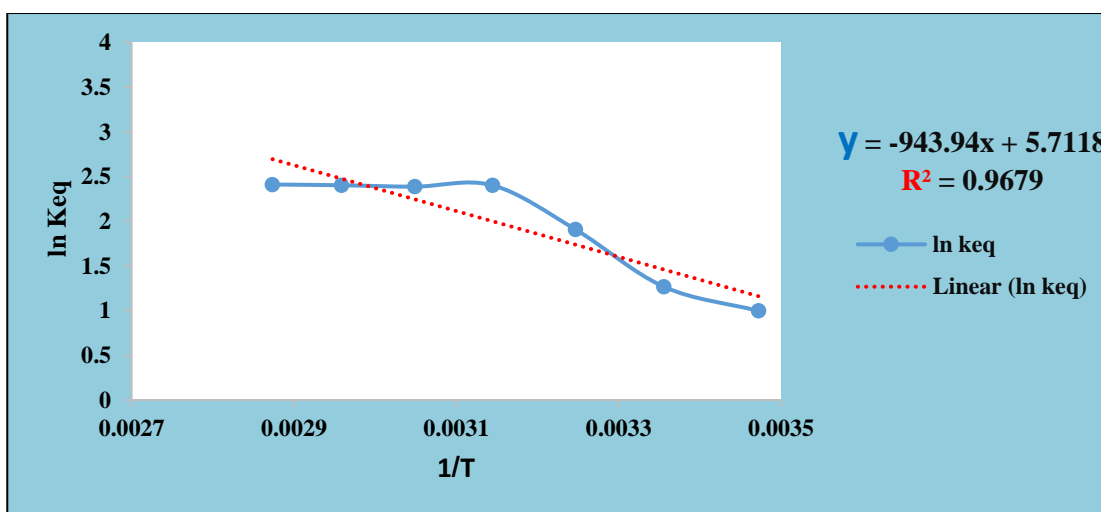
Fig. (3-51): Van't Hoff plot for adsorption of (5 mg.L $^{-1}$) BPB dye on NGO-C composite
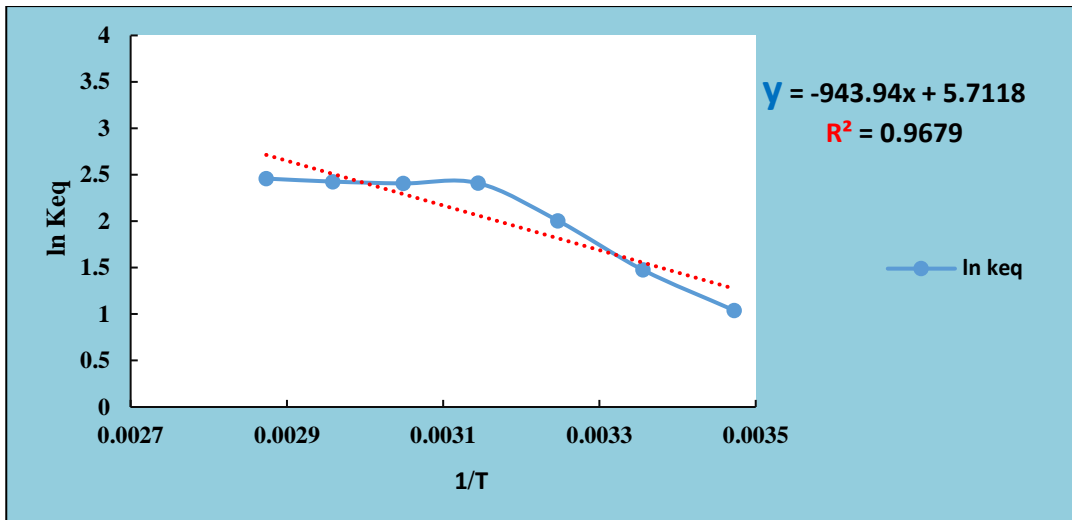
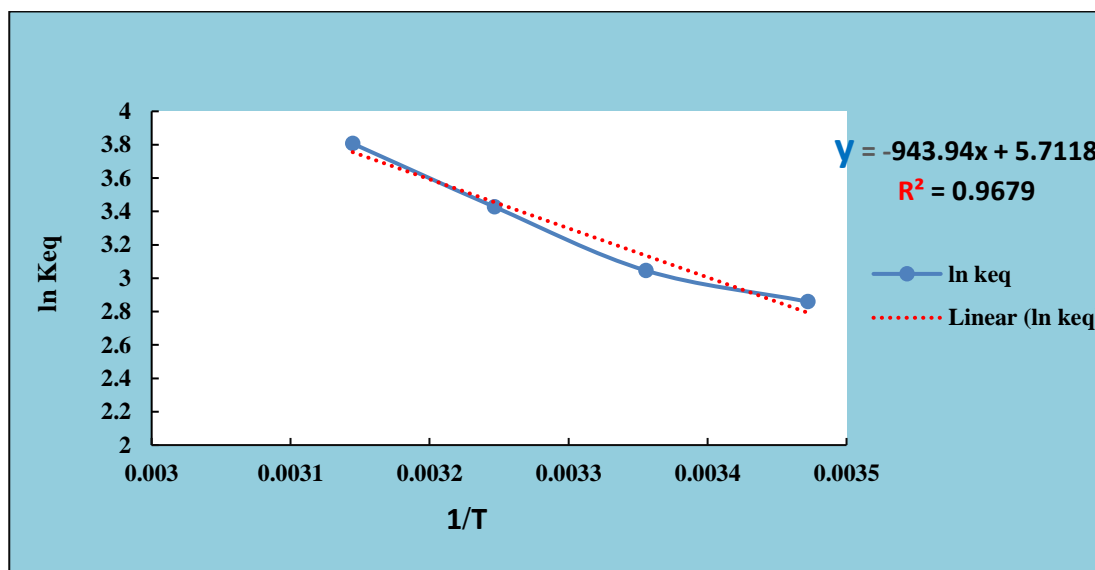Fig. (3-52): Van't Hoff plot for adsorption of (10 mg.L $^{-1}$) BPB dye on NGO-C composite
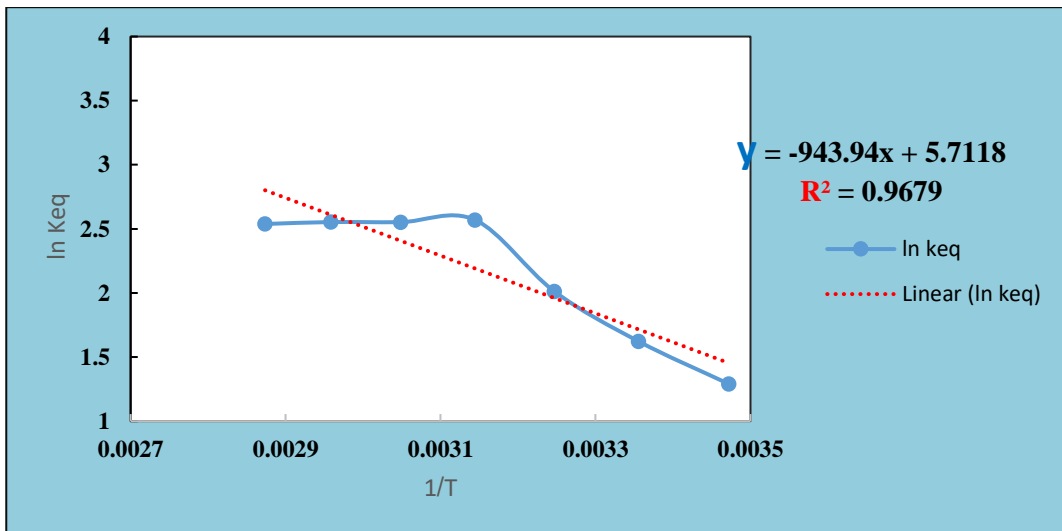
Fig. (3-53): Van't Hoff plot for adsorption of (15 mg.L $^{-1}$) BPB dye on NGO-C composite
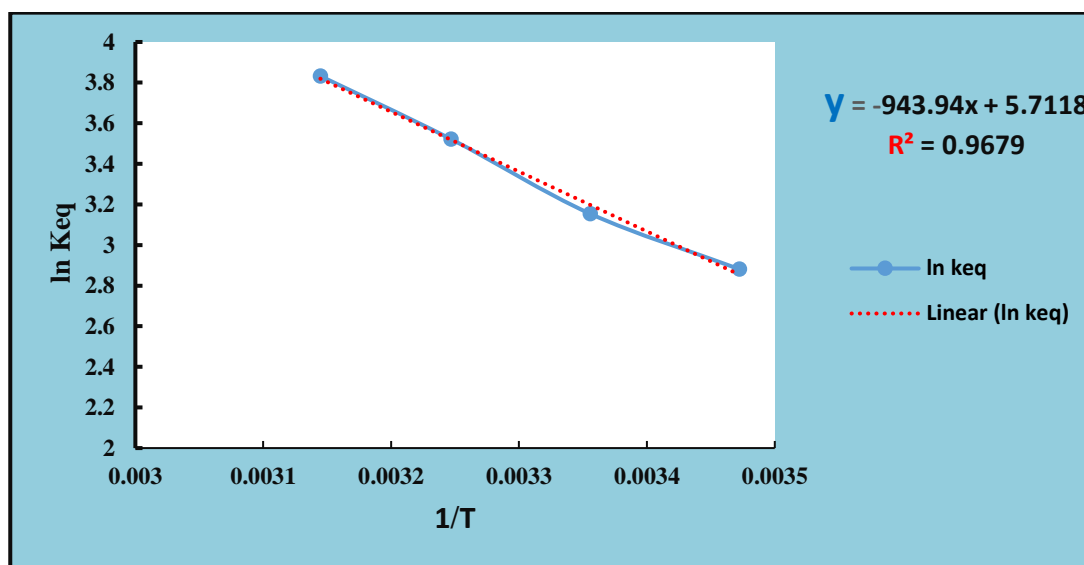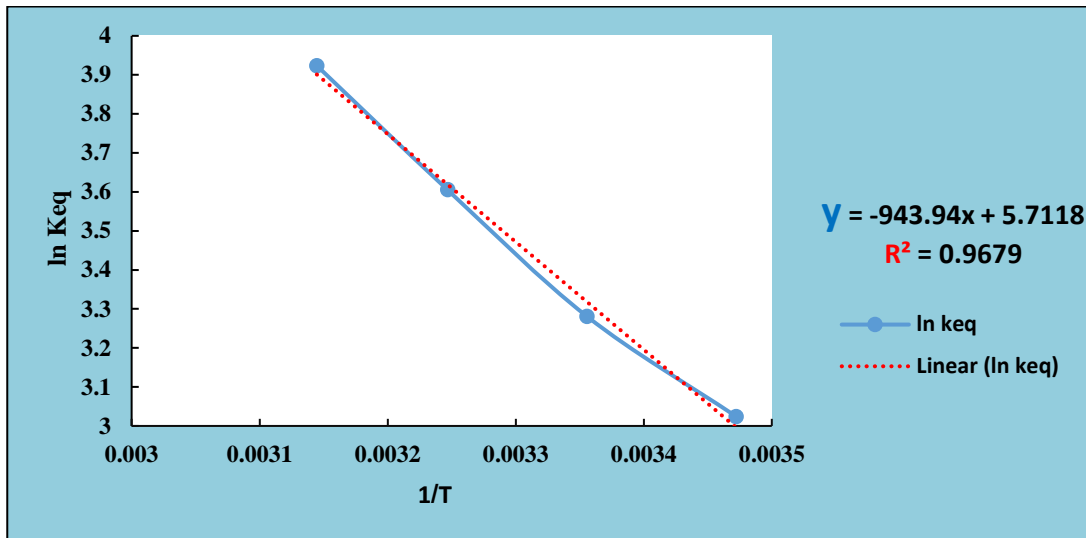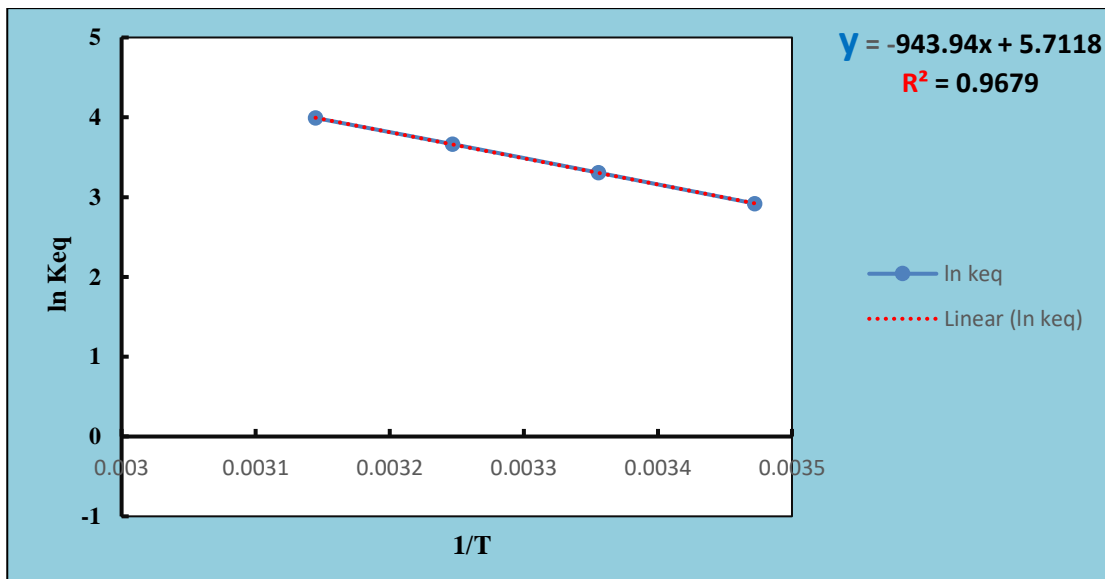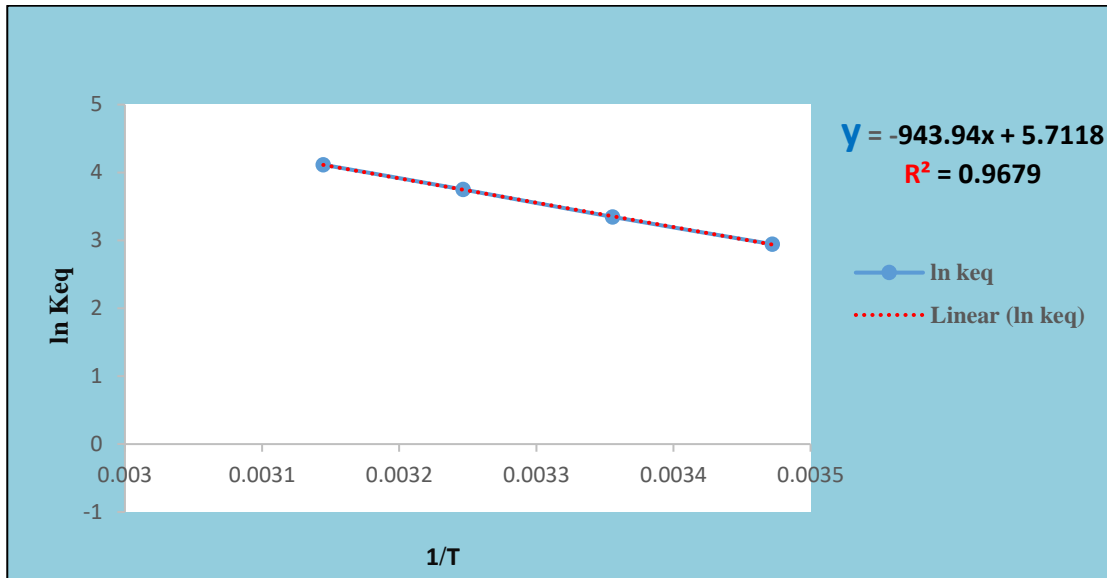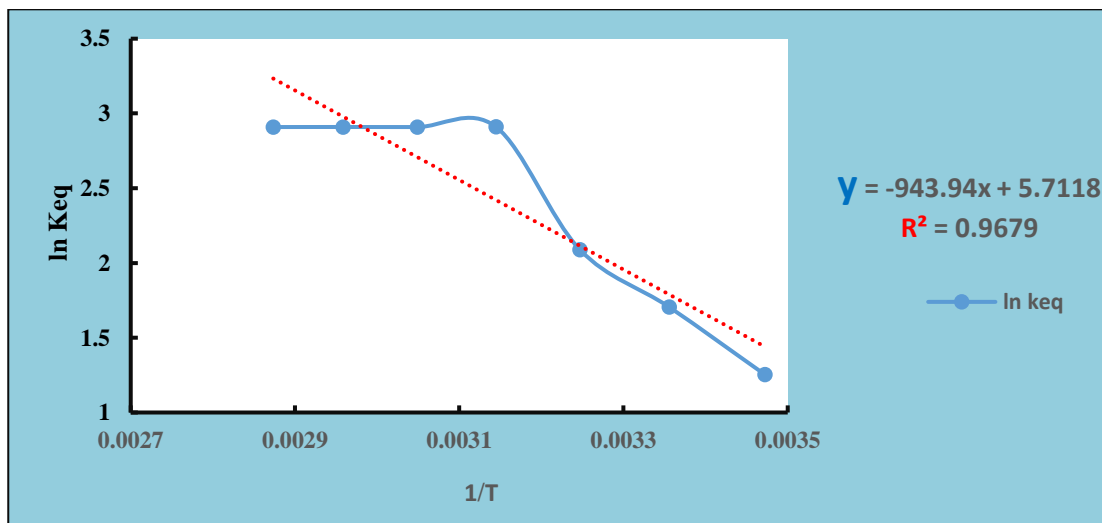

Fig. (3-54): Van't Hoff plot for adsorption of (20 mg.L $^{-1}$) BPB dye on NGO-C composite

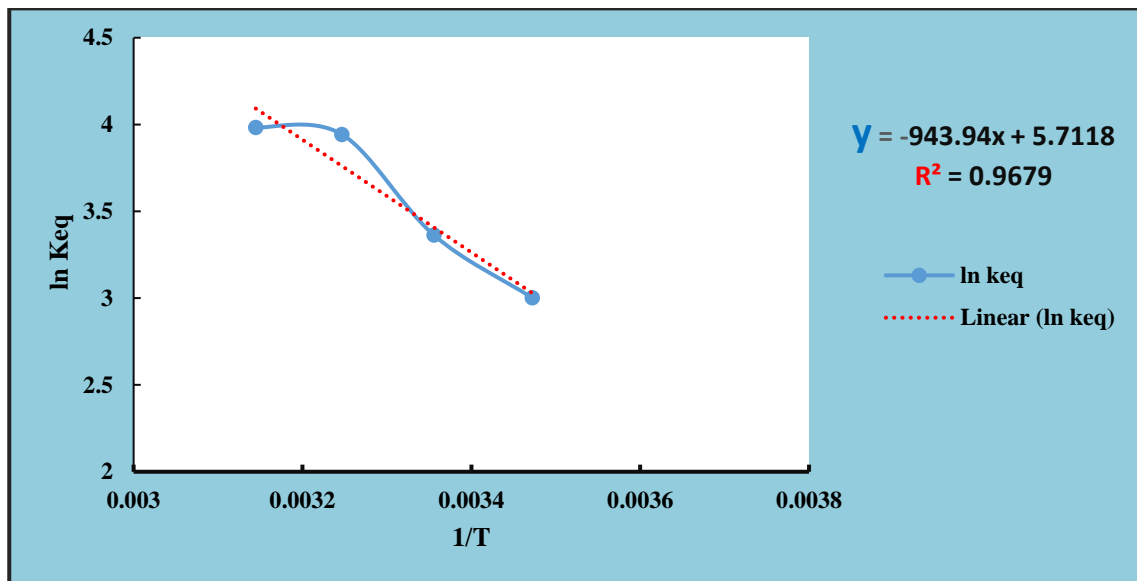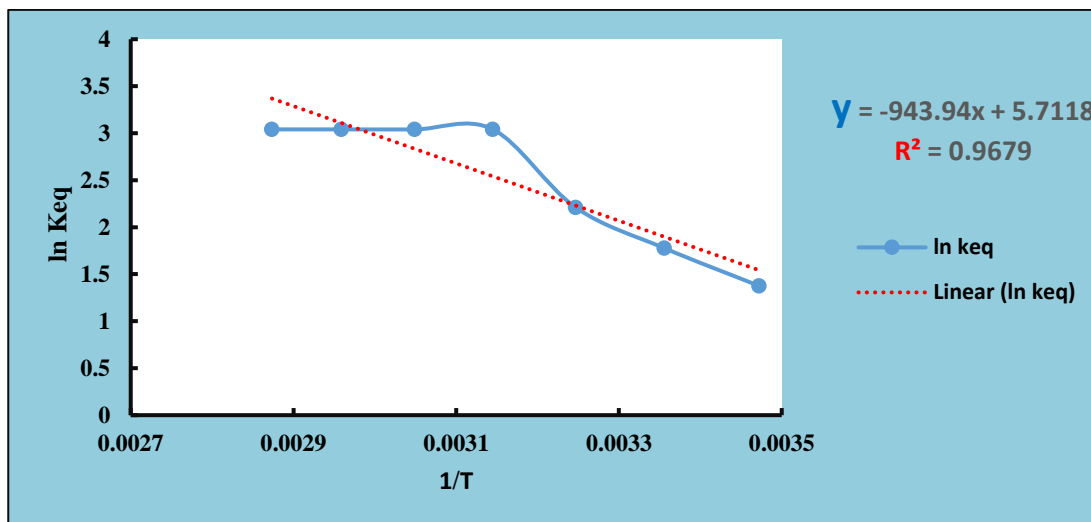Fig. (3-55): Van't Hoff plot for adsorption of (25 mg.L^{-1}) BPB dye on NGO-C composite
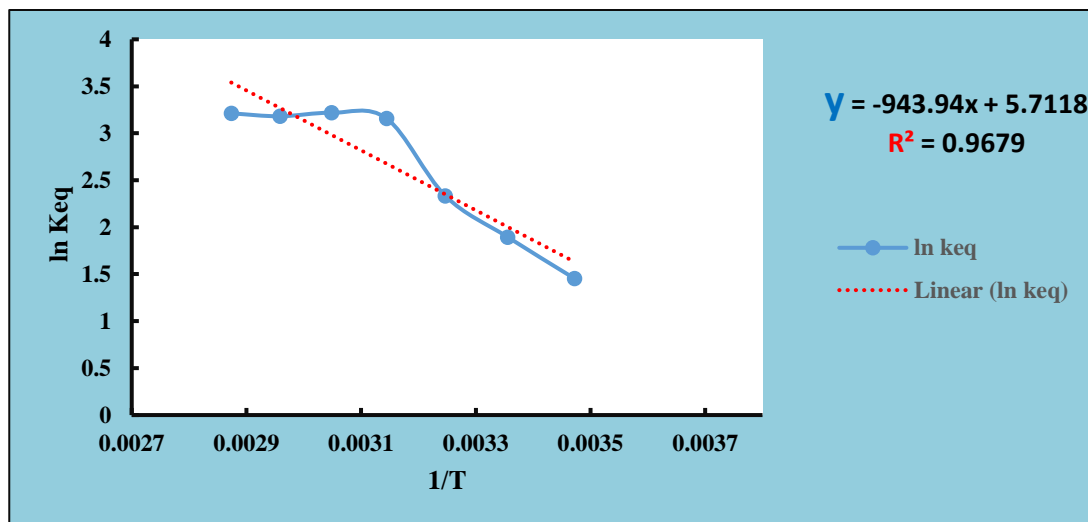
Fig. (3-56): Van't Hoff plot for adsorption of (30 mg.L^{-1}) BPB dye on NGO-C composite

Table (3-17): Thermodynamic parameters for the adsorption of BPB dye on NGO-C composite

Ci mg/L	ΔH (KJ/mol)	ΔS (J/K.mol)	ΔG (KJ/mol)						
			288 K	298 K	308 K	318 K	328 K	338 K	348 K
5	21.2871	83.56	-2.7793	-3.6150	-4.450	-5.2863	-6.121	-6.957	-7.793
10	19.998	80.03	-3.0510	-3.8513	-4.651	-5.452	-6.252	-7.052	-7.853
15	18.7203	77.082	-3.4794	-4.2502	-5.021	-5.791	-6.562	-7.333	-8.104
20	24.901	98.43	-3.4484	-4.4328	-5.417	-6.4015	-7.385	-8.370	-9.354
25	253665	100.9032	-3.6935	-4.7026	-5.711	-6.7206	-7.729	-8.738	-9.747
30	26.5136	105.621	-3.9052	-4.9615	-6.017	-7.0739	-8.130	-9.186	-10.24

3.5 Adsorption Kinetic

Two models, pseudo-first-order and pseudo-second-order, may be used to explain the experimental data to characterise the mechanism of adsorption and the potential rate[100].

3.5.1 Pseudo-First Order Model

The pseudo-first-order kinetic model is given by the following equation[98][100].

ln (Qe - Qt) = ln Qe - K$_1$ .t .... (3.7)

Where: Q_t: is the adsorption capacity(mg.g^{-1}) at any time (min), Q_e: is the adsorption capacity at equilibrium (mg. g^{-1}), K_1: is the pseudo-first-order rate constant for the adsorption process (min^{-1}).

The linearity of ln ($Q_e - Q_t$) vs (t).), the slope equal K_1, Qe calculated from intercept as shown in Table (3-18, 3-19 and 3-20) , Fig. (3-57, 3-58 and 3-59) show the pseudo-first-order data for BPB dye adsorption on NGO-CS, NGO-C and NGO-M composites.

Table (3-18): Pseudo-first order parameters for the adsorption of the BPB on NGO-CS composite

t (min)	Qt (mg/g)	t/Qt(min.g/mg)	Qe-Qt	ln (Qe-Qt)	Ce (ppm)
15	58.9211	0.2545	8.2987	2.1161	4.1078
30	64.3153	0.4664	2.9045	1.0662	3.5684
45	65.5601	0.6863	1.6597	0.5066	3.4439
60	66.3900	0.9037	0.8298	-0.1864	3.3609

Table (3-19): Pseudo-first order parameters for the adsorption of the BPB on NGO-M composite

t(min)	Qt(mg/g)	t/Qt (min. g/mg)	Qe-Qt	ln (Qe-Qt)	Ce(ppm)
15	23.0645	0.6503	5.6451	1.7308	5.3871
30	27.0968	1.1071	1.6129	0.4780	4.5806
45	27.5806	1.6315	1.1290	0.1213	4.4838

Table (3-20): Pseudo-first order parameters for the adsorption of the BPB on NGO-C composite

t(min)	Qt(mg/g)	t/Qt (min. g/mg)	Qe-Qt	ln (Qe-Qt)	Ce(ppm)
15	42.3611	0.3541	22.2222	3.1010	5.76389
30	52.0833	0.5761	12.5002	2.5257	4.79167
45	54.1667	0.8307	10.4166	2.3434	4.58333
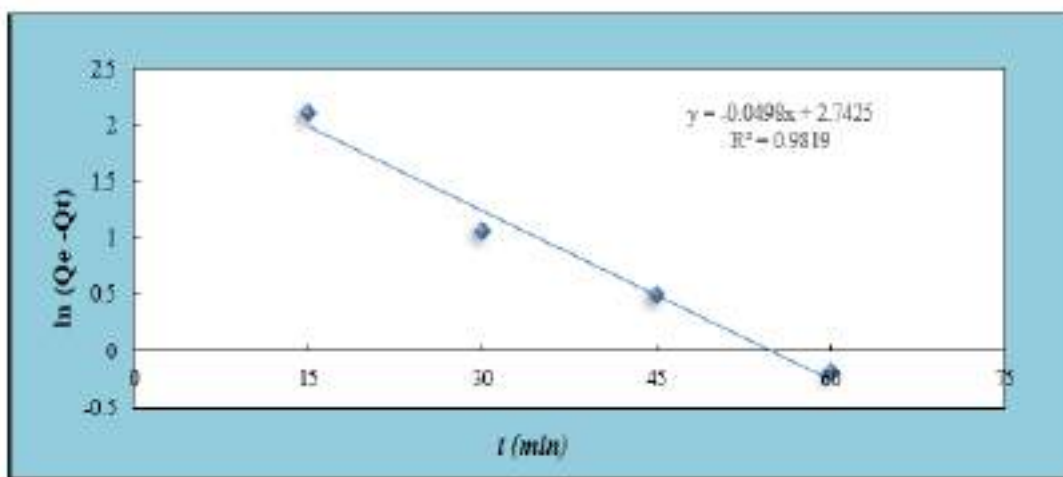
Fig. (3-57): Pseudo-first orders kinetic plots for BPB dye adsorption on NGO-CS composite

92
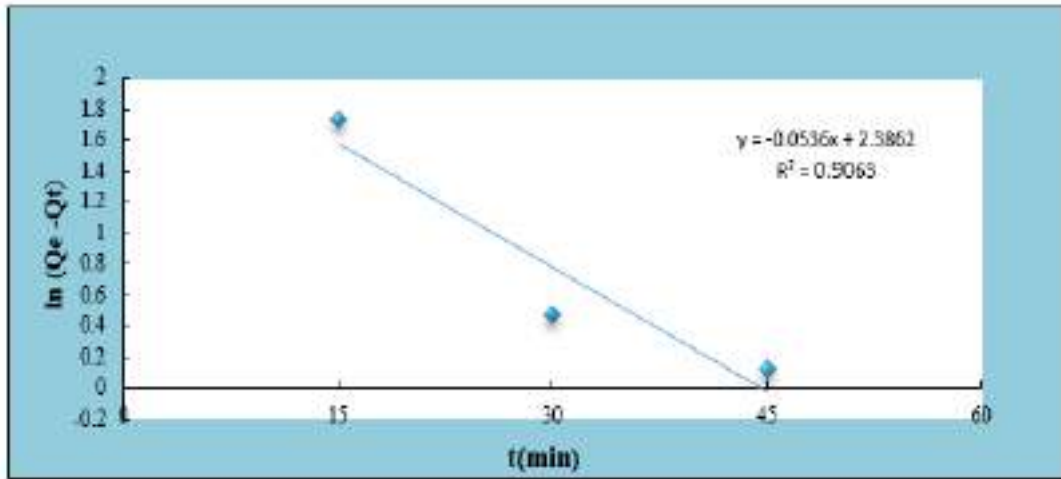
Fig. (3-58): Pseudo-first orders kinetic plots for BPB dye adsorption on NGO-M composite
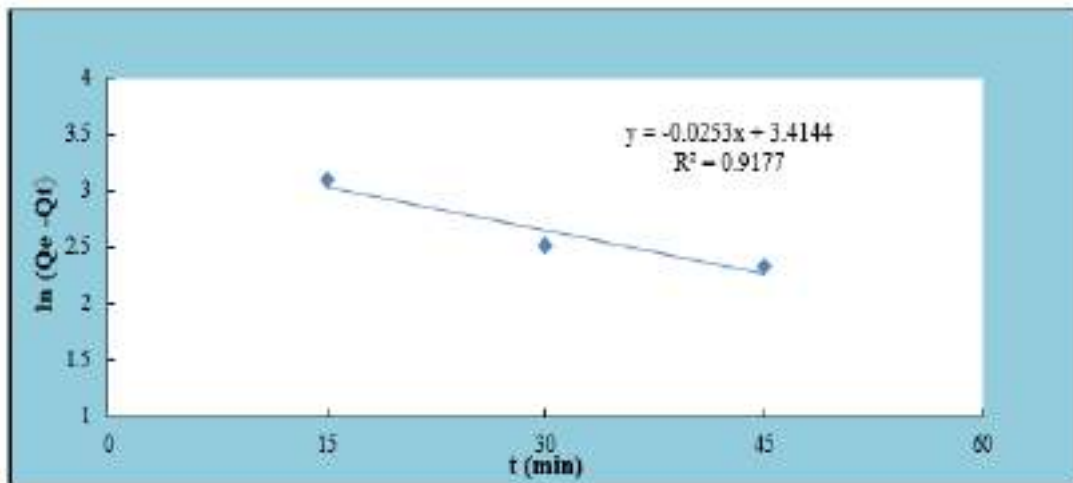
Fig. (3-59): Pseudo-first orders kinetic plots for BPB dye adsorption on NGO-C composite

3.5.2 Pseudo-Second Order Model

Pseudo-second order kinetic model is given by the Equation (3.7)[98] [100].

t /Qt= 1 /K₂   Qe² + (1∕Qe). t .... (3.8)

Where: Q_t is the adsorption capacity at any time (mg/g), Q_e is the adsorption capacity at equilibrium (mg/g), t: is the adsorption time (min), K_2 is the rate constant (g/mg. min).
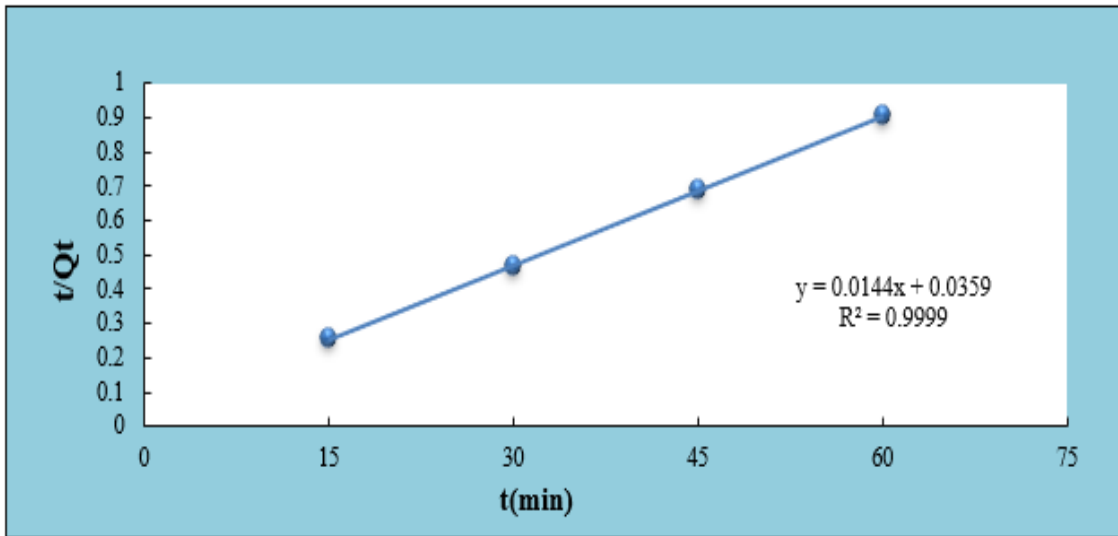
Fig. (3-60): Pseudo-second order parameters for the adsorption of the BPB dye on NGO-CS composite
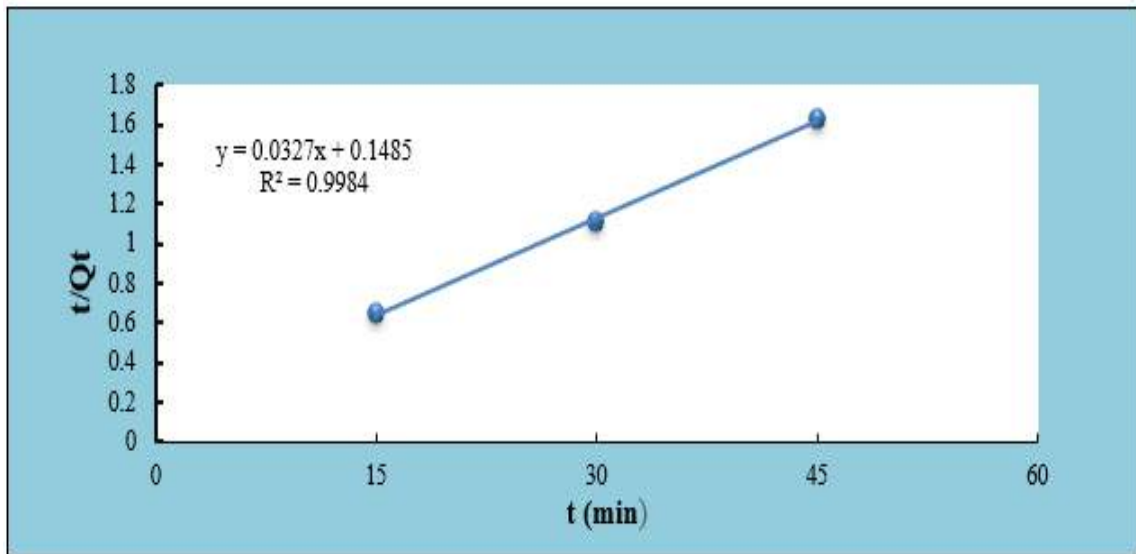
Fig. (3-61): Pseudo-second order parameters for the adsorption of the BPB dye on NGO-M composite
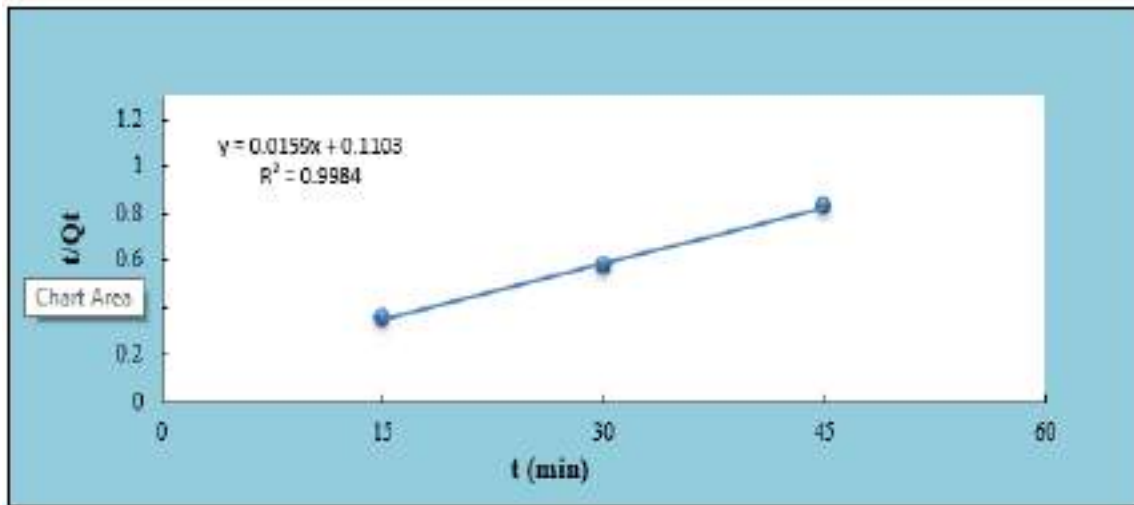
Fig. (3-62): Pseudo-second order parameters for the adsorption of the BPB dye on NGO-C composite

Table (3-21): R^2, K_1, K_2 and Qe (cal.) of Pseudo-first and second order for the adsorption of the BPB dye on NGO-CS, NGO-M and NGO-C composites

First order				
Composite	**Qe Exp.**	**Qe Cal.**	**R^2**	**K_1 (min^{-1})**
NGO-CS	67.2199	15.5255	0.9819	-0.0497
NGO-M	28.7096	10.8717	0.9068	-0.0536
NGO-C	64.5833	30.3995	0.9177	-0.0252
Second order				
Composite	**Qe Exp.**	**Qe Cal.**	**R^2**	**K_2 g/mg.min^{-1}**
NGO-CS	67.2199	69.2054	0.9999	0,0061
NGO-M	28.7096	30.5738	0.9984	0.0072
NGO-C	64.58333	62.9365	0.9984	0.0022

The calculated (Qe, cal.) from the pseudo-second order model matches well the experimental data (Qe, exp.), good linearity with correlation coefficients (R^2) above 0.99. These results confirm that pseudo-second order kinetic model is more valid to describe the adsorption behavior of BPB dye on NGO-CS, NGO-C and NGO-M composites [100].

3.6 Desorption

Equation (1.8) used to calculate the percentage of desorption of BPB dye was (42.126%) from NGO-CS composite, at λ max =409.5 nm.

3.7 Applications of Membranes

3.7.1 Separation of BPB Dye by NGO, CS, NGO-CS, NGO-M and NGO-C Membranes

The experimental data is show the removal % of BPB dye by the membranes in the order NGO-CS > CS > NGO-C >NGO-M > NGO, the best membrane is NGO-CS, where % R (98.5%), as show in Fig.(3-63). The mechanism analysis indicated that this membrane adsorbed dyes mainly through physical sieving, electrostatic interaction, and hydrogen bonds[69].
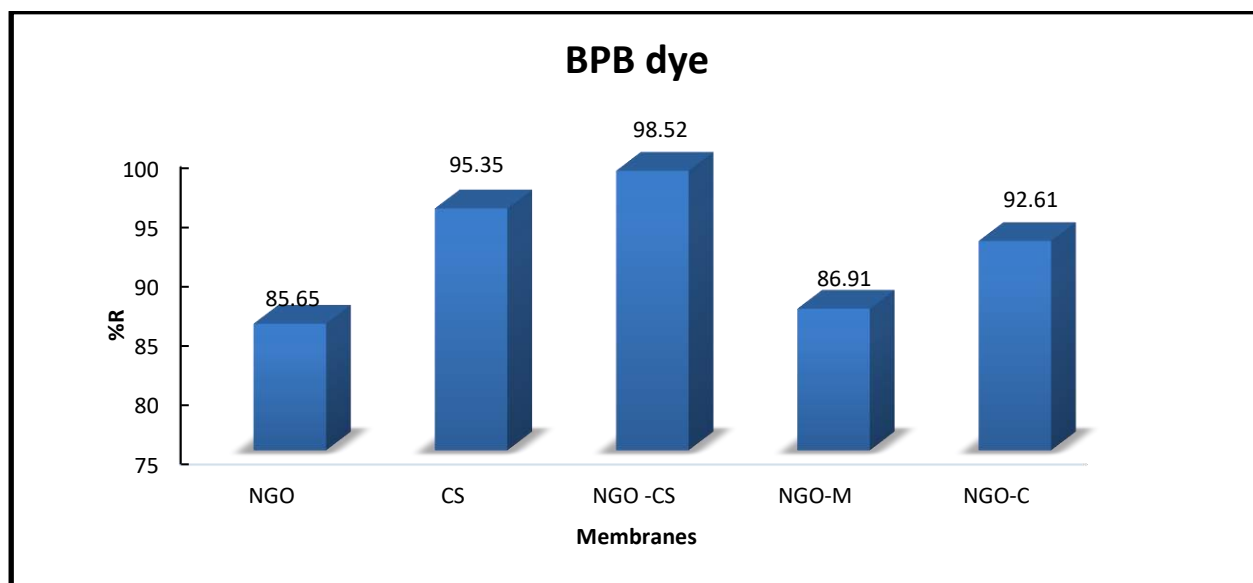
Fig. (3-63): Removal percentage of BPB dye by NGO, CS, NGO-CS, NGO-M and NGO-C membranes

(A)	(B)	(C)
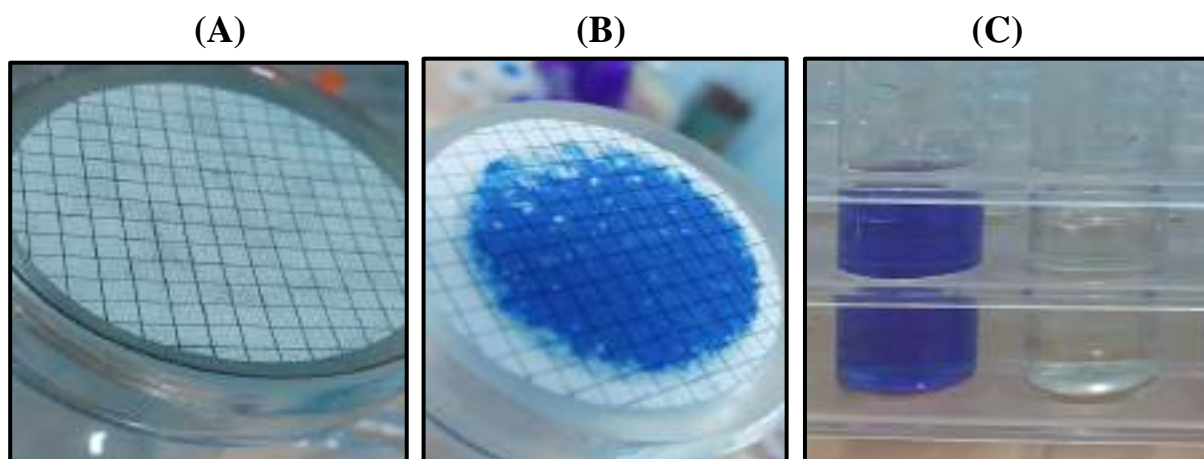
Fig. (3-64): NGO-CS membrane (A, B) before and after separation of BPB dye respectively (B) Solution of BPB dye before and after separation by NGO-CS membrane

3.7.2 Separation of Ni²⁺, Cd²⁺, Co²⁺, Cu²⁺ and Pb²⁺ Ions by NGO, CS NGO-CS, NGO-M and NGO-C Membranes

The results of separation the heavy metal ions by the membranes are fluctuating and irregular, the experimental data shows the removal percentage of Ni^{2+} and Co^{2+} ions by the membranes were in the order NGO-CS > NGO-C >NGO-M > CS > NGO, the best membrane is NGO-CS, R% (48.47%) and (68.17%) as show in Fig.(3-65) and Fig.(3-67) respectively.While, Cd^{2+} ions follow the order CS > NGO-M > NGO > NGO-CS > NGO-C, the best membrane is CS, where R% (52.2 %) as show in Fig.(3-66) .The Cu^{2+} ions follow the order NGO-M > NGO-C > NGO> NGO-CS> CS, the best membrane is NGO-M, ,where R% (66.47%) as show in Fig.(3-68). On the other hand, Pb^{2+} ions follow the order NGO-CS > NGO >NGO-M > NGO-C > CS, the best membrane is NGO-CS where R% (67.04%), as show in Fig.(3-69).
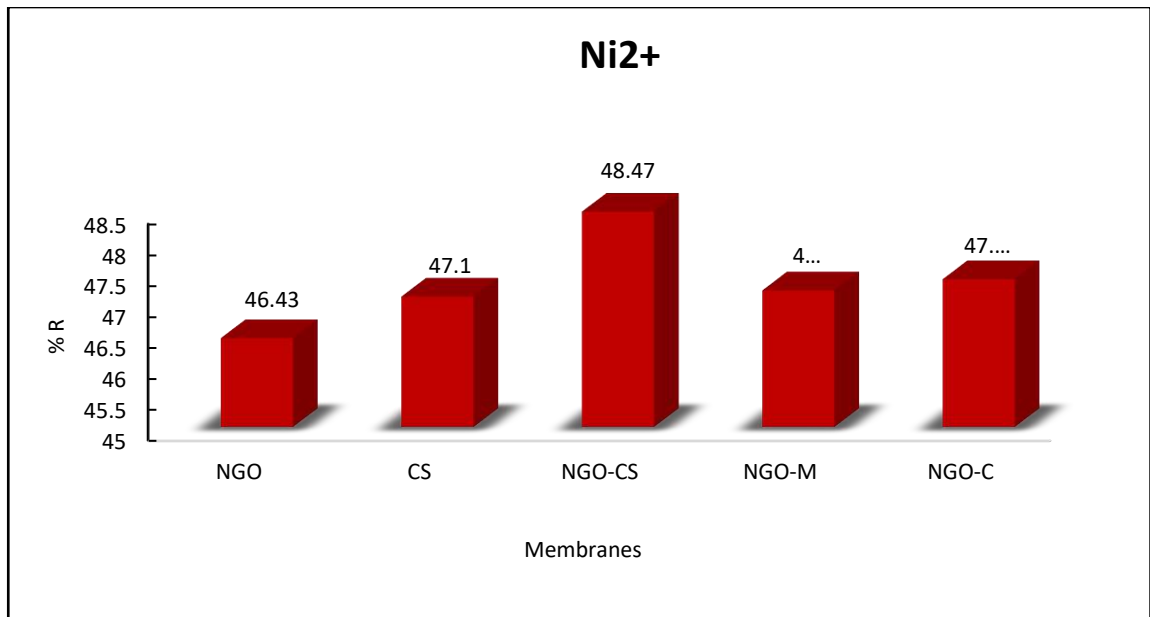
Fig. (3-65): Removal % of Ni^{2+} ions by NGO, CS, NGO-CS, NGO-M and NGO-C membranes
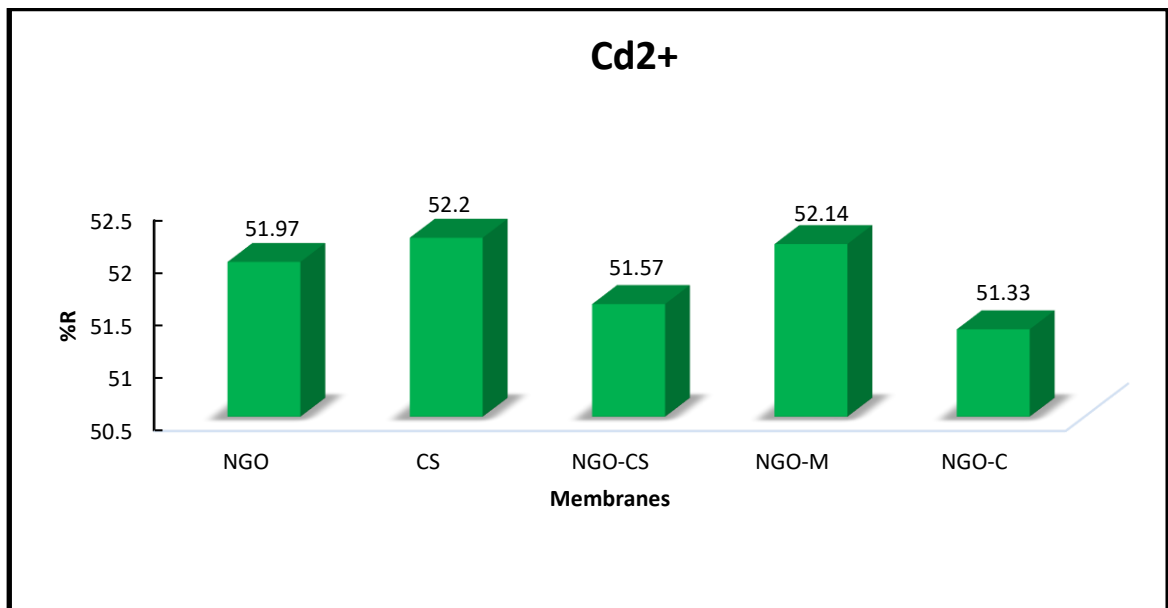
Fig. (3-66): Removal % of Cd^{2+} ions by NGO, CS, NGO-CS, NGO-M and NGO-C membranes
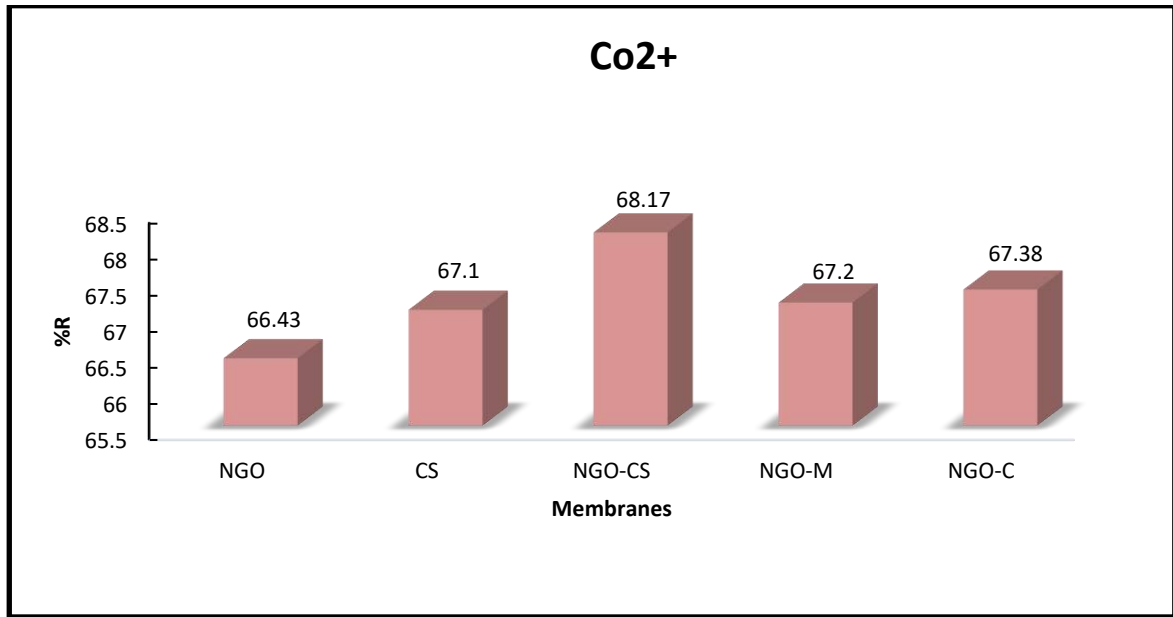
Fig. (3-67): Removal % of Co^{2+} ions on NGO, CS, NGO-CS, NGO-M and NGO-C membranes
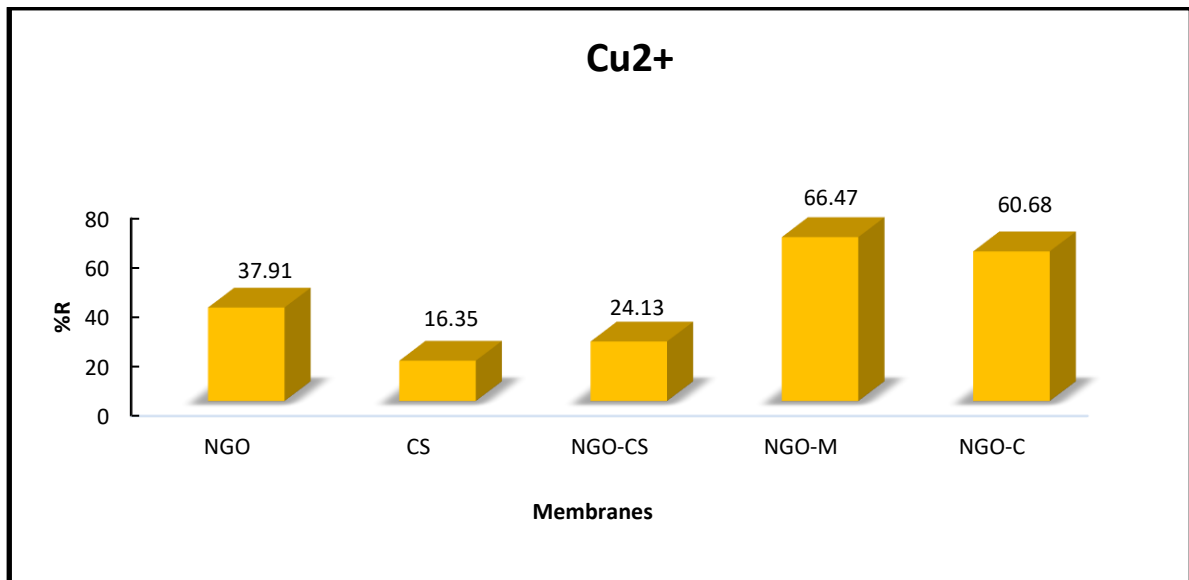
Fig. (3-68): Removal % of Cu^{2+} ions on NGO, CS, NGO-CS, NGO-M and NGO-C membranes
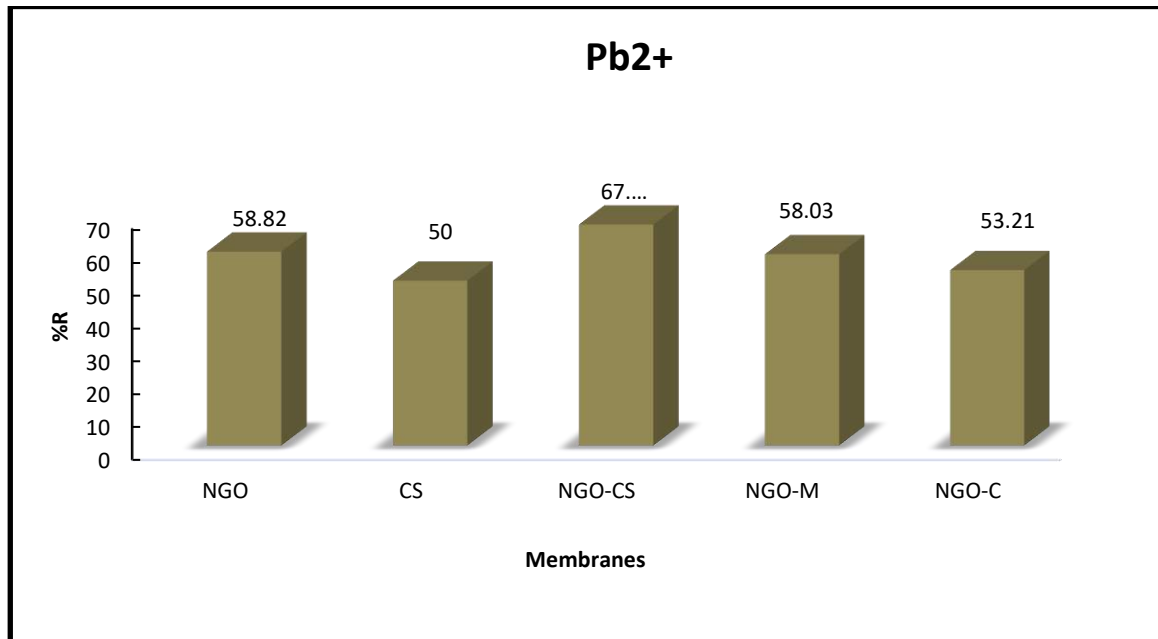
Fig. (3-68): Removal % of Cu^{2+} ions on NGO, CS, NGO-CS, NGO-M and NGO-C membranes

Table (3.22): Removal % of Ni^{2+}, Cd^{2+}, Co^{2+}, Cu^{2+} and Pb^{2+} ions by NGO, CS, NGO-CS, NGO-M and NGO-C membranes

Membranes	Removal %				
	Ni^{2+}	Cd^{2+}	Co^{2+}	Cu^{2+}	Pb^{2+}
NGO	46.43	51.97	66.43	37.91	58.82
CS	47.1	**52.2**	67.1	16.35	50
NGO-CS	**48.47**	51.57	**68.17**	24.13	**67.04**
NGO-M	47.2	52.14	67.2	**66.47**	58.03
NGO-C	47.38	51.33	67.38	60.68	53.21

100
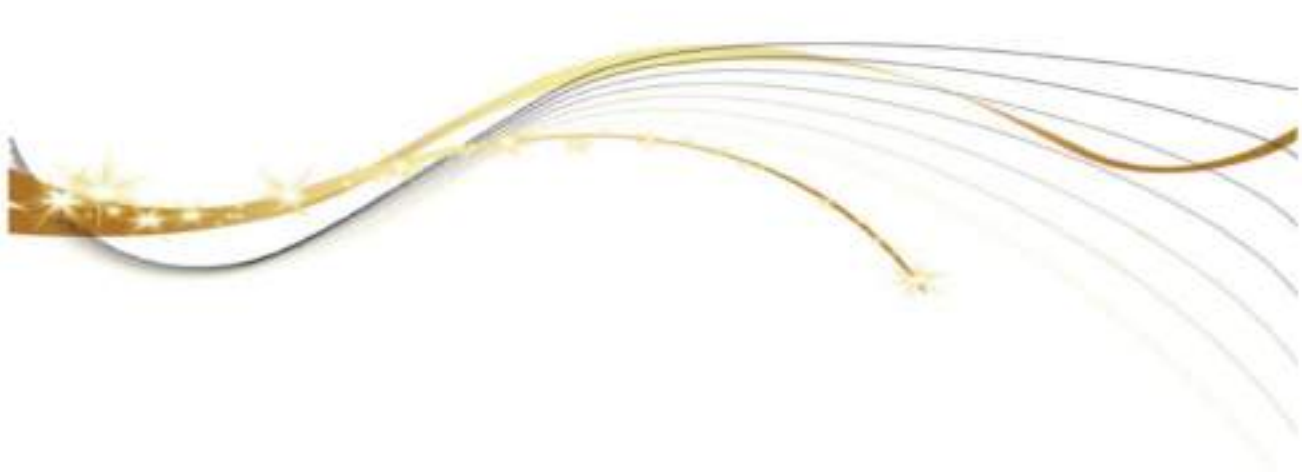
Conclusions and Recommendation

Conclusions and Recommendation

Conclusions

1- The following composites (NGO-CS, NGO-M, NGO-C) are formed, the amine group in chitosan polymers, amino acids (methionine and cysteine) are binding with the carboxylic acid or the epoxide group on the surface of nano-graphene oxide, according to FT-IR analysis.

2- The adsorption capacity Qe (mg/g) of the BPB dye on NGO-CS, NGO-M and NGO-C composites, were affected with the adsorption conditions, it was found to decrease with raising the pH, the best adsorption capacity occurs in the acidic medium, decreases with increasing the dosage of the composite and increasing the ionic strength, while increases with the contact time, temperature and dye concentration.

3- The general form of adsorption isotherms of BPB dye on NGO-CS, NGO-M and NGO-C composites is S-type according to the Giles classification.

4- The adsorption of BPB dye on NGO-CS, NGO-M and NGO-C composites are spontaneous ΔG (-) and endothermic ΔH (+) process. The results confirm that pseudo-second order kinetic model is more valid to describe the adsorption behavior of BPB dye on NGO-CS, NGO-C and NGO-M composites.

5- The distribution of pores in the membranes are irregular and the size of the pores are heterogeneous, fluctuate from one membrane to another and in the membrane itself as well. The removal% of BPB dye by these membranes are high, compared to removal% of trace metal ions.

Conclusions and Recommendation

Recommendations

1-Synthesis of other nano-graphene oxide composites using other polymers and metal oxides.

2- Using (NGO-CS, NGO-M and NGO-C) composites and membranes to remove other organic dyes and metal ions

3- Characterizing the (NGO-CS, NGO-M and NGO-C) composites by other instruments such as H-NMR, C-NMR, TEM, EDX.

4- Applying other isotherm models, BET, Temkin, Dubinin–Radushkevich isotherm models, as well as calculating the activation energy by applying the Arrenius equation.

5- Studying the biological activity of (NGO-CS, NGO-M and NGO-C) composites against bacteria and fungi.

6- Study of the mechanical properties of these (NGO-CS, NGO-M and NGO-C) membranes.

References

The References

[1] S. Sharma and A. Bhattacharya, "Drinking water contamination and treatment techniques," *Appl. Water Sci.*, vol. 7, no. 3, pp. 1043–1067, 2017.

[2] I. W. W. Smith, C. S. Cockell, and S. Leach, *Physical Chemistry in Action*. 2013.

[3] and A. K. F. L. Braghiroli, H. Bouafif, C. M. Neculita, "'Activated biochar as an effective sorbent for organic and inorganic contaminants in water,'" *"Water. Air. Soil Pollut*, vol. 229, p. 7, 2018.

[4] WHO, "Management of rcostadioactivity in drinking-water," *Who*, p. 104, 2018.

[5] "Heavy metal CU , NI and ZN : Toxicity , health hazards and their removal techniques by low cost adsorbents : A short overvlew revised: 20 th June-2013 1 M . Tech Research Scholar , Depa," pp. 143–157, 2013.

[6] R. A. Ahmed and A. M. Fekry, "Preparation and Characterization of a Nanoparticles Modified Chitosan Sensor and Its Application for the Determination of Heavy Metals from Different Aqueous Media," vol. 8, pp. 6692–6708, 2013.

[7] A. M. Ahmed, R.A., and Fekry, "Preparation and characterization of a nanoparticles modified chitosan sensor and its application for the determination of heavy metals from different aqueous media .," *Int. J. Electrochem. Sci.*, vol. 8, pp. 6692–6708.

[8] S. K. Sharma, S. Mahiya, G. Lofrano, A. Á. Biosorption, and Á. Carissa, "Removal of divalent nickel from aqueous solutions using Carissa carandas and Syzygium aromaticum : isothermal studies and kinetic modelling," *Appl. Water Sci.*, vol. 7, no. 4, pp. 1855–1868, 2017.

The References

[9]   M. Kaji, "Role of experts and public participation in pollution control: The case of Itai-itai disease in Japan," *Ethics Sci. Environ. Polit.*, vol. 12, no. 2, pp. 99–111, 2012.

[10]   S. Mehdipour, V. Vatanpour, and H. R. Kariminia, "Influence of ion interaction on lead removal by a polyamide nanofiltration membrane," *Desalination*, vol. 362, pp. 84–92, 2015.

[11]   T. Pradeep and Anshup, "Noble metal nanoparticles for water purification: A critical review," *Thin Solid Films*, vol. 517, no. 24, pp. 6441–6478, 2009.

[12]   G. Zolfaghari, A. Esmaili-Sari, M. Anbia, H. Younesi, and M. B. Ghasemian, "A zinc oxide-coated nanoporous carbon adsorbent for lead removal from water: Optimization, equilibrium modeling, and kinetics studies," *Int. J. Environ. Sci. Technol.*, vol. 10, no. 2, pp. 325–340, 2013..

[13]   P. E. Greeson, *P. E. Greeson, "Organic substances in water.". US Geological Survey,*. 1981.

[14]   GERAND, "'Drinking water and health, '.," *Natl. Res. Counc. Safe Drink. Water Comm.*, vol. 1, 1977.

[15]   E. Diamanti-Kandarakis *et al.*, "Endocrine-disrupting chemicals: An Endocrine Society scientific statement," *Endocr. Rev.*, vol. 30, no. 4, pp. 293–342, 2009.

[16]   and T. J. M. L. Cizmas, V. K. Sharma, C. M. Gray, "'HHS Public Access,'" *Pharmaceuticals.*, vol. 13, no. 4, pp. 381–394, 2017.

[17]   L. Pereira and M. Alves, "'Dyes-environmental impact and remediation,'" in *In Environmental protection strategies for sustainable development.*, 2012, pp. 112–154.

The References

[18] S. Activities et al., "'Geneural introduction to the chemistry of dyes,'" *Biol. Conserv*, vol. 99, pp. 1–91, 2010.

[19] "World health organization international agency for research on cancer iarc Monographs on the Evaluation of Carcinogenic Risks to Humans VOLUME 83 Tobacco Smoke and Involuntary Smoking," vol. 83, 2004.

[20] A. E. Al Prol, "Study of Environmental Concerns of Dyes and Recent Textile Effluents Treatment Technology: A Review," *Asian J. Fish. Aquat. Res.*, vol. 3, no. 2, pp. 1–18, 2019.

[21] P. G. and I. Introduction, "'Classification of dyes by chemical structure,'" *Chem. Appl. Dye.*, pp. 17–47, 1990.

[22] T. S. Technol, "'Methods of Applying Dyes to Textiles,'" vol. 11, no. C, pp. 112–192, 1994.

[23] R. Kant, "'Textile dyeing industry an environmental hazard,'" vol. 4, no. 1, pp. 22–26, 2012.

[24] and J. C. P. B. Lellis, C. Z. Fávaro-polonio, J. A. Pamphile, "'Effects of textile dyes on health and the environment and bioremediation potential of living organisms,'" *Biotechnol. Res.*, pp. 275---290, 2019.

[25] and S. K. S. Hussain, N. Khan, S. Gul, "'Contamination of water resources by food dyes and its removal technologies.,'" in *In Water Chemistry*, p. 113,2019.

[26] M. Hassaan, A. El Nemr, and M. A. Hassaan, "Health and Environmental Impacts of Dyes: Mini Review," *Am. J. Environ. Sci. Eng.*, vol. 1, no. 3, pp. 64–67, 2017.

[27] Y. Liu, Y. Huang, A. Xiao, H. Qiu, and L. Liu, "Preparation of magnetic Fe3O4/MIL-88A nanocomposite and its adsorption properties for bromophenol blue dye in aqueous solution," *Nanomaterials*, vol. 9, no. 1, 2019.

[28] S. Dutta, B. Gupta, S. K. Srivastava, and A. K. Gupta, "Recent advances on the removal of dyes from wastewater using various adsorbents: A critical review," *Mater. Adv.*, vol. 2, no. 14, pp. 4497–4531, 2021.

[29] A. P. Sachidhanandham, A.; Periyasamy, "Environmentally Friendly Wastewater Treatment Methods for the Textile Industry.," *Handb. of Nanomaterials Nanocomposites Energy Environ. Appl. Springer Cham, Switzerland,* pp. 1–40, 2020.

[30] P. V. Nidheesh, M. Zhou, and M. A. Oturan, "An overview on the removal of synthetic dyes from water by electrochemical advanced oxidation processes," *Chemosphere*, vol. 197, no. January, pp. 210–227, 2018, doi: 10.1016/j.chemosphere,12.195, 2017.

[31] P. R. De Souza and T. Moreira, "Removal of bromophenol blue anionic dye from water using a modified exuviae of Hermetia illucens larvae as biosorbent," 2020.

[32] G. Crini, E. Lichtfouse, L. D. Wilson, and N. Morin-Crini, "Conventional and non-conventional adsorbents for wastewater treatment," *Environ. Chem. Lett.*, vol. 17, no. 1, pp. 195–213, 2019.

[33] C. Bellmann, "Surface Modification by Adsorption of Polymers and Surfactants," in *Polymer Surfaces and Interfaces: Characterization, Modification and Applications*, p. Chapter 12.

[34] and S. S. R. R. Gusain, N. Kumar, "'Recent advances in carbon nanomaterial-based adsorbents for water purification,'" *Elesvier*, vol. 405, p. 213111, 2020.

[35] O. Sahu and N. Singh, "'Significance of bioadsorption process on textile industry wastewater,'" *Impact Prospect. Green Chem. Text. Technol.*, vol. 13, pp. 367–416., 2019.

[36] A. Fakhri, "Adsorption characteristics of graphene oxide as a solid adsorbent for aniline removal from aqueous solutions: Kinetics, thermodynamics and mechanism studies," *J. Saudi Chem. Soc.*, vol. 21, pp. S52–S57, 2017.

[37] L. Pereira and M. Alves, *"Dyes-environmental impact and remediation,". In Environmental protection strategies for sustainable development. Springer, Dordrecht. pp.* 2012.

[38] G. Uyar, "'A low-cost adsorbent for dye removal: methylene blue removal by alginatemontmorillonite hybride beads,'" *Istanbul Tech. Univ.*, 2012.

[39] S. Sohni *et al.*, "Highly Efficient Removal of Acid Red-17 and Bromophenol Blue Dyes From Industrial Wastewater Using Graphene Oxide Functionalized Magnetic Chitosan Composite," 2019.

[40] M. S. Amin and M. A. Ahmed, "Journal of Environmental Chemical Engineering Removal of methyl orange and bromophenol blue dyes from aqueous solution using Sorel ' s cement nanoparticles," *Biochem. Pharmacol.*, vol. 3, no. 3, pp. 1702–1712, 2015.

[41] G. Lofrano, "Emerging compounds removal from wastewater: natural and solar based treatments.," *Springer Sci. Bus. Media.*

[42] M. Chiou and H. Li, "Equilibrium and kinetic modeling of adsorption of

reactive dye on cross-linked chitosan beads," vol. 93, pp. 233–248, 2002.

[43] J. German-heins, "Sorption of Brilliant Blue FCF in soils as affected by pH and ionic strength," 2000.

[44] M. A. Mehmet Do gan, "Adsorption kinetics of methyl violet onto perlite," *Chemosphere*, vol. 50, pp. 517–528.

[45] L. You, Z. Wu, T. Kim, and K. Lee, "Kinetics and thermodynamics of bromophenol blue adsorption by a mesoporous hybrid gel derived from tetraethoxysilane and bis (trimethoxysilyl) hexane," vol. 300, pp. 526–535, 2006.

[46] M. A. Mohammad Razi, M. N. A. Mohd Hishammudin, and R. Hamdan, "Factor Affecting Textile Dye Removal Using Adsorbent from Activated Carbon: A Review," *MATEC Web Conf.*, vol. 103, pp. 1–17, 2017.

[47] C. Bellmann, "Surface Modification by Adsorption of Polymers and Surfactants," pp. 235–236.

[48] Y. Liu *et al.*, "Highly effective adsorption of cationic and anionic dyes on magnetic Fe/Ni nanoparticles doped bimodal mesoporous carbon," *J. Colloid Interface Sci.*, vol. 448, pp. 451–459, 2015.

[49] S. J. Shan, Y. Zhao, H. Tang, and F. Y. Cui, "A Mini-review of Carbonaceous Nanomaterials for Removal of Contaminants from Wastewater," *IOP Conf. Ser. Earth Environ. Sci.*, vol. 68, no. 1, 2017.

[50] N. M. Abbasi, S., Peerzada, M.H., Nizamuddin, S. and Mubarak, "Functionalized nanomaterials for the aerospace, vehicle, and sports industries," *Handb. Funct. Nanomater. Ind. Appl.*, pp. 795–825, 2020.

[51] S. S. N. and H. H. R. Ahmed Abd ulwahid Mohammed, "Using Solid Phase

Micro Extraction Method to Separate The Trace Elements from Crude Oil Samples by Nano Graphene Oxide as a Sorbent," *Turkish J. Physiother. Rehabil.*, vol. 32, no. 3, pp. 23182–23191, 2021.

[52] E. and Samiee, R., Ramezanzadeh, B., Mahdavian, M., Alibakhshi and G. Bahlakeh, "Graphene oxide nano-sheets loading with praseodymium cations: adsorption-desorption study, quantum mechanics calculations and dual active-barrier effect for smart coatings fabrication.," *J. Ind. Eng. Chem.*, vol. 78, pp. 143–154, 2019.

[53] J. Y. X. Xu, L. Zhao, H. Bai, W. J. Hong, C. Li and G. Q. Shi, "Chemically Converted Graphene Induced Molecular Flattening of 5,10,15,20-Tetrakis(1-methyl-4-pyridinio)porphyrin and Its Application for Optical Detection of Cadmium(II) Ions," *Am. Chem. Soc*, vol. 131, pp. 13490–13497., 2009.

[54] X. Yang, Y. Tu, L. Li, S. Shang, and X. Tao, "Well-Dispersed Chitosan/Graphene Oxide Nanocomposites," vol. 2, no. 6, pp. 1707–1713, 2010.

[55] M. N. V. R. Kumar, "A review of chitin and chitosan applications q," vol. 46, pp. 1–27, 2000.

[56] Y. Chung, Y. Li, and C. Chen, "Journal of Environmental Science and Health , Part A : Toxic / Hazardous Substances and Environmental Engineering Pollutant Removal From Aquaculture Wastewater Using the Biopolymer Chitosan at Different Molecular Weights," no. October 2014, pp. 37–41.

[57] Y. I. T. Sannan, K. Kurita, "'Studies on Chitin. 2. Effect of Deacetylation on solubility,'" *Die Makromol. Chem*, vol. 177, no. 12, p. 3589 ..

[58] N. Y. H. Sashiwa, N. Kawasaki, A. Nakayama, E. Muraki and S. Aiba, "'Chemical modification of chitosan 14: Synthesis of water- soluble chitosan derivatives by simple acetylation,'" *Biomacromol*, vol. 3, p. 1126.

The References

[59] A. Spoial, C. Ilie, D. Ficai, and A. Ficai, "Chitosan-Based Nanocomposite Polymeric Membranes for Water Purification — A Review," pp. 1–29, 2021.

[60] K. D. M. S. Jisha, "Chitosan nanoparticles preparation and applications," *Environ. Chem. Lett.*, 2017.

[61] J. Wang, S. Zhuang, and J. Wang, "Technology Removal of various pollutants from water and wastewater by modified chitosan adsorbents," vol. 3389, 2018.

[62] H. Bai, C. Li, X. Wang, and G. Shi, "On the gelation of graphene oxide," *J. Phys. Chem. C*, vol. 115, no. 13, pp. 5545–5551, 2011.

[63] H. Bai, C. Li, X. Wang, and G. Shi, "A pH-sensitive graphene oxide composite hydrogel," *Chem. Commun.*, vol. 46, no. 14, pp. 2376–2378, 2010.

[64] C. De Spectrome, "Recent developments in polysaccharide-based materials used as adsorbents in wastewater treatment," vol. 30, pp. 38–70, 2005.

[65] S. İlknur Şentürk, "Adsorption of Acid Violet 17 Onto Acid-Activated Pistachio Shell: Isotherm, Kinetic and Thermodynamic," *Chem. Biochem. Environ. Eng.*, vol. 67, no. 1, 2020.

[66] T. Robinson, G. McMullan, R. Marchant, and P. Nigam, "Remediation of dyes in textile effluent: A critical review on current treatment technologies with a proposed alternative," *Bioresour. Technol.*, vol. 77, no. 3, pp. 247–255, 2001..

[67] Z. Karim, A. P. Mathew, M. Grahn, J. Mouzon, and K. Oksman, "Nanoporous membranes with cellulose nanocrystals as functional entity in chitosan: Removal of dyes from water," *Carbohydr. Polym.*, vol. 112, pp. 668–676, 2014.

[68] J. R. Werber, C. O. Osuji, and M. Elimelech, "Materials for next-generation

desalination and water purification membranes," *Nat. Rev. Mater.*, vol. 1, 2016.

[69] Z. Wang, A. Wu, L. C. Ciacchi, and G. Wei, "Recent advances in Nanoporous Membranes for Water Purification," *Nanomaterials*, vol. 8, no. 2, 2018.

[70] Y. Han, Z. Xu, and C. Gao, "Ultrathin graphene nanofiltration membrane for water purification," *Adv. Funct. Mater.*, vol. 23, no. 29, pp. 3693–3700, 2013.

[71] J. Yin and B. Deng, "Polymer-matrix nanocomposite membranes for water treatment," *J. Memb. Sci.*, vol. 479, pp. 256–275, 2015.

[72] S. Pandit and M. De, "Interaction of Amino Acids and Graphene Oxide: Trends in Thermodynamic Properties," no. December, 2016.

[73] A. Shahzad *et al.*, "RSC Advances Heavy metals removal by EDTA-functionalized chitosan graphene oxide nanocomposites †," *RSC Adv.*, vol. 7, pp. 9764–9771, 2017.

[74] H. Hosseinzadeh and S. Ramin, "PT SC," p. #pagerange#, 2018.

[75] A. K. Sarkar, "Functionalized magnetic biopolymeric graphene oxide with outstanding performance in water puri fi cation," *NPG Asia Mater.*, 2019.

[76] M. Fathy, T. A. Moghny, M. A. Mousa, O. H. Abdelraheem, and A. A. Emam, "Synthesis and study bromophenol blue dye adsorption efficiency of reduced graphene oxide produced by catalytic acid spray (CAS) method," pp. 567–577, 2020.

[77] M. Sahli *et al.*, "Chitosan-graphene oxide nanocomposites as water-solubilising agents for rotenone pesticide," *J. Mol. Liq.*, vol. 318, p. 114066, 2020.

[78] X. Jin, X. Wen, S. Lim, and R. Joshi, "Size-Dependent Ion Adsorption in Graphene Oxide Membranes," pp. 1–8, 2021.

The References

[79]   S. Samhan Zahran and F. Takrori, "Faculty of Graduate Studies Chemistry Department An Efficient Removal of Bromophenol Blue Dye from Contaminated Water Using Nanographene Oxide as a Novel Adsorbent," 2021.

[80]   J. Chen, B. Yao, C. Li, and G. Shi, "An improved Hummers method for eco-friendly synthesis of graphene oxide," *Carbon N. Y.*, vol. 64, no. 1, pp. 225–229, 2013.

[81]   A. el Sana Frindy, Ana Primo, Hamid Ennajih, E. M. kacem Qaiss, Rachid Bouhfid, Mohamed Lahcini, and A. E. K. Essassi, Hermenegildo Garcia, "Chitosan-graphene oxide films and CO2-dried porous aerogel microspheres: Interfacial interplay and stability," *Carbohydr. Polym.*, 2017.

[82]   A. Croitoru *et al.*, "materials Chitosan / Graphene Oxide Nanocomposite Water Purification," pp. 1–13.

[83]   H. H. Radey, "Surface Functionalization of Nano Graphene Oxide by Amino Acid," vol. 6, no. March, pp. 941–951, 2022.

[84]   K. Narayanan, T.S., Jegannathan, S. and Ravichandran, "Corrosion resistance of phosphate coatings obtained by cathodic electrochemical treatment: Role of anode–graphite versus steel," *Prog. Org. coatings*, vol. 55(4), pp. 355–362.

[85]   R. Justin and B. Chen, "Characterisation and drug release performance of biodegradable chitosan – graphene oxide nanocomposites," *Carbohydr. Polym.*, vol. 103, pp. 70–80, 2014.

[86]   L. Stobinski *et al.*, "Graphene oxide and reduced graphene oxide studied by the XRD, TEM and electron spectroscopy methods," *J. Electron Spectros. Relat. Phenomena*, vol. 195, no. March 2018, pp. 145–154, 2014.

[87]   M. Sahli *et al.*, "Chitosan-graphene oxide nanocomposites as water-

solubilising agents for rotenone pesticide," vol. 318, pp. 1–13, 2020.

[88] S. Mustapha *et al.*, "Comparative study of crystallite size using Williamson-Hall and Debye-Scherrer plots for ZnO nanoparticles," *Adv. Nat. Sci. Nanosci. Nanotechnol.*, vol. 10, no. 4, 2019.

[89] Y. Chen, L. Chen, H. Bai, and L. Li, "Graphene oxide-chitosan composite hydrogels as broad-spectrum adsorbents for water purification," *J. Mater. Chem. A*, vol. 1, no. 6, pp. 1992–2001, 2013.

[90] Y. Xu *et al.*, "Synthesis and characterization of additive graphene oxide nanoparticles dispersed in water: Experimental and theoretical viscosity prediction of non-Newtonian nanofluid," *Math. Methods Appl. Sci.*, 2020.

[91] F. Varenne *et al.*, "Evaluation of zeta potential of nanomaterials by electrophoretic light scattering: Fast field reversal versus Slow field reversal modes," *Talanta*, vol. 205, no. June, p. 120062, 2019.

[92] G. D. C. P. and KAS., *Analytical Chemistry*. 2014.

[93] J. Ferreira and E. M. Girotto, "PH effects on the ohmic properties of bromophenol blue-doped polypyrrole film," *J. Braz. Chem. Soc.*, vol. 21, no. 2, pp. 312–318, 2010.

[94] A. Hicham, J. Hussein, and H. Siba, "Kinetic, isotherm and thermodynamic studies on the ciprofloxacin adsorption from aqueous solution using Aleppo bentonite," *Baghdad Sci. J.*, vol. 19, no. 3, pp. 680–692, 2022.

[95] V. A. Online, "broad-spectrum adsorbents for water puri fi cation †," pp. 1992–2001, 2013.

[96] Y. Hu *et al.*, "Dye adsorption by resins: Effect of ionic strength on hydrophobic and electrostatic interactions," *Chem. Eng. J.*, vol. 228, pp. 392–397, 2013.

[97] C. H. Giles and D. Smith, "A General Treatment and Classification of the Solute Adsorption Isotherm," *Dep. Math. Univ. Strat. Glas. G1, Scotl.*, vol. 47, no. 3, pp. 755–765, 1973.

[98] A. M. Rheima, M. A. Mohammed, S. H. Jaber, and S. A. Hameed, "Adsorption of selenium (Se4+) ions pollution by pure rutile titanium dioxide nanosheets electrochemically synthesized," *Desalin. Water Treat.*, vol. 194, pp. 187–193, 2020.

[99] A. A. A. Darwish, M. Rashad, and H. A. AL-Aoh, "Methyl orange adsorption comparison on nanoparticles: Isotherm, kinetics, and thermodynamic studies," *Dye. Pigment.*, vol. 160, pp. 563–571, 2019.

[100] F. Wang, "Adsorption of Anionic Dye on Graphene Nanosheets Doped with Ag Nanoparticles: Kinetics and Thermodynamic Study," *Russ. J. Phys. Chem. A*, vol. 93, no. 7, pp. 1357–1364, 2019.

الخلاصة

يعد تلوث المياه مشكلة واسعة النطاق في جميع أنحاء العالم. ففي الوقت الحاضر، أدت الأنشطة الصناعية المتنامية إلى توليد كميات هائلة من المواد الخطرة؛ النفايات الصناعية غير المعالجة والملوثات غير الخاضعة للرقابة التي تنطلق في المياه البيئية. من بينها، تولد الأصباغ الناتجة عن الصناعات النسيجية كمية كبيرة من مياه الصرف الصناعي بسبب الطلب الكبير على المياه ويتم تصريفها بشكل متكرر في البيئة طوال عملية الإنتاج ولها تأثير مباشر على صحة الإنسان، ونتيجة لذلك، تعد معالجة تلوث المياه أحد أهم الحلول. القضايا الحتمية التي أولها المجتمع العلمي اهتمامًا كبيرًا بهدف أساسي هو حماية الموارد المائية الطبيعية والحفاظ عليها. تتضمن هذه الدراسة ثلاثة أجزاء تخليق، تشخيص و تطبيق متراكبات اوكسيد الجرافين النانوي جرافين لإزالة بعض ملوثات المياه.

القسم الاول يتضمن تخليق اوكسيد الجرافين النانوي (NGO) وثلاثة متراكبات، اوكسيد الجرافين النانوي-الكيتوسان (NGO-CS), اوكسيد الجرافين النانوي-الميثيونين (NGO-M) و اوكسيد الجرافين النانوي-السيستين (NGO-C).

القسم الثاني يتضمن تشخيص هذه المتراكبات بواسطة تقنية (FT-IR) و تقنية (XRD) لإيجاد حجم الجسيمات المتكونة حيث وجدت (7.4, 10.8, 16.83 and 19.52 nm) للمتراكبات NGO-M, NGO-CS و NGO-C على التوالي من خلال تطبيق معادلة Debye-.Scherrer, وكذالك شخصت بواسطة تقنية جهد زيتا لمعرفة شحنة السطح للمتراكبات.

القسم الثالث يتضمن إستخدام هذه المتراكبات في معالجة المياة وذلك بإزالة الملوثات العضوية (صبغة برموفينول الزرقاء) وكذلك الملوثات اللاعضوية (ايونات المعادن الثقيلة النزره) وبطريقتين : الأولى (الإمتزاز) لصبغة BPB على المتراكبات الثلاثة، وتحديد الظروف المثلى لكل متراكب، النتائج كانت كالاتي (الدالة الحامضية = 3،2 و 1، وزن المتراكب =2،2و2 مليغرام، زمن التماس =75،60و 60 دقيقة، درجة الحرارة= 45،55 و55 درجة مئوية، تركيز الصبغة =40،25 و 25جزء من المليون) للمتراكبات NGO-M,CS و NGO-C على التوالي , وكذلك تم دراسة ايزوثيرم الإمتزاز حيث اظهرت منحنيات الإمتزاز الشكل العام للإمتزاز للمتراكبات من نوع S حسب تصنيف Gilles ، وطبقت معادلات فرندلش و لانكماير ، وكذلك تم دراسة الثرموديناميكا الحرارية للمتراكبات حيث كانت (+) ΔS ,(+) ΔH اي ان امتزاز صبغة BPB على المتراكبات الثلاثة هي عملية ماصة للحرارة, وان (-) ΔG لذلك العملية تكون تلقائية .

أظهرت النتائج أن معادلة الدرجة الثانية الكاذبة أكثر صحة لوصف سلوك حركية الإمتزاز لصبغة BPB على المتراكبات الثلاث.

الطريقة الثانية (الأغشية) حيثُ صنعت أغشية NGO-M,NGO-CS, CS,NGO وNGO-C عن طريق الترشيح التقريبي ، وتم تحديد متوسط حجم المسام لهذه الأغشية حيث كانت (52.31-613.2) , (36.43-400.7),(49.53-347.5) , (326.0 -84.8) و(55.32-147.01) نانومتر على التوالي بواسطة تقنية FESEM استخدمت هذه الأغشية لفصل ملوث عضوي (صبغة BPB) ، حيث كانت نسبة الإزالة على النحو التالي (85.65 ، 95.35 ، 98.52 ، 86.91 و 92.61٪) على التوالي ، حيث كان أفضل غشاء NGO -CS. استخدمت هذه الأغشية أيضًا لفصل أيونات المعادن الثقيلة Ni^{+2} , Cd^{+2}, Co^{+2}, Cu^{+2} و Pb^{+2} من المحاليل ، وتظهر البيانات التجريبية أن نسبة إزالة أيونات Ni^{+2} وCo^{+2} بواسطة الأغشية كانت بالترتيب NGO > CS > NGO-M > NGO-C > NGO-CS، أفضل غشاء هو NGO-CS، R% (48.47%) و (68.17%) بينما أيونات Cd^{+2} تتبع الترتيب NGO-CS > NGO > NGO-M > CS > NGO- C >، وأفضل غشاء هو CS، حيث R% (52.2%). وتتبع أيونات Cu^{+2} الترتيب NGO-M > CS > NGO-CS > NGO > NGO-C، وأفضل غشاء هو NGO-M، حيث R% (66.47%) . من ناحية أخرى، تتبع أيونات Pb^{+2} الترتيب CS > NGO-C > NGO-M > NGO > NGO-CS، وأفضل غشاء هو NGO-CS حيث R% (67.04%).

جمهورية العراق

وزارة التعليم العالي و البحث العلمي

جامعة ميسان

كلية العلوم

قسم الكيمياء

تخليق و تشخيص بعض اغشية اوكسيد الجرافين النانوي لإزالة بعض ملوثات المياه

رسالة مقدمة الى

كلية العلوم / جامعة ميسان جزء من متطلبات نيل
شهادة الماجستير في علوم الكيمياء

الطالبة

سماح نعيم غازي

بكالوريوس علوم كيمياء/ جامعة ميسان   (2018)

بإشراف

أ.م

صفاء صبري نجم

أ.م.د

احمد مجيد عباس

١٤٤٥ هـ   ٢٠٢٣ م